SANDIA REPORT
SAND201X-XXXX
Unlimited Release
Printed Month and Year

Fluxional Monomers for Enhanced Thermoset Materials

Brad H. Jones, Todd M. Alam, Hayden T. Black, Mathias C. Celina, and David R. Wheeler

Prepared by
Sandia National Laboratories
Albuquerque, New Mexico 87185 and Livermore, California 94550

Sandia National Laboratories is a multimission laboratory managed and operated by National Technology and Engineering Solutions of Sandia, LLC, a wholly owned subsidiary of Honeywell International, Inc., for the U.S. Department of Energy's National Nuclear Security Administration under contract DE-NA0003525.

Issued by Sandia National Laboratories, operated for the United States Department of Energy by National Technology and Engineering Solutions of Sandia, LLC.

Available to DOE and DOE contractors from
U.S. Department of Energy
Office of Scientific and Technical Information
P.O. Box 62
Oak Ridge, TN 37831

Telephone: (865) 576-8401
Facsimile: (865) 576-5728
E-Mail: reports@osti.gov
Online ordering: http://www.osti.gov/scitech

Available to the public from
U.S. Department of Commerce
National Technical Information Service
5301 Shawnee Rd
Alexandria, VA 22312

Telephone: (800) 553-6847
Facsimile: (703) 605-6900
E-Mail: orders@ntis.gov
Online order: https://classic.ntis.gov/help/order-methods/

SAND201X-XXXX
Printed September 2017
Unlimited Release

Fluxional Monomers for Enhanced Thermoset Materials

Brad H. Jones,[1] Todd M. Alam,[1] Hayden T. Black,[1] Mathias C. Celina,[1] and David R. Wheeler[2]
Organic Materials Science[1] and Special Technologies[2]
Sandia National Laboratories
P. O. Box 5800
Albuquerque, New Mexico 87185-MS0888

Abstract

This report catalogues the results of a project exploring the incorporation of organometallic compounds into thermosetting polymers as a means to reduce their residual stress. Various syntheses of polymerizable ferrocene derivatives were attempted with mixed success. Ultimately, a diamine derivative of ferrocene was used as a curing agent for a commercial epoxy resin, where it was found to give similar cure kinetics and mechanical properties in comparison to conventional curing agents. The ferrocene-based material is uniquely able to relax stress above the glass transition, leading to reduced cure stress. We propose that this behavior arises from the fluxional capacity of ferrocene. In support of this notion, nuclear magnetic resonance spectroscopy indicates a substantial increase in chain flexibility in the ferrocene-containing network. Although the utilization of fluxionality is a novel approach to stress management in epoxy thermosets, it is anticipated to have greater impact in radical-cured thermosets and linear polymers.

ACKNOWLEDGMENTS

We are indebted to the following people, whose contributions were instrumental to the work described in this report. Mark Stavig conceived and designed the measurement fixture used in Chapter 3 for the evaluation of residual stress, while Lam Banh assisted in its construction and testing. In addition, Mark Stavig provided valuable support and guidance in a variety of experimental measurements. Patricia Sawyer assisted with preparation of a large number of samples, as well as thermal characterization. Nicholas Giron and Estevan Martinez performed FTIR spectroscopic measurements and analyzed much of the FTIR data presented in Chapter 3. Timothy Lambert provided assistance for the synthetic component of the work. Robert Bernstein, Erica Redline, and Jamie Kropka provided valuable support and insight through helpful discussions. Finally, we thank Doug Wall and Jim McElhanon for their aid in initiating this research project.

TABLE OF CONTENTS

FIGURES

TABLES

NOMENCLATURE

Abbreviation	Definition
E_a	activation energy
ASAP	atmospheric solids analysis probe
FcDA	1,1'-bis(α-aminoethyl)ferrocene
S_b	bond order parameter
v_e	calculated concentration of elastically effective strands at final conversion
CAN	covalent adaptable network
Cp	cyclopentadienyl ligand
DSC	differential scanning calorimetry
DGEBA	diglycidyl ether of bisphenol A
DMSO	dimethylsulfoxide
DQ	double quantum
DMA	dynamic mechanical analysis
G''	dynamic shear loss modulus
G'	dynamic shear storage modulus
G_f'	dynamic shear storage modulus at final conversion
828	EPON® 828 epoxy resin
α_f	final epoxy conversion
FTIR	Fourier transform infrared
t_{gel}	gel time
T_g	glass transition temperature
HRMS	high resolution mass spectrometry
IPD	isophorone diamine
T_{cure}	isothermal cure temperature
D-230	Jeffamine® D-230 curing agent
LDRD	Lab-Directed Research and Development
MAS	magic angle spinning
MDA	methylenedianiline
NMR	nuclear magnetic resonance
NW	nuclear weapon
R&D	research and development
RDC	residual dipolar coupling
T	temperature
TGA	thermogravimetric analysis

Abbreviation	Definition
$T_{g\infty}$	ultimate glass transition temperature at full cure
ε_V	volumetric shrinkage from gelation to final conversion

1. INTRODUCTION

Thermoset materials are created by the conversion of one or more monomers bearing reactive functional groups into a crosslinked network, as shown in Figure 1-1 for the example of tetra- and di-functional compounds depicted by red chevrons and blue triangles, respectively. The starting monomers are typically a readily processable liquid mixture, while the final polymeric product is tough, insoluble, and infusible, on account of its crosslinked chemical structure. As such, thermosets are used in a variety of applications, including many NW components. During cure, the average molecular weight of the species present progressively increases and the mixture eventually gels. At the gel point, the material is effectively a single, infinite network and it behaves as a rubbery, viscoelastic solid, *i.e.*, it is able to resist deformation. Beyond the gel point, the material continues to cure and the density of crosslinks increases further. This is accompanied by an increase in the T_g of the material. Below T_g, a thermoset behaves as a glassy solid having a modulus (stiffness) orders of magnitude greater than above T_g.

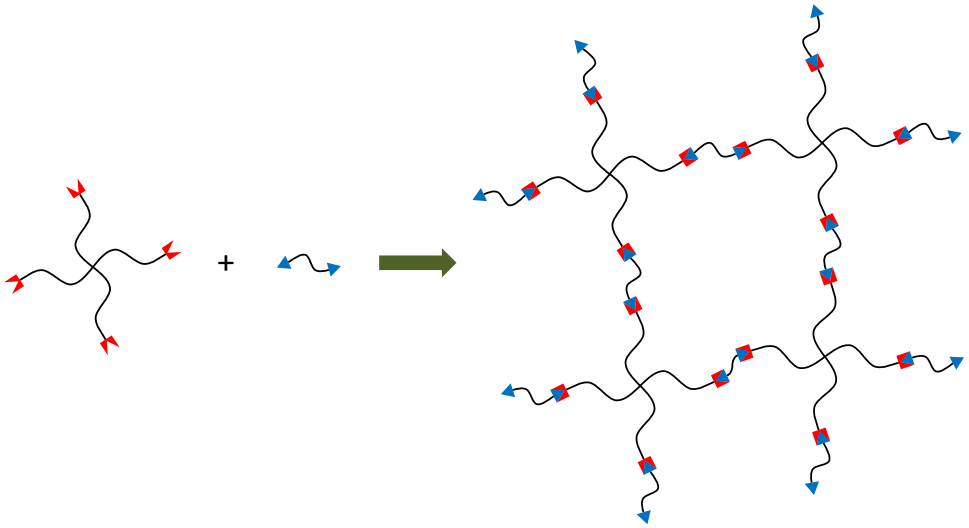

Figure 1-1. Schematic diagram of a thermoset polymerization.

The reaction of functional groups in thermosets essentially substitutes weak van der Waals interactions with strong covalent bonds, resulting in an overall decrease in interatomic distances within the polymerizing network. This substitution drives a volumetric contraction of the material, which is the origin of the well-known Achilles' heel of thermosets – residual stress. In practice, the processing of thermosets necessitates contact with one or more dissimilar materials, such as a mold or a substrate. As cure progresses beyond gelation, the progressively increasing drive for volumetric contraction is resisted by the adhesive constraints of such contacts, resulting in a situation where the thermoset is perturbed from its equilibrium state, *i.e.*, it possesses residual internal stress. This situation is frequently exacerbated by changes in temperature, where the differing propensities for expansion or contraction

of the thermoset and, for example, a surrounding mold generate additional stress in the material. The magnitude of the overall residual stress in a processed thermoset is a complex function of the thermal history of the material, the constraints imposed by processing, the volumetric shrinkage that would occur in the absence of such constraints, and the modulus of the material, which itself evolves in a complex manner during cure. In general, the stress imparted by reaction shrinkage or thermal excursions is proportional to the modulus of the material and is appreciably greater when the material is glassy (below T_g) compared to when it is rubbery (above T_g). Nevertheless, for a particular system, significant residual stress can be built up in either regime.

The residual stress that exists in a processed thermoset can be relieved through various phenomena, many which are deleterious or even catastrophic for the performance of a device, such as internal cracking or interfacial delamination. Therefore, any general strategy by which residual stress can be reduced or eliminated will have a direct and immediate benefit to applications in which thermosets are employed. Traditionally, residual stress is addressed through optimization of cure schedules or through the addition of inert fillers.[1-14] In addition, residual stress can be partially relaxed (relieved) by annealing a thermoset near its T_g, wherein molecular reorientation occurs to accommodate the imposed stress, with a concomitant reduction in the free volume of the material.[15-17] Nevertheless, there are significant limitations in the extent to which these strategies can reduce stress. Furthermore, in practice, they are often unfeasible to implement; for example, the ideal cure schedule from a stress standpoint may extend the cure time by a financially-prohibitive amount.[18] Indeed, millions of R&D dollars are spent each year at Sandia optimizing the processing conditions for thermosets. In contrast, a general chemistry-based solution to this problem offers a platform by which residual stress can be reduced across all thermosets independent of processing conditions, thereby saving Sandia significant R&D investments in the long term while enhancing material performance.

The intent of this LDRD project has been to create new fluxional thermoset monomers and explore their capacity to reduce residual stress. In general, the term fluxional describes a molecule or a portion of a molecule that undergoes spontaneous interchange between different structures or bonding configurations. We use the term fluxional more specifically to describe the dynamics of cyclopentadienyl (Cp)-metal groups, such as metallocenes.[19,20] A general example is shown in Figure 1-2 for a metal, M, bonded in a sandwich configuration to two Cp rings. The metal can be bonded through the electron cloud of one, two, three, or all five of the carbon atoms of the Cp rings, termed η_1, η_2, η_3, and η_5 configurations, respectively. More importantly, the Cp rings can rotate around the ring-metal bond. In solution, the energy barrier to ring rotation in ferrocene (where M = Fe^{+2}), for example, is 4 kJ/mol; by comparison, the energy barrier to simple carbon-carbon bond rotation – a bond rearrangement process that is considered to be relatively facile – is three times greater.[21] The potential ability of Cp-metal functionalities for residual stress relaxation when incorporated into a polymeric network is depicted in Figure 1-3. A general metallocene group is highlighted in red, exhibiting fluxional motion about the Cp-metal axis, while wavy lines indicate continued polymer structure. An imposed stress, such as that resulting

from the curing processes described above, can be relaxed (relieved) by molecular reorientation. Generally speaking, stress can be relaxed in polymeric materials above T_g, wherein carbon-carbon bond rotation occurs rapidly and the corresponding conformational rearrangements (*e.g.*, trans-gauche) provide a mechanism for relaxation. However, as discussed in greater detail in Chapter 3, the introduction of crosslinks severely inhibits such conformational rearrangements. Nevertheless, the degree to which Cp ring rotation will contribute to stress relaxation will be far greater and it will be more readily activated on account of its substantially lower energy requirements, in comparison to conventional polymeric materials.

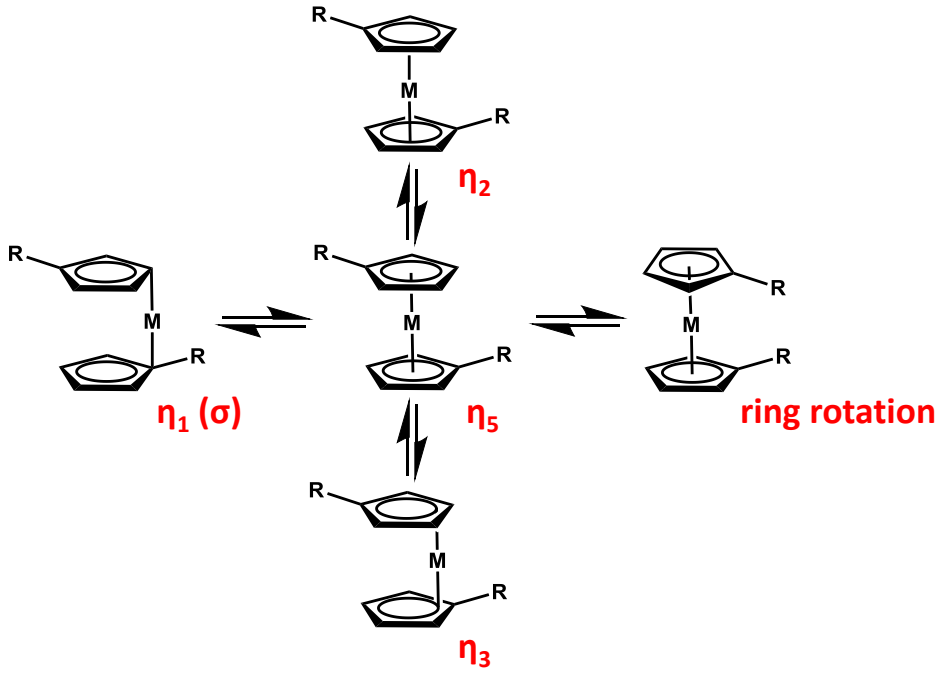

Figure 1-2. Several typical bonding configurations observed in fluxional Cp-metal groups.

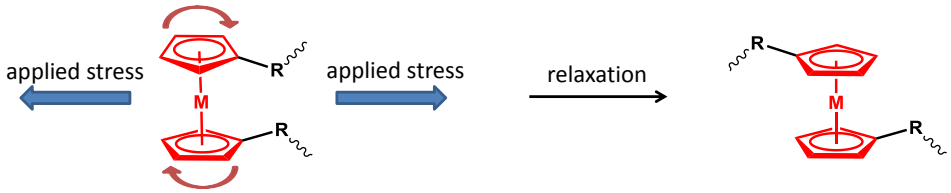

Figure 1-3. Schematic diagram depicting hypothetical mechanism for stress relaxation in polymers incorporating Cp-metal backbone functionality.

It is important to emphasize that the approach described above and depicted in Figure 1-3 requires chain connectivity through the Cp-metal axis. In other words, appropriate

monomers comprise symmetrically disubstituted metallocene derivatives. Therefore, this project began with an exploration of synthetic strategies by which reactive functionalities suitable for thermoset polymerizations (*e.g.*, amine, epoxide, vinyl) can be installed onto metallocenes. We chose to work with ferrocene derivatives, due to the widespread commercial availability and cost of key precursors, as well as a relative abundance of past literature in which ferrocenes are incorporated onto polymers. These syntheses, described in Chapter 2, were discovered to be much more challenging than anticipated, often yielding undesirable products or compounds with low purity. Ultimately, a symmetrically substituted diamine of ferrocene – FcDA – was the only compound we were able to obtain at a purity and scale suitable for further study. This led us to subsequently focus our study on epoxy thermosets derived from a common epoxy resin cured with FcDA. Unsurprisingly, we found that these materials exhibited unique stress relaxation behavior above T_g and reduced residual stress due to cure in comparison to conventional epoxy thermosets, which is the subject of Chapter 3. Similarly, we used solid state ^{1}H NMR to investigate the segmental dynamics of these materials and observed abnormally high chain flexibility, which is the subject of Chapter 4. Finally, Chapter 5 compares the outcomes of this project against the overall goal to minimize residual stress in thermosets and provides several suggestions for future work on that basis.

2. SYNTHESIS OF REACTIVE, DISUBSTITUTED FERROCENES

2.1. Ferrocene Diepoxides

Initially, a symmetrically substituted diepoxide derivative of ferrocene was targeted as a seemingly straightforward compound to synthesize. Diepoxides and triepoxides are widely used as resins in the preparation of epoxy thermosets. In particular, DGEBA, formed from the reaction of bisphenol A with epichlorohydrin, and similar compounds are used as the base resin for the overwhelming majority of commercial epoxy formulations, in combination with a wide variety of curing agents. Thus, a ferrocene diepoxide would permit comparison of the stress relaxation characteristics and dynamics of DGEBA-based and ferrocene-based epoxy networks.

Several literature procedures exist for the preparation of epoxide-substituted ferrocenes reporting high yield.[22-25] Several of these procedures were attempted in the synthesis of the diepoxide with little success (Figure 2-1). Generally, reactions would give the monoepoxide intermediate without progressing to the diepoxide. As an example, the full synthetic details leading to compound **1** in Figure 2-1 are provided below. A typical solution ^{1}H NMR spectrum of compound **1** is provided in Figure 2-2. Attempts to drive the reaction to the diepoxide with heat or concentration of reactants mostly led to byproducts. We attributed the retardation of the epoxidation reaction to an intramolecular ‘isomerization’, where the epoxide group of the monoepoxide intermediate is attacked by the alcohol on the same molecule (under basic conditions). This initial intramolecular attack opens the epoxide, which can then close again by cyclization to the epoxide on the other side of the molecule. We believe that fast switching between these two states leads to a stable intermediate that is unreactive to additional epichlorohydrin.

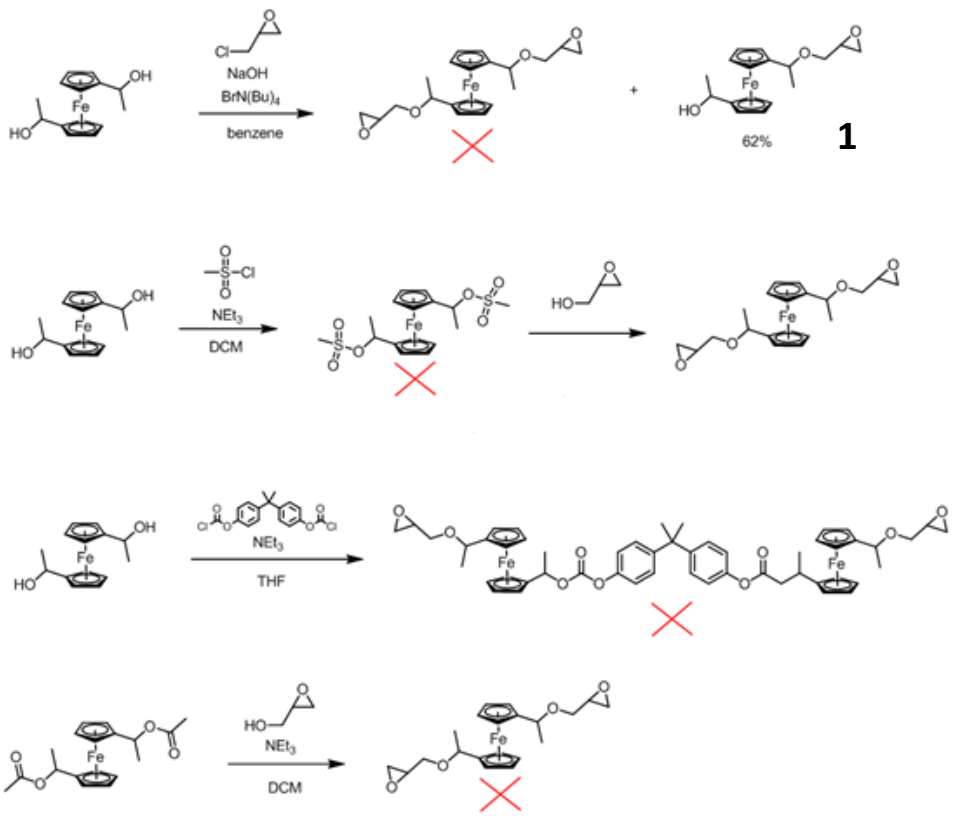

Figure 2-1. Attempted synthetic routes to diepoxide derivatives of ferrocene.

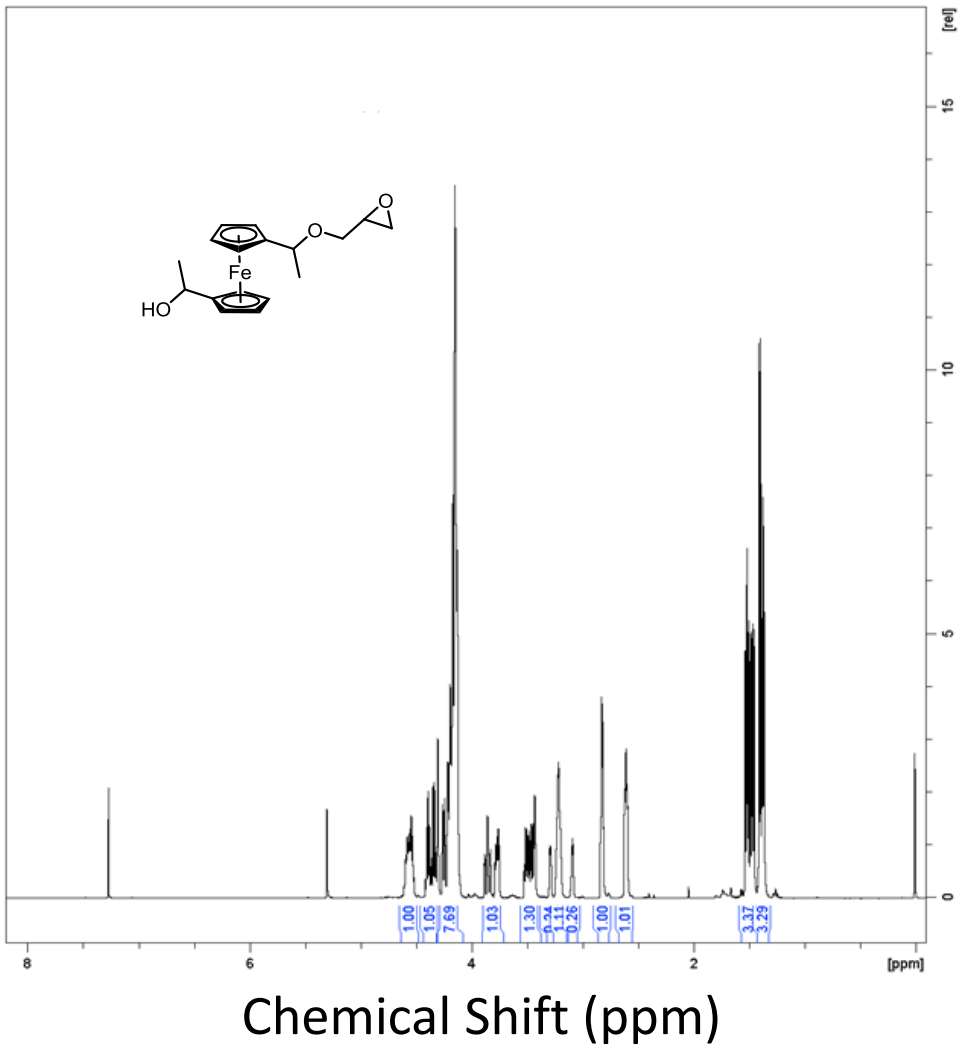

Figure 2-2. ^{1}H NMR spectrum of monoepoxide 1.

1-(1'-(1-(oxiran-2-ylmethoxy)ethyl)-[ferrocene]-1-yl)ethan-1-ol (1). A solution of 1,1'-ferrocenbis(ethan-1-ol) (2.0 g, 7.2 mmol) in benzene (20 mL) was prepared in a 100 mL round bottom flask. To the flask was added tetrabutylammonium bromide (0.28 g, 0.58 mmol) and an aqueous solution of NaOH (20 mL, 50% wt/wt). The biphasic mixture was then stirred at room temperature and epichlorohydrin was added dropwise via syringe. The reaction was stirred at room temperature for 16 hr, then warmed to 45 °C and stirred for 4 hr. The reaction mixture was then cooled to room temperature and poured into a separatory funnel. The aqueous layer was extracted with ethyl acetate (2 x 40 mL), and the combined organic fractions were washed with brine (1 x 50 mL). The organic layer was dried with $MgSO_4$, filtered, and concentrated under vacuum. The crude mixture was chromatographed on silica gel using 5:1 dichloromethane:ethyl acetate as eluent to afford the pure product as an orange/brown oil (1.46 g, 61%). ^{1}H NMR (500 MHz, $CDCl_3$): δ (ppm) 4.56 (1H, m), 4.36 (1H, m), 4.13-4.30 (8H, m), 3.75-3.88 (1H, m), 3.43-3.51 (1.25H, m), 3.30 (0.25H, m), 3.22

(1.25H, m), 3.09 (0.25H, m), 2.83 (1H, m), 2.61 (1H, m), 1.36-1.41 (3H, m), 1.46-1.54 (3H, m). HRMS-ASAP$^+$ (m/z) calculated for $C_{17}H_{22}FeO_3$: 330.0919, found: 330.0909.1511 (M^+).

Intramolecular reactions were consistently problematic in many different attempts to produce disubstituted ferrocenes. In theory it would always be best to design a synthetic route in which the monofunctional intermediate cannot be attacked by itself in an intramolecular fashion. This was attempted by introducing a leaving group onto the ferrocene substituents and reacting with glycidol; however, these attempts were unsuccessful (Figure 2-1).

2.2. Ferrocene Diamines

In light of our inability to produce a suitable diepoxide, we also pursued a diamine derivative of ferrocene. However, undesirable intramolecular reactions were also encountered in the diamine syntheses (Figure 2-3). This fact was, again, somewhat surprising, as there are numerous prior reports of synthetic routes to diamine derivatives of ferrocene that contain no mention of a propensity for intramolecular reaction.[26-33] For example, reductive amination, as described in detail below, led to an intramolecular cyclization affording the cyclized secondary amine **3** in moderate yield. The best result for a ferrocene diamine was obtained by treating an acetoxy derivative with ammonium hydroxide to obtain FcDA (**2**, see below for full synthetic details); however, intramolecular cyclization and polymerization still affords a product with relatively low purity (~ 85 – 92%). The reaction is somewhat heterogeneous due to the limited solubility of the acetoxy derivative in ammonium hydroxide, as well as the need for a large excess of ammonium hydroxide in order to avoid polymerization and cyclization. Additional purification of FcDA on silica gel was unsuccessful, as the material seemed to decompose (thin-layer chromatography showed low retention factor streaks even in polar solvents).

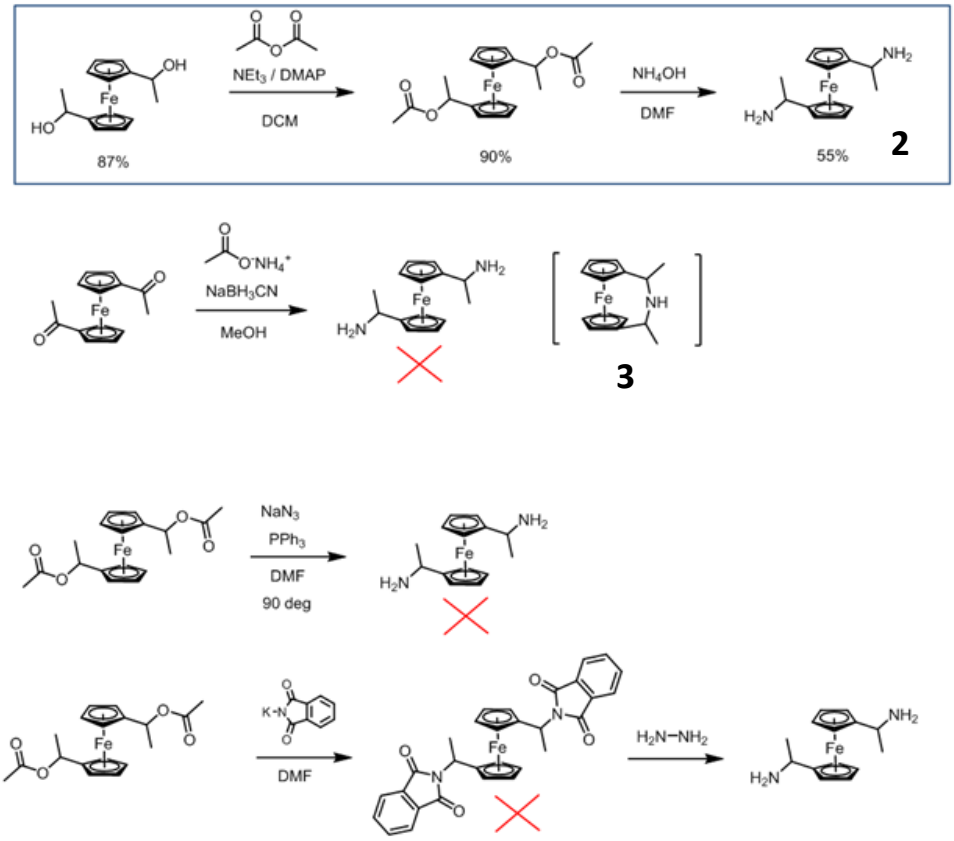

Figure 2-3. Attempted synthetic routes to diamine derivatives of ferrocene.

1,1'-(iminodiethylidene)-ferrocene (3). To a dry 2 L round bottom flask was added 1,1'-diacetylferrocene (75.0 g, 276 mmol), ammonium acetate (500 g, 6.5 mol), and anhydrous methanol (700 mL). The solution was warmed to 60 °C and sodium cyanoborohydride (50.0 g, 800 mmol) was added in portions over 10 min. After stirring at 60 °C for 48 hr the mixture was cooled to room temperature and slowly poured into saturated $NaHCO_3$ (aq, 800 mL). The aqueous layer was extracted with dichloromethane (3 x 300 mL) and the combined organic fractions were washed with saturated $NaHCO_3$ (aq, 1 x 200 mL). The organic layer was then dried with $MgSO_4$, filtered, and concentrated under vacuum. To this crude residue was added HCl (2M, 800 mL), and the mixture was allowed to stir for 1 hr. **[CAUTION! The addition of acid to residual cyanoborohydride forms highly poisonous hydrogen cyanide gas. This step should be done slowly in a fume hood and all subsequent waste should be handled properly.]** The dihydrochloride salt precipitated as a yellow powder and was collected on a Buchner funnel and washed with H_2O (200 mL). The dihydrochloride salt was then slowly added to a stirring solution of KOH (2M, 500 mL)**,** which led to the precipitation of the neutral amine product. The orange solid was collected on a Buchner funnel, washed with H_2O (400 mL) and dried under vacuum to afford the pure product as an orange powder (31.7 g, 42%).

1,1'-(ferrocene-1,1'-diyl)bis(ethan-1-acetoxy). To a dry 25 mL 3-neck round bottom flask was added ferrocenebis(ethan-1-ol) (3.0 g, 10.9 mmol) and 4-dimethylaminopyridine (13 mg, 0.11 mmol) under a flow of N_2. Anhydrous dichloromethane (60 mL) and triethylamine (3.2 mL) were added via syringe. The solution was stirred at room temperature and acetic acid (2.4 g, 23.0 mmol) was added dropwise via syringe over 30 min. The reaction was stirred at room temperature for 16 hr and then poured into a separatory funnel. The organic phase was washed with saturated $NaHCO_3$ (aq, 2 x 30 mL) and brine (1 x 30 mL), dried with $MgSO_4$, filtered and concentrated under vacuum to afford the pure product as a viscous oil (3.65 g, 93%, sometimes solidified over long periods of time). ^{1}H NMR (500 MHz, $CDCl_3$): δ (ppm) 5.8 (2H, m), 4.25 (2H, m), 4.19 (2H, m), 4.14 (4H, m), 2.05 (6H, s), 1.55 (6H, m).

1,1'-bis(α-aminoethyl)ferrocene (FcDA, 2). A solution of dimethylformamide (110 mL) and ammonium hydroxide (30-33% in H_2O) was prepared in a 1 L flask equipped with stir bar and addition funnel. The solution was warmed to 50 °C with stirring, and a solution of 1,1'-(ferrocene-1,1'-diyl)bis(ethan-1-acetoxy) (16.8 g, 46.9 mmol) in 200 mL dimethylformamide was added dropwise over a period of 1 hr. The reaction was stirred at 50 °C for an additional 2 hr, then cooled to room temperature and poured into a 2 L Erlenmeyer flask. The mixture was acidified to pH = 0 by addition of 50% HCl and then added to a separatory funnel. The aqueous layer was washed with dichloromethane (3 x 150 mL) and then poured into another 2 L Erlenmeyer flask and basified to pH = 13 by addition of solid NaOH. This mixture was returned to the separatory funnel and extracted with dichloromethane (3 x 200 mL). The combined organic fractions were then washed with H_2O (4 x 200 mL) and brine (1 x 200 mL). The organic phase was then dried with $MgSO_4$ and concentrated under vacuum to afford the crude product as a mixture of brown oil and orange precipitate. Some of the precipitate could be removed by addition of dichloromethane/hexanes (1:1) and filtration. Yield: 6.5 g, 51%. ^{1}H NMR (500 MHz, $CDCl_3$): δ (ppm) 4.10-4.17 (8H, m), 3.80 (2H, m), 1.64 (4H, br), 1.35 (6H, d, J = 7 Hz). ^{13}C NMR (500 MHz, $CDCl_3$): δ (ppm) 25.1, 46.0, 66.0, 67.8, 96.6. Elemental analysis: calculated for $C_{14}H_{20}FeN_2$: C, 61.78; H, 7.41; Fe, 20.52; N, 10.29. Found: C, 62.12; H, 7.23; Fe, 19.4; N, 9.35.

The best purity for **2** obtained using the above procedure was 90-92%, as assessed by solution ^{1}H and ^{13}C NMR spectroscopy (Figure 2-4 and Figure 2-5). Expected impurities include oligomers and cyclized compounds, including **3** (Figure 2-6 and Figure 2-7)**.** At the last step of the procedure, a precipitate can be removed from the crude mixture. Typically, the ^{1}H NMR spectra of the crude mixture, the isolated precipitate, and the filtrate are essentially identical. This suggests that the precipitate is a crystalline stereoisomer of the product. It may be possible to skip the precipitation/filtration step and use the crude oil/powder mixture without loss of performance. It is also worth noting that the ^{13}C NMR spectrum contains additional peaks than those listed in the characterization above, but the additional peaks are not distinguishable within the typically reported tenth decimal place. The extra peaks are likely due to stereoisomers. Fluxional dynamics between different configurations, most notably in the aminoethyl side chain, are observable in the low temperature solution 13C NMR shown in Figure 2-8. At −50 °C, there are multiple similar

resonances observed in FcDA that are not observed in the monoamine **3**. As the temperature increases there is dynamic interchange between these different configurations in FcDA. These dynamics lead to a single, motionally-averaged ^{13}C NMR resonance for that carbon environment. This motional averaging is not seen in **3** since the bridging amine prevents any fluxional motion of the Cp ring.

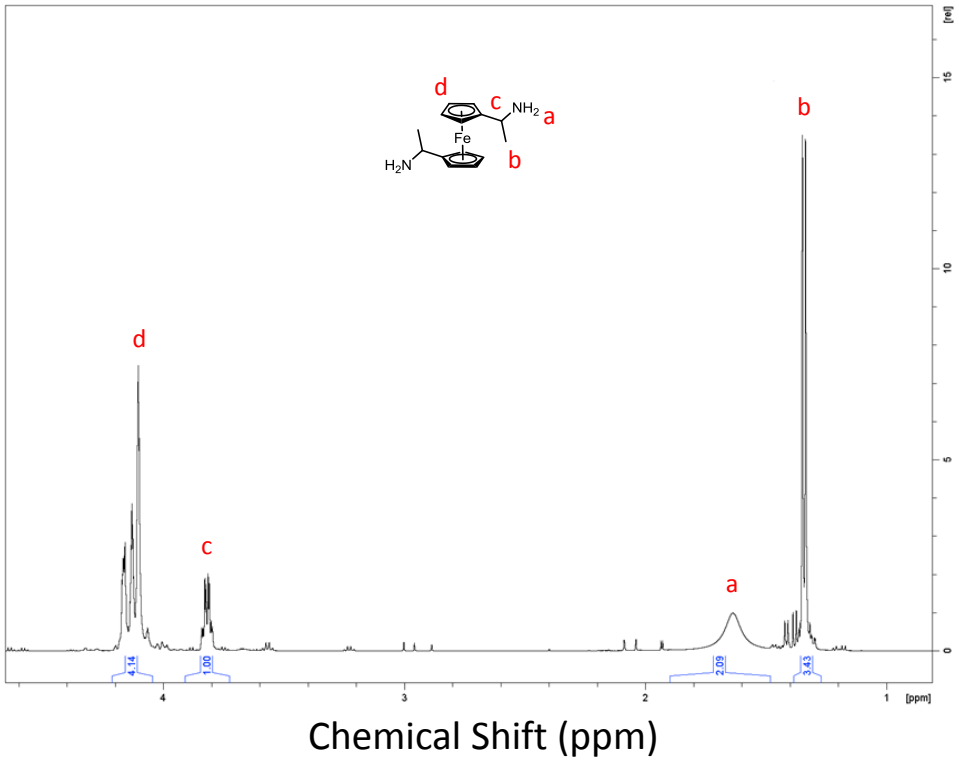

Figure 2-4. ^{1}H NMR spectrum of FcDA (2).

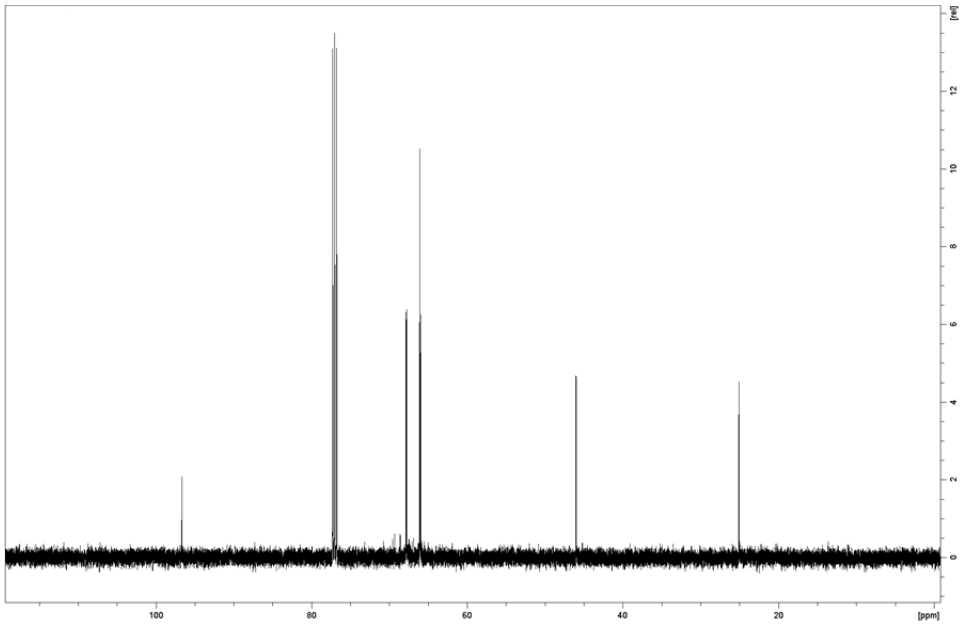

Figure 2-5. ^{13}C NMR spectrum of FcDA (2).

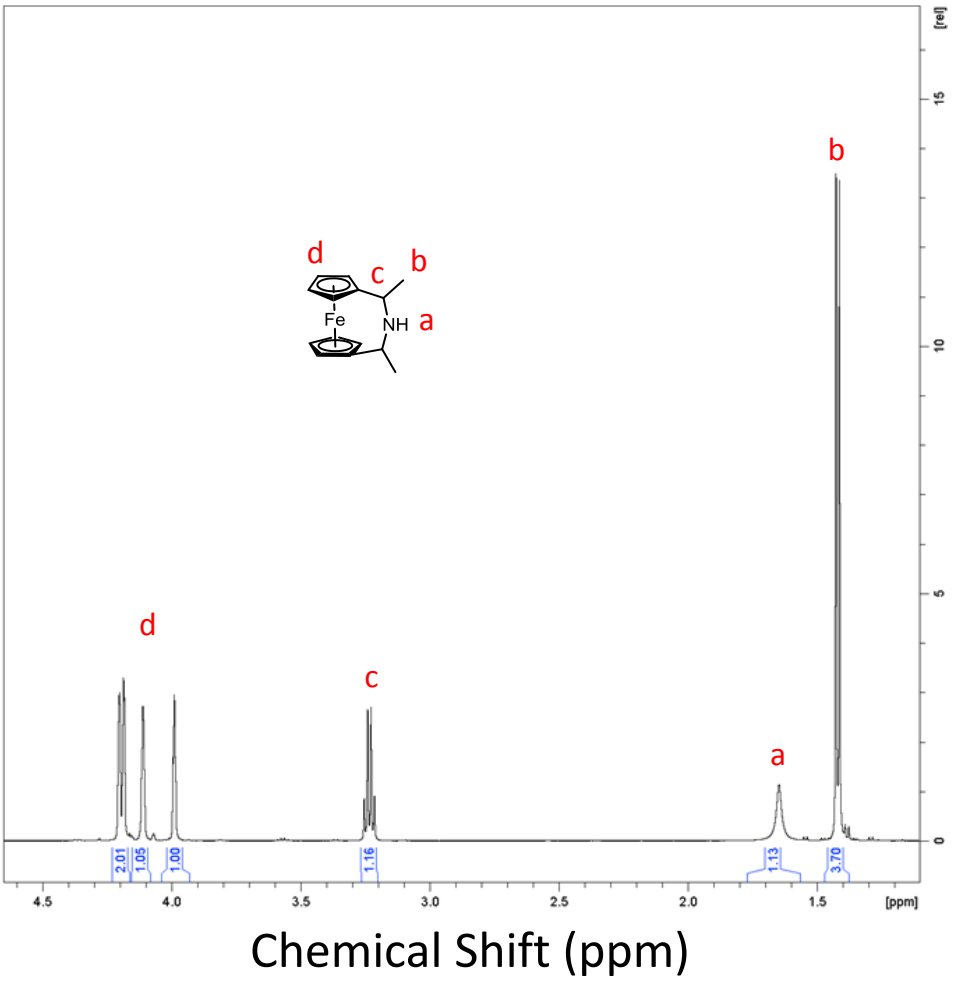

Figure 2-6. ^{1}H NMR spectrum of cyclic monoamine 3.

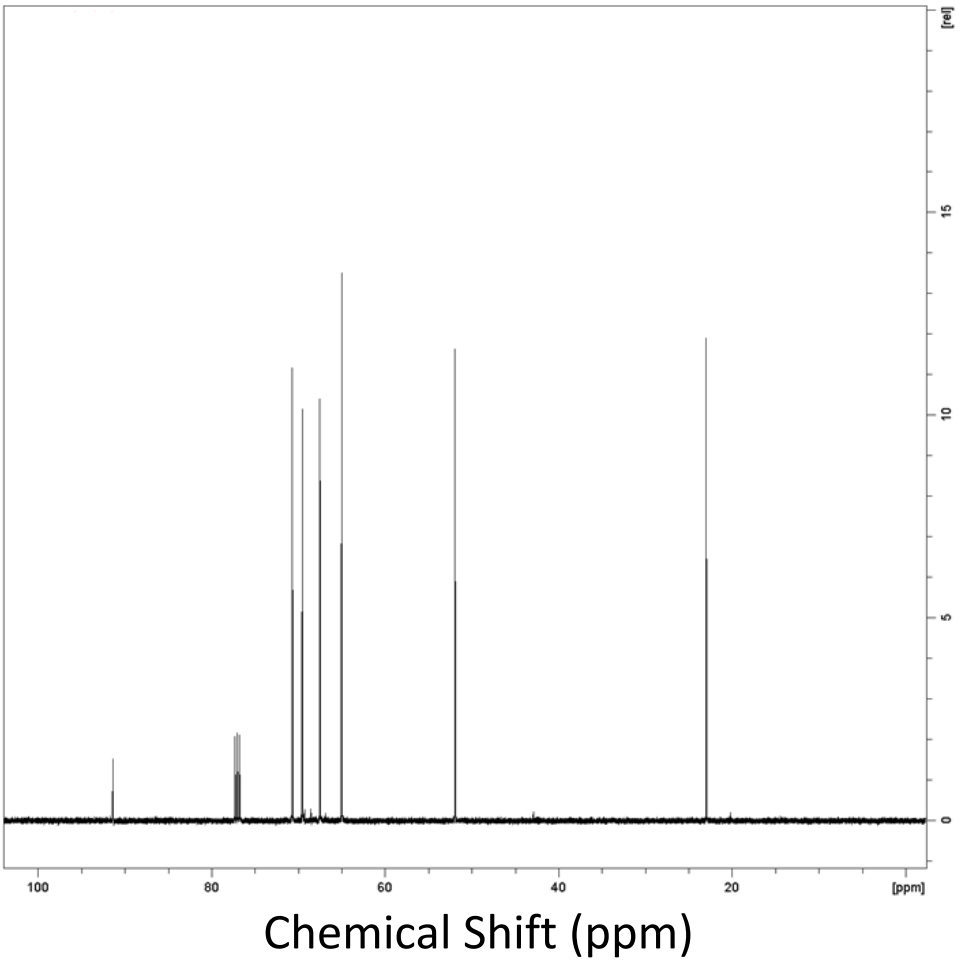

Figure 2-7. ^{13}C NMR spectrum of cyclic monoamine 3.

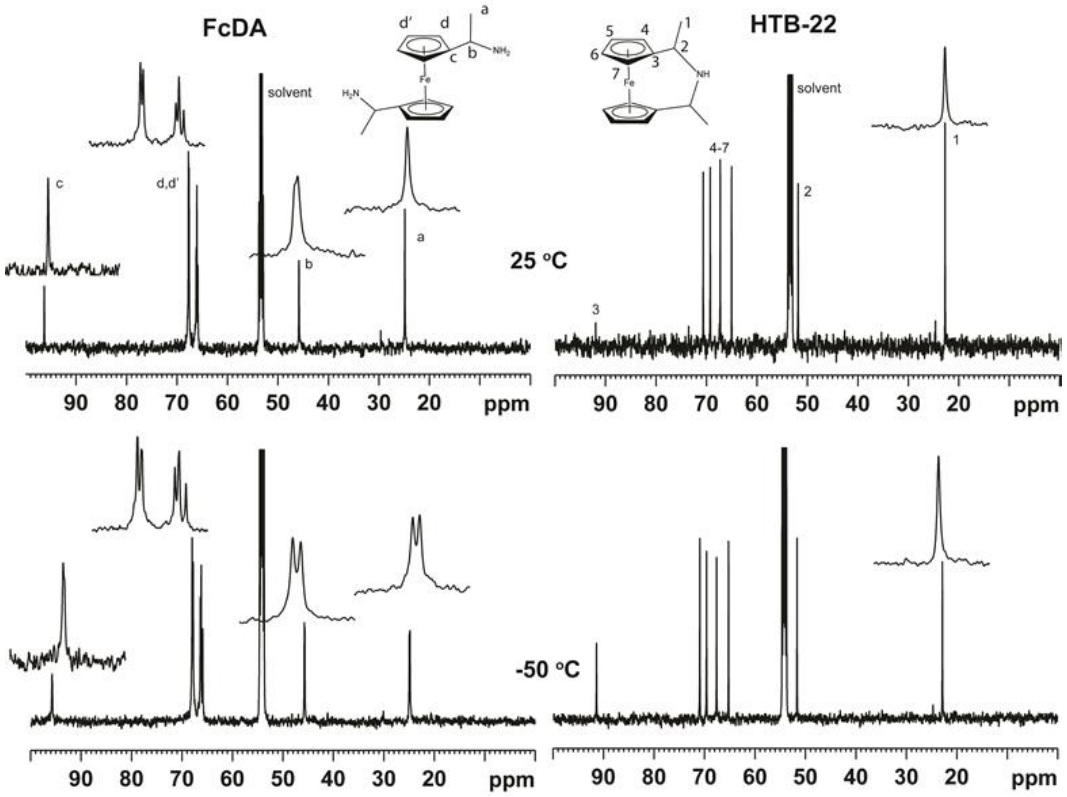

Figure 2-8. Variable temperature solution ^{13}C NMR of FcDA compared to cyclic monoamine 3.

2.3. Ferrocene Diacrylates

We also briefly attempted to synthesize a diacrylate derivative of ferrocene. In theory, such a compound could be polymerized into a thermoset material with a small amount of free radical initiator. Radical-based systems are chain-growth polymerizations, yielding substantially different network structures than step-growth polymerizations (*e.g.*, epoxy-amine systems), with significant implications for residual stress and stress relaxation among other important characteristics. Hence, a ferrocene diacrylate would provide an ideal thermoset system by which to compare the ferrocene-based material described in Chapter 3.

The synthetic procedure described below gave a seemingly pure product after simple work-up, isolated as a relatively low viscosity oil. After several days, the product became more viscous and exhibits behavior suggesting of premature polymerization, although the NMR spectrum (Figure 2-8) remains similar to that of the initial product. This issue may potentially be circumvented through the addition of a radical scavenger or by conducting the synthesis in stabilized tetrahydrofuran to incorporate residual inhibitor into the product. Such modifications have not yet been attempted.

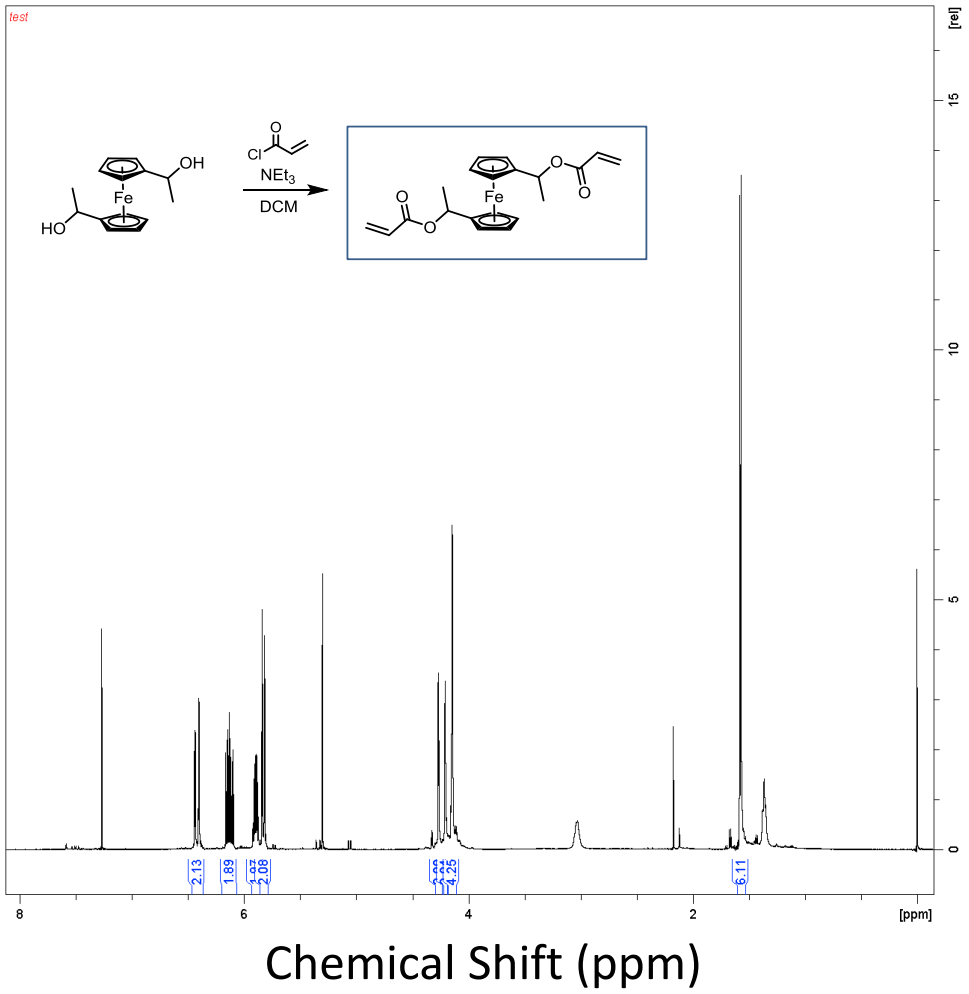

Figure 2-9. Chemical structure and ^{1}H NMR spectrum of 1,1'-ferrocenebis(ethane-1,1-diyl) diacrylate.

1,1'-ferrocenebis(ethane-1,1-diyl) diacrylate. To a dry 250 mL 3-neck round bottom flask was added 1,1'-ferrocenbis(ethan-1-ol) (3.0 g, 10.9 mmol) under a flow of N_2. Anhydrous dichloromethane (75 mL) and anhydrous triethyl amine (12 mL) were then added via syringe and the solution was cooled to 0 °C. Acryloyl chloride (3.56 mL, 43.8 mmol) was added dropwise via syringe and the reaction was slowly warmed to room temperature and stirred for 16 hr. The mixture was filtered and then washed in a separatory funnel with 0.5 M KOH (aq, 2 x 100 mL) and brine (2 x 100 mL). The organic layer was then dried with $MgSO_4$ and concentrated to afford the product as a viscous orange/brown oil (3.35 g, 80%). ^{1}H NMR (500 MHz, $CDCl_3$): δ (ppm) 6.41-6.49 (2H, ddd, *J* = 17.5, 2.5, 1.5 Hz), 6.10-6.17 (2H, dq, *J* = 17.5, 5.5 Hz), 5.89-5.91 (2H, m), 10.5, 1.5 Hz), 4.27 (2H, m), 4.22 (2H, m), 4.15 (4H, m), 1.58 (6H, d, *J* = 10.5 Hz).

3. STRESS RELAXATION IN EPOXY THERMOSETS *VIA* A FERROCENE-BASED AMINE CURING AGENT

From the synthetic work described in Chapter 2, FcDA emerged as the only reactive, disubstituted ferrocene derivative that we could reliable produce at a purity and scale suitable for further study. Therefore, we chose to investigate its behavior as a curing agent for a commercial DGEBA resin and to compare it to a series of conventional diamine curing agents (Figure 3-1) with a specific emphasis on residual cure stress and stress relaxation. The information presented herein provides a comprehensive illustration of the similarities and differences between our unique, ferrocene-based thermoset and more traditional materials.

3.1. Background

First, it is important to frame this work in the context of other historical approaches to stress reduction in highly crosslinked polymers. Early efforts to reduce and eliminate cure stress in thermosets involved copolymerization of traditional monomers with ring-opening compounds, such as spiro ortho-esters.[34-38] Ring-opening reactions of the corresponding moieties within the polymer network were then used to offset cure shrinkage. More recently, a significantly more robust approach has been widely investigated, based on reversible crosslinks.[39-64] The presence of dynamic, covalent bonds in crosslinked polymers – so-called CANs – enables terminal-like viscoelastic behavior, as molecular rearrangement can be accommodated through the transient characteristics of these bonds. Such materials are able to fully relax stress at elevated temperature and can be self-healed, welded, or otherwise reprocessed, yet they exhibit many of the desirable chemical and mechanical traits of traditional thermosets, provided that the concentration of transient species is appropriately controlled. This extraordinary behavior has been demonstrated across a diverse set of lightly to highly crosslinked polymers, including thiol-enes,[40,41] thiol-ynes,[43] poly(acrylate)s,[44,46,51] epoxies,[45,47,50,53,54] poly(diene)s,[49,61,64] poly(lactide)s,[55] poly(urethane)s and related materials,[42,56,57,60] poly(triazole)s,[58] and even deoxyribonucleic acid-based networks.[59] The covalent adaptable functionalities of these materials exploit addition-fragmentation chain transfer,[40,41,43,44,46,51] transesterification,[45,47,50,54,55,61] Diels-Alder,[39,64] oxetane ring-opening,[42] metathesis,[49] disulfide-disulfide,[56] thiol-disulfide,[53] transcarbamoylation,[57] transamination,[60] or transalkylation[58] reactions. CANs are further distinguished by whether these reactions preserve the crosslink density of the network (commonly referred to as vitrimers), which has important implications for its rheological properties.

Although the terminal-like viscoelastic behavior exhibited by CANs imparts several advantageous characteristics atypical of thermoset materials (*e.g.*, self-healing), a critical implication is that CANs flow at long times and/or elevated temperature. This fact will render CANs wholly unsuitable for many traditional applications of thermosets, particularly those requiring consistent performance over long lifetimes, as is typically the case for NWs. Through our approach, stress relaxation can be significantly enhanced in a highly crosslinked polymer containing only permanent crosslinks, i.e., devoid of the transient bonds that lead to terminal behavior.

A large number of polymers have been synthesized containing ferrocene and other organometallic sandwich moieties incorporated along the polymer backbone, as highlighted in several reviews.[65-67] Kulbaba, *et al.*, prepared linear poly(ferrocenylsilane)s with selective deuterium labeling of the Cp ligands and used ^{2}H NMR spectroscopy to show that rapid Cp rotation, or torsional flexing, occurs above T_g.[68-70] In light of this fact, we were encouraged that Cp rotation could be exploited in crosslinked ferrocene-containing materials above T_g. Although the topological constraints imposed by permanent crosslinks impede large-scale segmental motion (*i.e.*, reptation), stress can still be relaxed via diffusion of network defects (*e.g.*, chain ends).

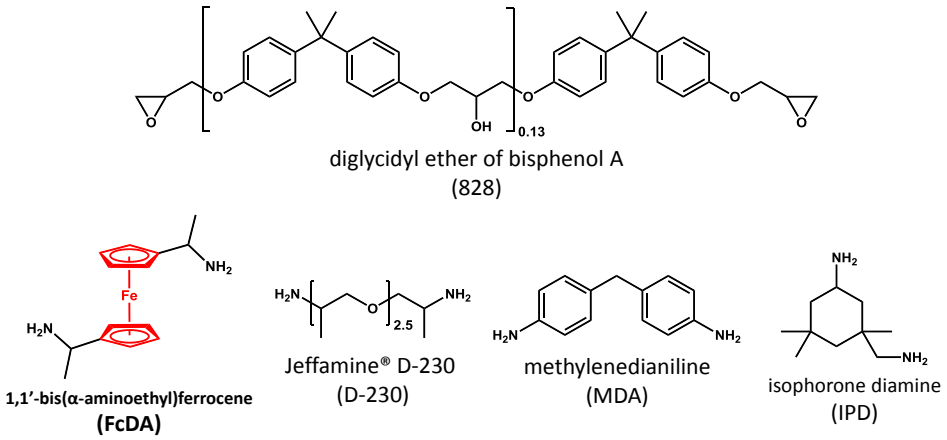

Figure 3-1. Epoxy resin and curing agents studied in this work.

3.2. Experimental Methods

3.2.1. Materials

EPON 828, a DGEBA of number-average molecular weight 377 g/mol, was obtained from Momentive Performance Materials (Waterford, NY). D-230, a polyether diamine of number-average molecular weight 230 g/mol, was obtained from Huntsman Corporation (The Woodlands, TX). MDA and IPD were obtained from Sigma-Aldrich (Saint Louis, MO). The epoxy resin and curing agents were used without further purification. FcDA was synthesized as described in Section 2.2.

3.2.2. Thermoset Preparation

Thermosets were prepared by blending 828 resin and the desired curing agent such that the epoxy and amine reactive, functional groups were present in equimolar amounts, based on the theoretical molecular weight of the constituents. This condition corresponds to mass compositions (*i.e.*, g curing agent/g 828) of 0.305, 0.263, 0.226, and 0.361 for D-230, MDA, IPD, and FcDA, respectively. For D-230, IPD, and FcDA, a stoichiometrically-balanced amount of 828 and curing agent was mixed by hand at room temperature. For MDA, mixing was performed at 100 °C. To prepare

fully cured specimens using D-230 and FcDA, the mixtures were cured overnight at room temperature, followed by a 2 hr post-cure at 120 °C or 140 °C, respectively. Using IPD, the mixture was cured overnight at 80 °C, followed by a 1 hr post-cure at 180 °C. Using MDA, the mixture was cured overnight at 100 °C, followed by a 1 hr post-cure at 200 °C. The post-cure temperatures were selected to be *ca.* 20-25 °C above $T_{g\infty}$ (Table 3-1) of the fully cured materials.

Table 3-1. Key properties of 828 cured with diamine curing agents under isothermal conditions.

Curing Agent	FcDA			D-230			MDA			IPD		
$T_{g\infty}$ (°C)[a]	113			90			180			155		
T_{cure} (°C)[b]	**70**	**90**	**110**	**50**	**70**	**90**	**90**	**110**	**130**	**70**	**90**	**110**
α_f[c]	0.89	0.94	0.95	0.88	0.96	0.99	0.88	0.92	0.97	0.83	0.89	0.96
ν_e (mol/kg)[d]	1.9	2.4	2.5	1.7	2.6	2.9	1.7	2.2	2.8	1.3	1.9	2.7
t_{gel} (hr)[e]	0.75	0.31	0.14	4.0	1.3	0.45	0.79	0.38	0.20	0.51	0.25	0.10
ε_V (%)[f]	0.85	1.2	1.8	0.49	1.5	2.1	1.0	1.2	1.7	0.91	1.5	1.8
G_f' (MPa)[g]	680	130	15	530	400	12	560	530	320	580	530	470

[a] Ultimate glass transition temperature at full cure
[b] Isothermal cure temperature
[c] Final epoxy conversion
[d] Calculated concentration of elastically effective strands at final conversion
[e] Gel time
[f] Volumetric shrinkage from gelation to final conversion
[g] Dynamic shear modulus at final conversion

3.2.3. FTIR Spectroscopy

Near-IR spectroscopy was performed using a custom temperature-controlled vial holder transmission accessory with a Bruker Equinox 55 FTIR spectrometer for isothermal cure monitoring studies. A mixture of 828 and curing agent was dispensed into a 2.2 mm diameter vial and placed in the transmission accessory at a pre-set temperature. IR spectra were acquired sequentially by averaging eight scans (~13.7 seconds) between 8000-4000 cm^{-1} at 4 cm^{-1} resolution. Spectra were normalized to the peak height at 6060 cm^{-1} (C−H stretch overtone) to correct for physical NIR scattering effects. Epoxy consumption was quantified by determining the integrated area of the 4528 cm^{-1} band (combination band of epoxy ring stretch overtone and fundamental C−H stretch) from minima to minima between 4560-4497 cm^{-1}. Epoxy conversion was computed by normalizing the 4528 cm^{-1} band area relative to an initial spectrum and a spectrum of material fully cured above $T_{g\infty}$.

3.2.4. DSC

DSC was performed using a TA Instruments (New Castle, DE) Q200 calorimeter. Analyzed samples comprised 5-15 mg material loaded in an aluminum pan. Analyses were performed under 10 mL/min nitrogen flow.

3.2.5. TGA

TGA was performed using a TA Instruments Q500 analyzer. Analyzed samples comprised 5-15 mg material loaded in a platinum pan. Analyses were performed under 90 mL/min nitrogen flow.

3.2.6. DMA

DMA was performed using a TA Instruments ARES AR-G2 rheometer. Fully cured rectangular specimens of approximate dimensions 3.5 cm length × 1.3 cm width × 0.2 cm thickness were prepared using a silicone mold. The temperature dependence of G' and G'' were measured in torsion at 1 Hz frequency and 5 °C/min ramp rate. The maximum strain amplitude was 1% and was automatically reduced to maintain torque values within transducer limits. T_g values for the fully cured materials (Table 3-1) were taken as the temperature at which the loss tangent (G''/G') achieved its maximum value. In addition, the time dependence of the dynamic shear moduli was also measured during cure. In such cases, a parallel plate fixture was used with 8 mm diameter disposable aluminum plates and a 2 mm gap. The desired mixture of 828 and curing agent was loaded into the gap and the temperature was raised to the desired cure temperature. The dynamic shear moduli were measured under 1 Hz frequency and 0.1% initial strain amplitude. Due to the substantial change in G' and G'' during cure, the strain amplitude was automatically reduced during the test to maintain torque values within transducer limits. Similarly, to accommodate the shrinkage that occurs during cure, the gap was automatically reduced during the test to maintain negligible axial force on the transducer.

3.2.7. Stress Relaxation

Stress relaxation tests were performed using two different deformation modes. Uniaxial tension was applied under flowing nitrogen using a TA Instruments Q800 dynamic mechanical analyzer. Torsional deformation was applied under flowing air using an ARES AR-G2 rheometer. For these tests, the same rectangular specimens described above were used. For both deformation modes, specimens were loaded into the test fixture and equilibrated for 30 min at the desired temperature, after which the desired strain step was applied. The corresponding tensile or shear moduli were monitored isothermally as a function of time.

3.2.8. Cure Stress

The stress build-up during cure of the thermosets was evaluated using a custom-built fixture (Figure 3-2). The fixture consisted of a fixed aluminum base plate and a movable aluminum upper plate. An Interface (Scottsdale, AZ) SSM-FDH, sealed, S-type, high-temperature load cell was affixed to the movable plate, and a 0.25 in diameter brass pin with a flat end was affixed to the load cell. A wide brass screw with a flat surface was attached to the base plate. Both surfaces of the upper pin and base screw were coarsely sanded prior to each test to ensure good adhesion. The gap between the upper pin and the base screw was set to 1 mm and the desired mixture of 828 and curing agent was loaded into the gap. The fixture was then heated to the desired cure temperature and the force exerted on the load cell was monitored over

time. An effective stress is reported as this force divided by the cross-sectional area of the upper pin. All reported stress build-up curves are an average of three duplicate measurements.

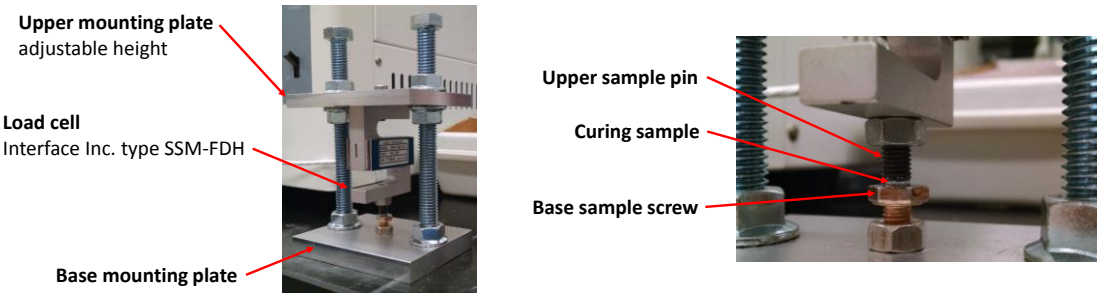

Figure 3-2. Fixture used to evaluate stress build-up during thermoset cure.

3.2.9. Mechanical Properties

The tensile and compressive properties of fully cured specimens were evaluated at room temperature using an Instron (Norwood, MA) 5900 Series Universal Testing Machine. For tensile tests, dog-bone specimens were fabricated according to ASTM standard D638 (Type V specimen dimensions) using a silicone mold. Uniaxial tension was applied with a crosshead speed of 1 mm/min. The strain was measured *via* an extensometer attached to the gage length of the specimen. Tensile properties are reported as an average of six specimens. For compression tests, cube specimens of approximate size 0.25 in were cut from rectangular bars prepared using a silicone mold. Uniaxial compression was applied using a sub-press and a crosshead speed of 0.5 mm/min. The strain was measured *via* an extensometer attached to the compression platens of the sub-press. Compressive properties are reported as an average of a minimum of ten specimens.

3.3. Results and Discussion

The kinetics of the curing reaction of 828 with the curing agents listed in Figure 3-1 were evaluated by FTIR spectroscopy. Figure 3-3 compares the conversion of epoxy functional groups over time during isothermal cure with FcDA or D-230 as curing agent at 70 °C, 90 °C, and 110 °C. The conversion values were obtained by monitoring the decrease in the characteristic absorbance at ~ 4528 cm^{-1} (Figure 3-4), commonly assigned as a combination band involving epoxy ring stretching.[71] From Figure 3-3, it is apparent that FcDA and D-230 give similar cure kinetics, which is unsurprising considering that both compounds possess identical α-aminoethyl functionalities (Figure 3-1). The conversion profiles are typical of thermally-activated, autocatalytic epoxy-amine reactions, with rate constants exhibiting Arrhenius temperature dependence. In particular, the measured E_a for 828 cured with FcDA is 56 kJ/mol, in reasonable agreement with typical reactions of epoxies and aliphatic amines (Figure 3-5).[72] The FTIR spectra indicated approximately 5% residual epoxy upon

complete consumption of the primary and secondary amine of FcDA (Figure 3-4). We attribute this discrepancy to non-reactive impurities in the FcDA. It is important to note, however, that increasing the FcDA content in the reactive mixture above the theoretical value for stoichiometric balance, in order to compensate for this discrepancy, produced a negligible effect on the glass transition (Figure 3-6). The final conversion of epoxy groups is listed in Table 3-1 at several cure temperatures for each curing agent. Using the method described by Charlesworth,[73] we have estimated the final concentration of elastically effective strands in the network at each cure temperature, also listed in Table 3-1. Despite 5% residual epoxy, the FcDA system reaches crosslink densities comparable to the conventional systems at the cure temperatures studied. Therefore, we believe the data presented hereafter are representative of a high crosslink density for this particular combination of resin and curing agent.

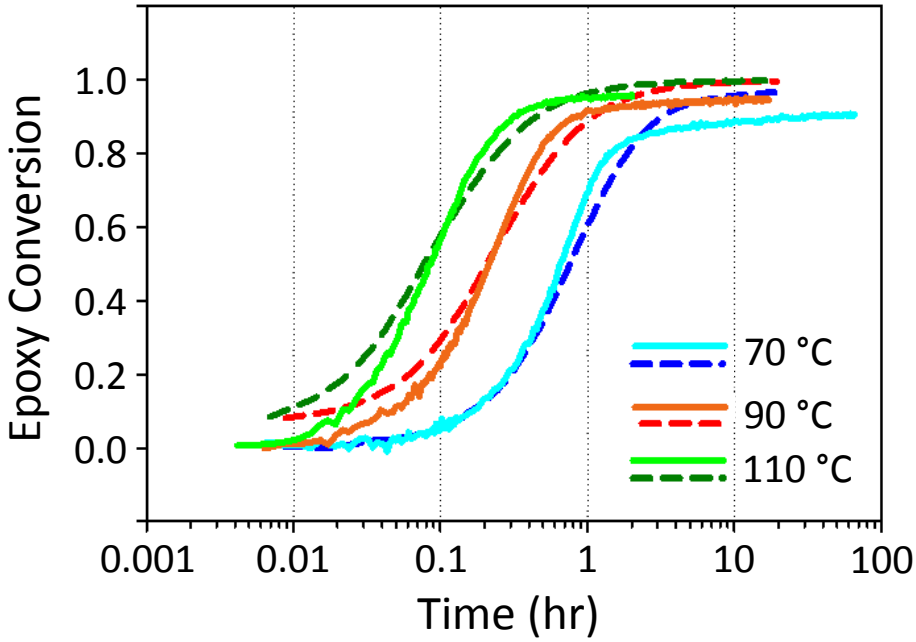

Figure 3-3. Isothermal cure kinetics of 828 cured with FcDA (solid) and D-230 (dotted), as assessed by FTIR spectroscopy.

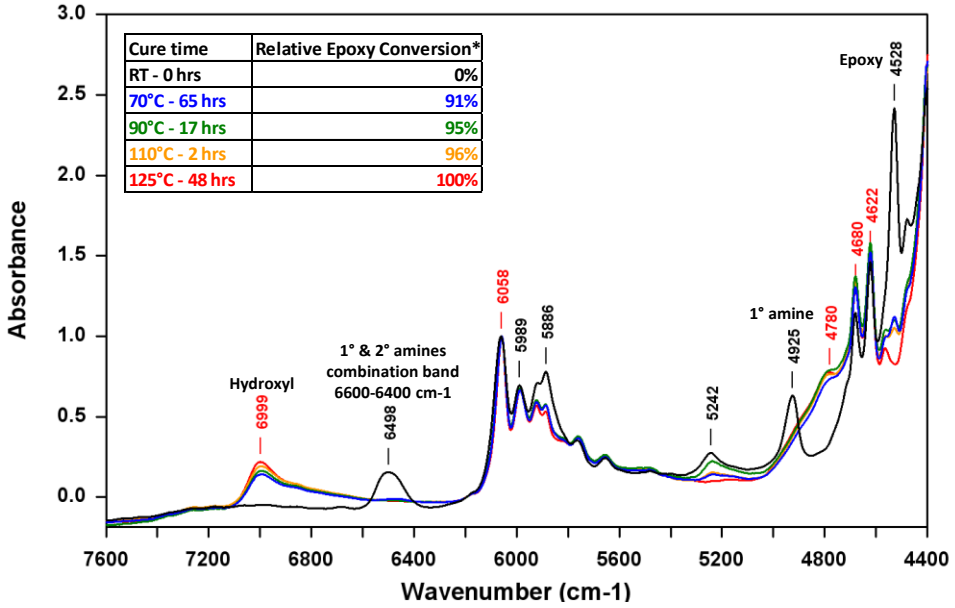

Figure 3-4. FTIR spectra of 828 cured with FcDA.

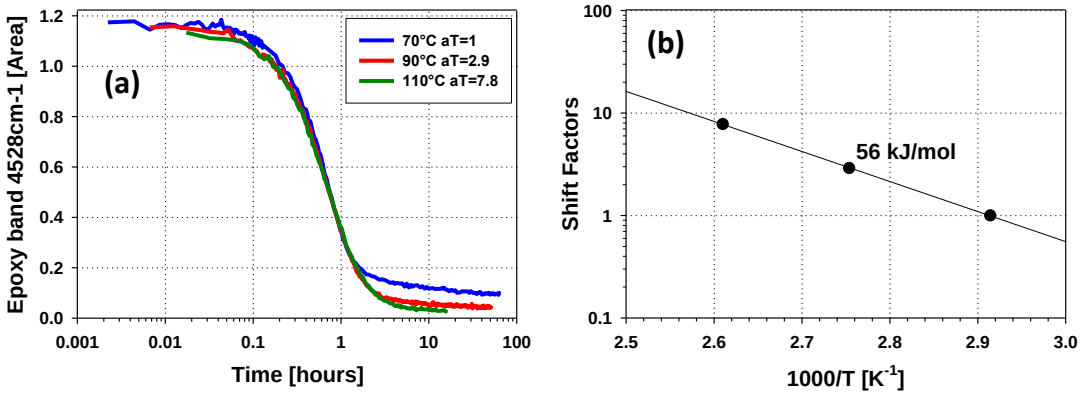

Figure 3-5. (a) Epoxy FTIR band area over time during isothermal cure of 828 with FcDA with horizontal shift factors applied. (b) Corresponding temperature dependence of the shift factors.

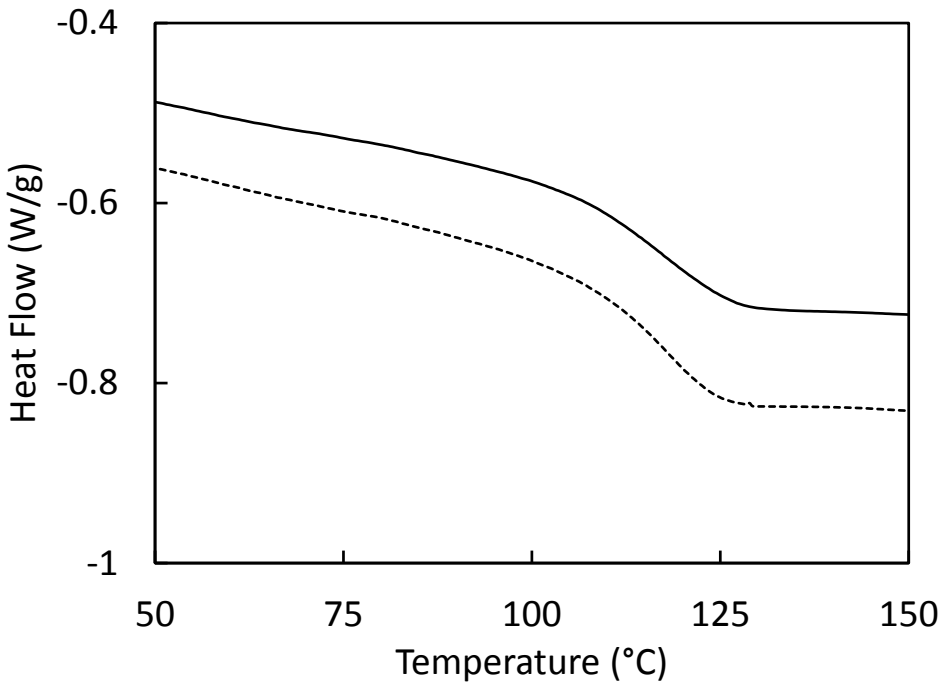

Figure 3-6. DSC heating traces (20 °C/min ramp rate) of 828 fully cured with FcDA at (solid) 0.361 g FcDA/1 g 828 and (dotted) 0.381 g FcDA/1 g 828.

Similarly, the dynamic shear moduli G' and G'' of 828 cured with FcDA evolve during cure in a manner consistent with step-growth thermoset polymerizations. As shown in Figure 3-7, gelation is characterized by a sudden increase in G', indicating the formation of an effectively infinite network with significant elastic character. The gel times measured by this method are provided in Table 3-1. The time to reach the gel point for 828 cured with FcDA at 70 °C is approximately 0.75 hr; by comparison with the conversion kinetics (Figure 3-3), we observe that the conversion at the gel point is approximately 0.56. This value is consistent with the theoretical value of 0.58 for a difunctional resin reacted with a stoichiometric equivalence of tetrafunctional curing agent.[74] For the cure temperatures used in Figure 3-7, cure is effectively arrested by vitrification of the sample, as $T_{g\infty}$ (Table 3-1) is greater than the cure temperature. At 70 °C, the material vitrifies deeply during cure, with G' reaching several hundred MPa and a well-defined maximum evident in G''. At 110 °C, G' increases gradually at long times, reaching only ~ 10 MPa after 4 hr, while G″ exhibits no well-defined maximum, suggestive of a material straddling the glassy and rubbery regimes. Table 3-1 further lists the final value of G' at each cure temperature and curing agent studied. All systems in Table 3-1, cured below their $T_{g\infty}$, show a monotonic decrease in modulus with increasing temperature. This behavior is consistent with shallower vitrification at higher cure temperatures, with the specific final value of G' attained being dictated by the proximity of the cure temperature to $T_{g\infty}$.

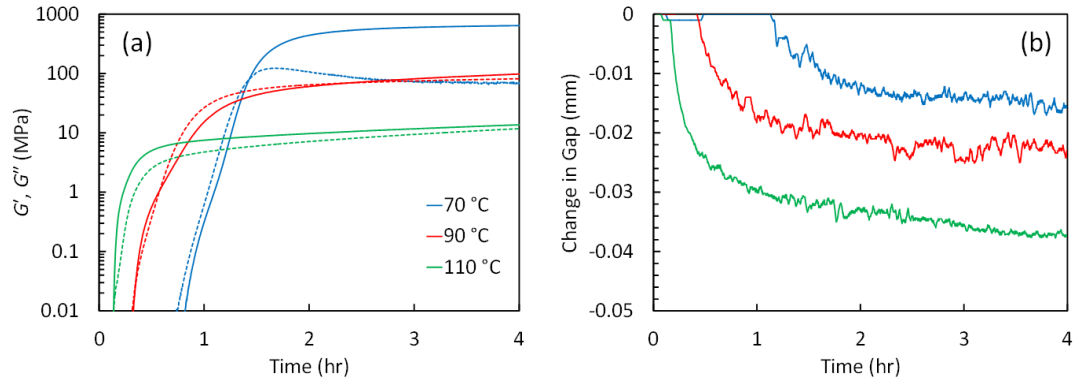

Figure 3-7. (a) *G′* (solid) and *G″* (dotted) measured during isothermal cure of 828 with FcDA. (b) Corresponding change in gap required to maintain zero axial force during cure.

The measurement of dynamic shear moduli during cure additionally provides the opportunity to evaluate the cure shrinkage of these materials. After gelation, cure shrinkage while confined between parallel plates is manifested by a build-up of stress in the material, which can be observed *via* the axial force exerted on the test fixture. If the gap is continually adjusted so as to accommodate cure shrinkage and maintain the material in a stress-free state (*i.e.*, zero axial force), then shrinkage can be evaluated from a measurement of the gap (h). This approach has been previously employed for epoxy thermosets, where a linear correlation between shrinkage and conversion was observed.[75-77] Figure 3-7b shows the corresponding change in gap for 828 cured with FcDA. The ultimate change in gap at the end of cure is used to calculate the volumetric shrinkage according to $\varepsilon_V = [1 + \Delta h/3h_0]^3 - 1$. It is important to note that this approach yields only the shrinkage from gelation to final conversion, not the total shrinkage over the entire duration of cure. The volumetric shrinkage for each system is listed in Table 3-1. Unsurprisingly, the measured cure shrinkage increases with increasing cure temperature, consistent with the greater extents of conversion reached at higher temperatures.

We further sought to characterize stress build-up during isothermal cure of 828 with FcDA and to compare FcDA to the traditional curing agents in this regard. Initially, we attempted to modify the above-mentioned approach, monitoring the evolution of axial force while maintaining a constant gap. However, we discovered that the axial force frequently exceeded the transducer limit for our instrument, even despite the small diameter (8 mm) of the plates. Consequently, we developed a simple, custom fixture designed to perform an analogous measurement. This fixture, inspired by a number of similar fixtures used to evaluate cure stress in UV-cured thermosets,[78-83] effectively consists of a parallel plate geometry in which a high-temperature load cell provides the same axial force measurement (Figure 3-2).

In Figure 3-8, we examine a series of stress build-up curves for isothermal cure of 828 with FcDA, D-230, MDA, or IPD. The particular curves shown correspond to the cure temperatures listed in Table 3-1, which were selected because they constitute the highest temperatures at which the measurement fixture could equilibrate to within 2

°C of its ultimate temperature prior to gelation of the sample (Figure 3-9). As with the measurement of dynamic shear moduli, gelation in these measurements is clearly evident from the onset of stress build-up. By comparison of Figure 3-7 and Figure 3-8, we see that the time to reach the gel point for 828 cured with FcDA is relatively consistent across both measurements. The slightly longer gel times observed in the stress build-up curves reflect the comparatively slow thermal equilibration of the test fixture.

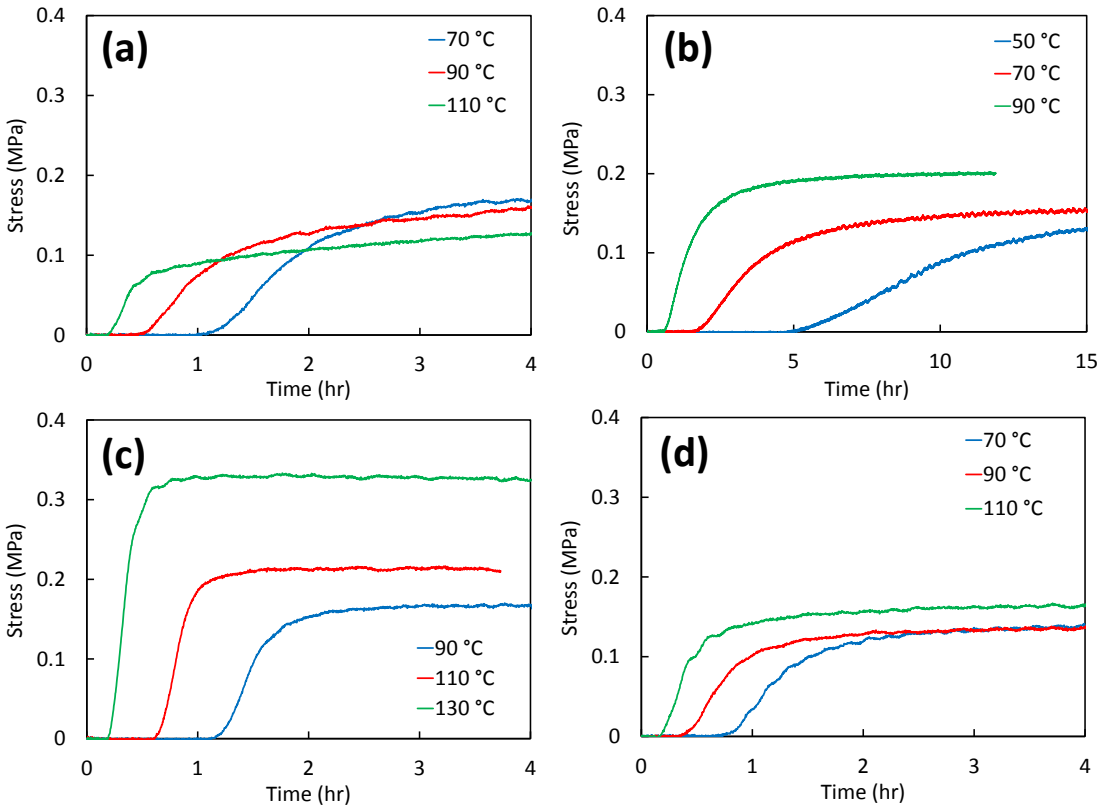

Figure 3-8. Stress build-up during isothermal cure of 828 with (a) FcDA, (b) D-230, (c) MDA, and (d) IPD.

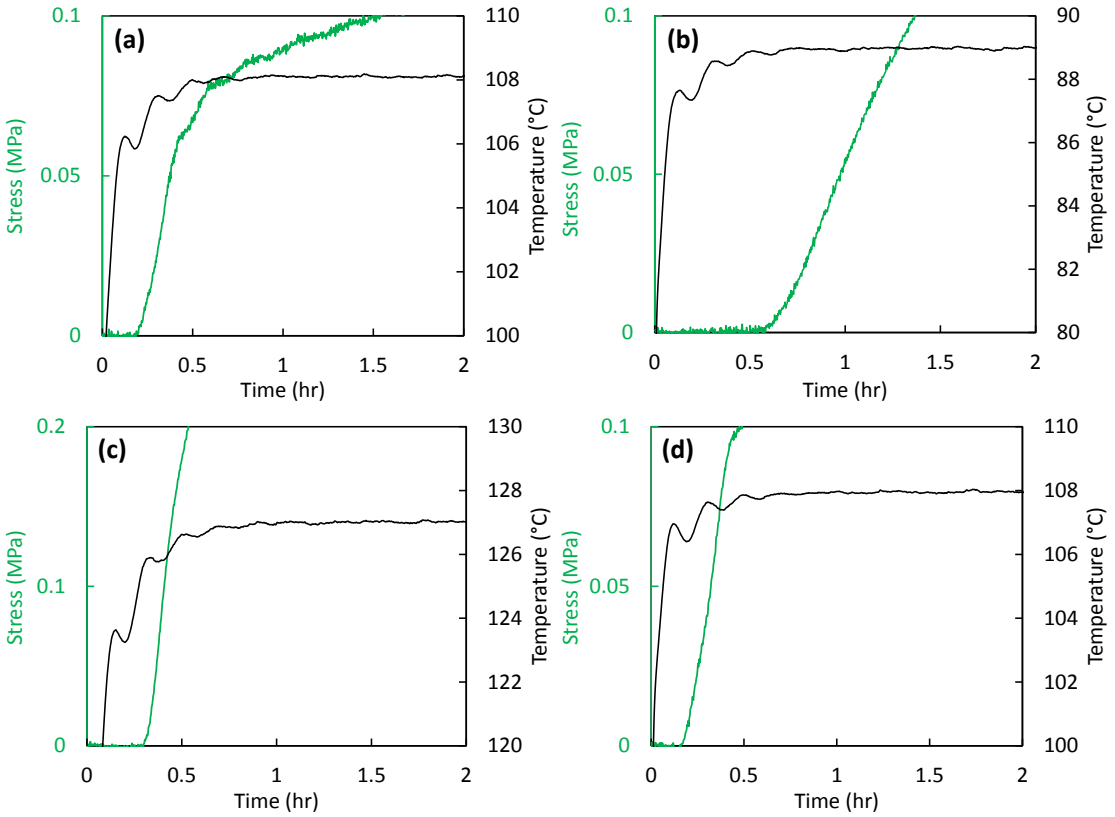

Figure 3-9. Thermal equilibration of cure stress fixture during measurement of stress build-up of 828 cured with (a) FcDA, (b) D-230, (c) MDA, and (d) IPD.

From the simplest perspective, the stress build-up after gelation will be dictated by the shrinkage, as well as the corresponding modulus evolution. Shrinkage stems from the conversion of functional groups and the consequent substitution of van der Waal's interactions by covalent bonds. As Table 3-1 indicates, all four systems shown in Figure 3-8 experience similar shrinkage from gel to final conversion at the cure temperatures studied. To reiterate, these cure temperatures are at or below $T_{g\infty}$. In this regime, the stress build-up of 828 cured with the traditional curing agents (D-230, MDA, or IPD) exhibits a distinct trend towards higher values at higher cure temperatures. We believe this is primarily driven by shrinkage, as we have noted that functional group conversion, hence shrinkage, can progress to greater extents before cure is effectively arrested by vitrification. Indeed, similar observations have been made in previous work.[84] On the other hand, the stress build-up of 828 cured with FcDA shows the *opposite* trend, wherein higher cure temperatures result in *lower* stress values. For example, the stress after 4 hr of cure is ~ 25% lower when cured at 110 °C versus 70 °C. As a result, the overall stress build-up of 828 cured with FcDA is significantly reduced relative to the traditional curing agents. At the highest cure temperature for each data set, the final stress is 0.13 MPa with FcDA, as compared to 0.20 MPa, 0.23 MPa, and 0.16 MPa with D-230, MDA, and IPD, respectively. Although the proximity of the cure temperatures to $T_{g\infty}$ varies among the four systems,

Table 3-1 shows that the FcDA system achieves similar conversions, crosslink densities, and shrinkage values as the traditional systems, thus the temperature dependence of stress build-up cannot be ascribed to these factors. In addition, we have measured the stress build-up for slightly modified formulations of 828 and D-230 (Figure 3-10) – one stoichiometrically balanced, but containing 5% DMSO as an impurity, and one stoichiometrically imbalanced with 5% excess epoxy groups *via* partial replacement of D-230 with DMSO. In Figure 3-10, the former and latter are demarcated by the medium lines and thin lines, respectively; the data for a stoichiometrically balanced mixture in the absence of DMSO are demarcated by the thick lines. While these modifications produce lower stress levels, the overall trend clearly remains the same. Therefore, the temperature dependence of stress build-up with FcDA cannot simply be ascribed to the 5% residual epoxy that we have previously noted.

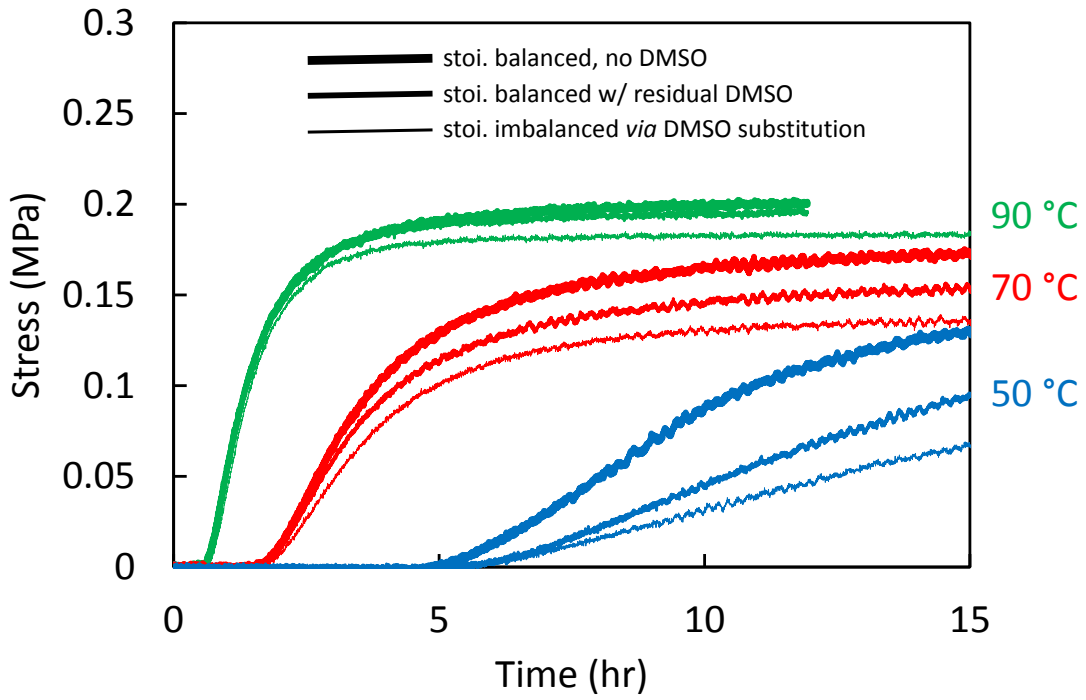

Figure 3-10. Stress build-up during isothermal cure of 828 with D-230 and with or without added DMSO.

Instead, we propose that the peculiar temperature dependence of stress build-up in 828 cured with FcDA is fundamentally connected to enhanced stress relaxation behavior imparted by the fluxional ferrocene units. Figure 3-11 compares the tensile relaxation of 828 fully cured with different curing agents. Each relaxation curve was measured under 1% strain at 25 °C above T_g (*i.e.*, at 138 °C, 115 °C, 205 °C, and 180 °C for FcDA, D-230, MDA, and IPD, respectively). The traditional curing agents yield

behavior that is expected for highly crosslinked materials, namely, there is negligible relaxation. In contrast, 828\FcDA relaxes a substantial portion of the imposed stress.

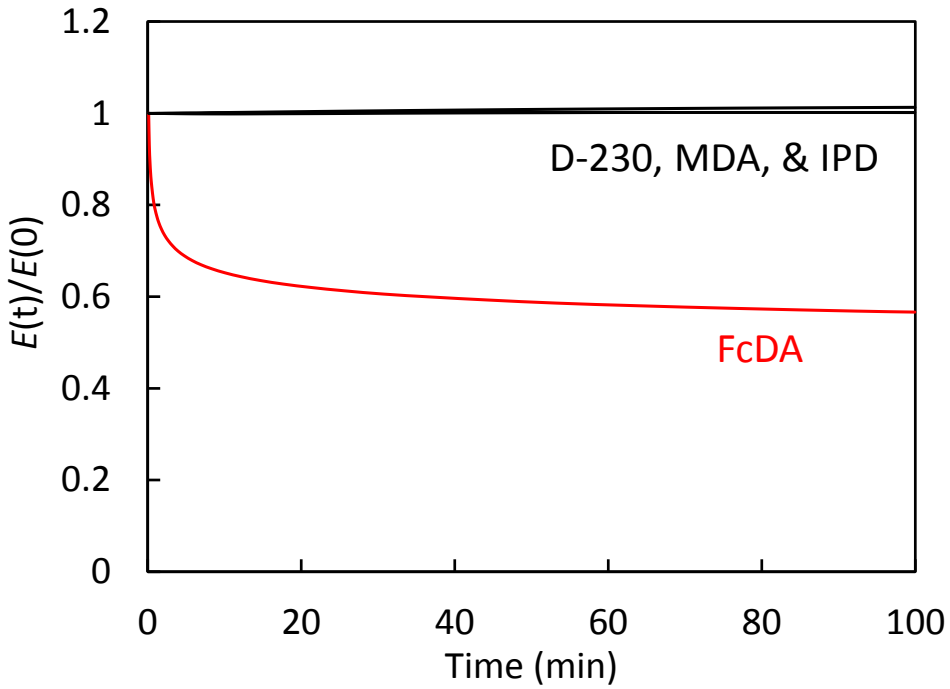

Figure 3-11. Time-dependent tensile relaxation modulus of 828 fully cured with FcDA, as compared to 828 fully cured with D-230, MDA, and IPD.

This phenomenon appears to be a physical relaxation process, and can be readily distinguished from chemical relaxation processes exhibited by networks containing transient bonds – specifically, CANs[39-64] or thermosets that exhibit stress relaxation *via* degradative pathways.[85,86] Figure 3-12 compares the tensile relaxation modulus of 828\FcDA at several different temperatures above T_g. Here, it is important to note that all relaxation curves for 828\FcDA were measured after annealing at 175 °C under nitrogen for 24 hr. Without this annealing step, we observed poor reproducibility of relaxation curves at higher temperatures, which we attribute to loss of non-reactive impurities contributed by the raw FcDA material (Figure 3-13). This annealing step causes a *ca*. 10-15 °C decrease in T_g, as indicated by the relative shift in the inflection point of the DSC heat flow shown in Figure 3-14. The tensile relaxation in Figure 3-12 is characteristic of a physical process in that its time scale is relatively short, occurring over seconds to minutes. Furthermore, the relaxation curves are well described by the empirical relationship $E(t) = E_\infty[1 + (t/\tau_0)^m]$, first proposed by Chasset and Thirion[87] to describe the relaxation of vulcanized natural rubber. As an example, the parameters E_∞, τ_0, and m obtained from fitting the 138 °C data are 3.8 MPa, 0.34 min, and 0.22, respectively. At the highest temperature, 175 °C, there is significant deviation between the experimental data and the fitting at longer times which is not

apparent from Figure 3-12, perhaps suggesting some contribution from chemical relaxation. However, the stress relaxation measured under torsional deformation in air is quite similar to that measured under tensile deformation in nitrogen (Figure 3-15), further corroborating the notion that this behavior is due to physical relaxation.

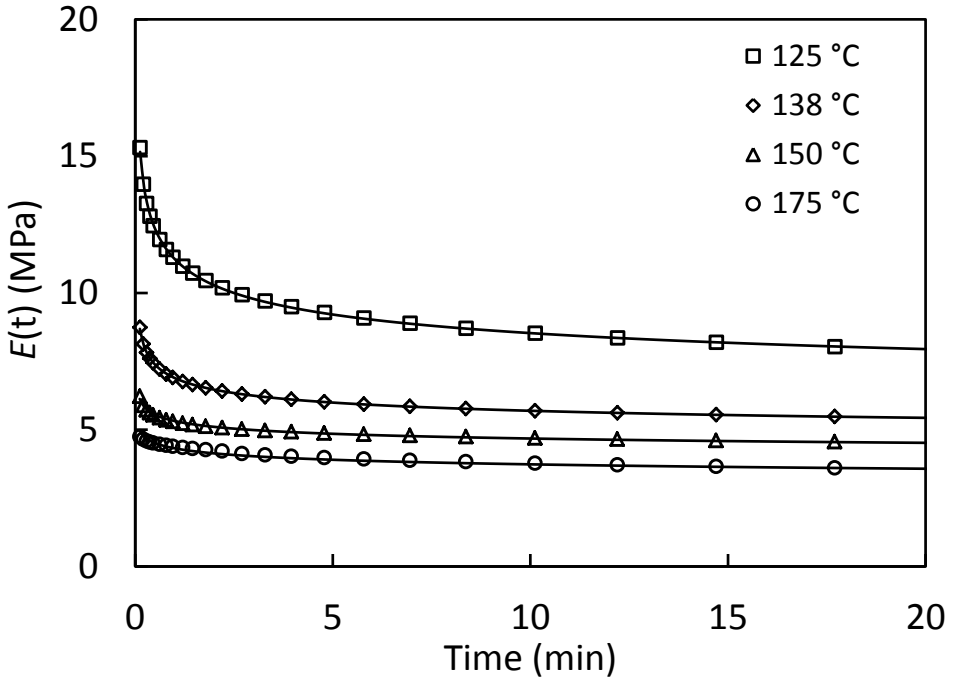

Figure 3-12. Time-dependent tensile relaxation modulus of 828 fully cured with FcDA at several temperatures above T_g.

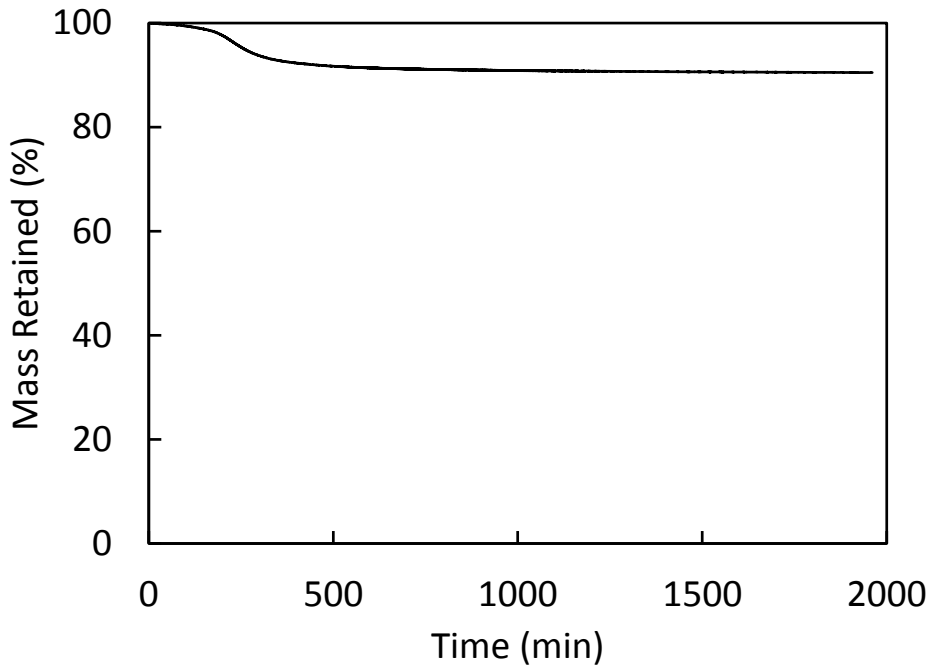

Figure 3-13. TGA of 828\FcDA annealed isothermally at 175 °C showing loss of volatile impurities.

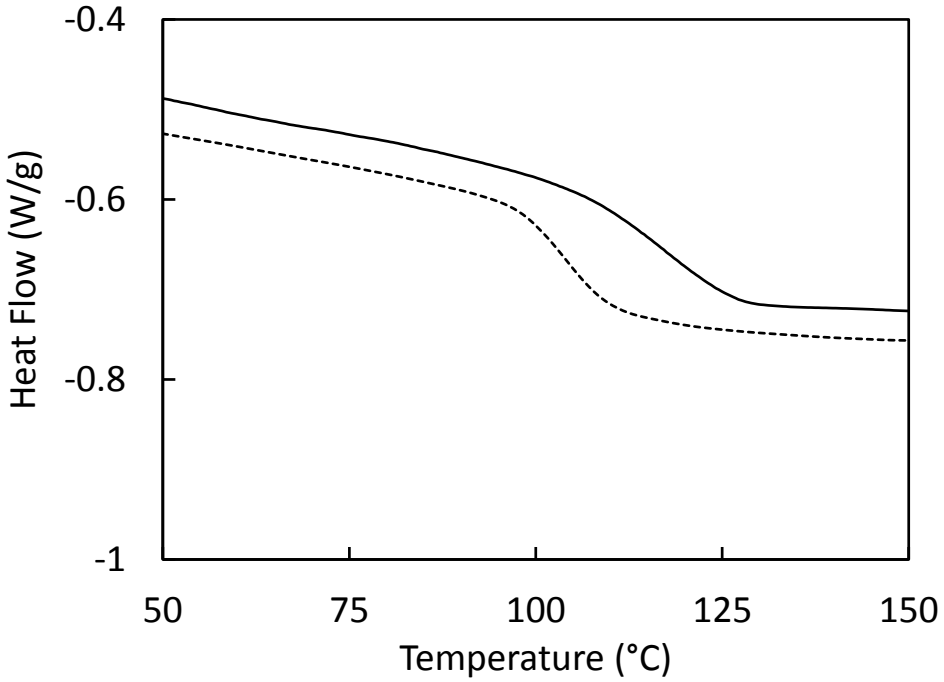

Figure 3-14. DSC heating traces (20 °C/min ramp rate) of 828\FcDA (solid) before and (dotted) after annealing at 175 °C.

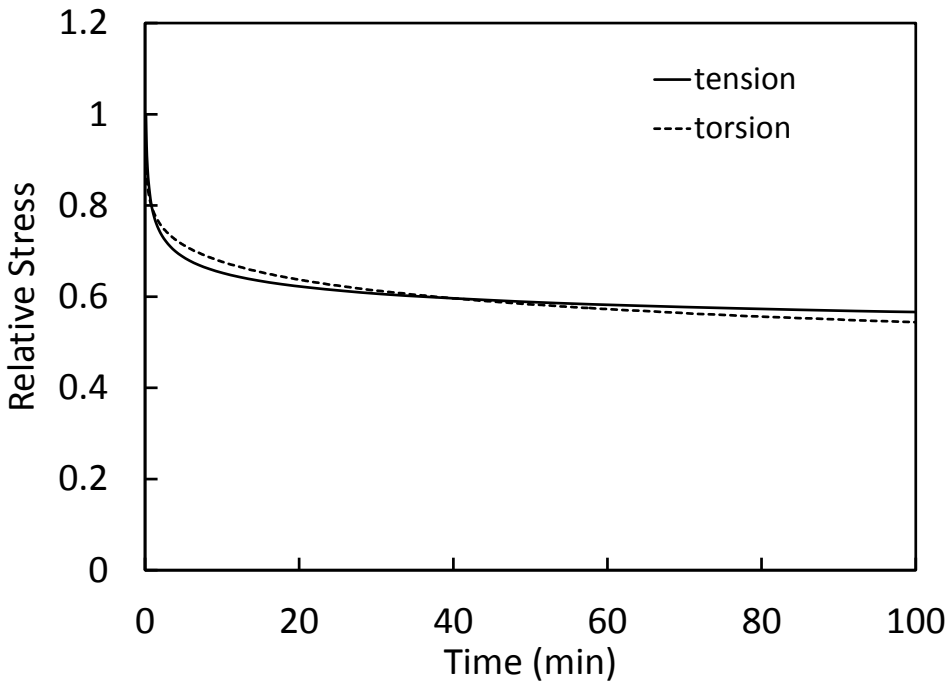

Figure 3-15. Relative stress during stress relaxation of 828\FcDA, measured under tensile deformation in nitrogen and under torsional deformation in air.

The unique stress relaxation of 828 cured with FcDA is also apparent when examining the temperature dependence of dynamic shear moduli. Figure 3-16 compares G', G'', and the loss tangent G''/G' for 828\FcDA to 828\D-230, 828\MDA, and 828\IPD. As mentioned previously, we have taken T_g to be the temperature at which the loss tangent achieves its maximum value. This choice yields good agreement with previously published T_g values for 828 cured with the traditional curing agents.[73,88-90] Yet again, the temperature dependence of G' for 828\FcDA is consistent with a highly crosslinked thermoset; the glass transition separates glassy and rubbery regimes characterized by G' values of ~ 1 GPa and several MPa, respectively. The rubbery regime, however, is atypical in that it exhibits a gradual decrease in G' with increasing temperature, and does not fully plateau until 50+ °C above T_g. In contrast, the traditional thermosets reach a well-defined plateau in G' *ca*. 15 °C above T_g and increases slightly with increasing temperature thereafter, as is normal for rubbers. At 25 °C above T_g, G' is measured to be 6.6 MPa and 6.4 MPa for 828\FcDA and 828\D-230, respectively. Crosslink densities are frequently estimated by using the classical scaling $G_r' \sim \nu$, where G_r' is the rubbery plateau modulus and ν is the concentration of elastically effective strands, despite known deviations at extremely high crosslink densities.[73] Although the unique behavior of 828\FcDA makes estimating G_r' dubious, these data certainly suggest that the materials possess similar crosslink densities. Indeed, after extended immersion in acetone, the mass of 828\FcDA increased by 1.5 times, while the mass of 828\D-230 increased by 1.3 times.

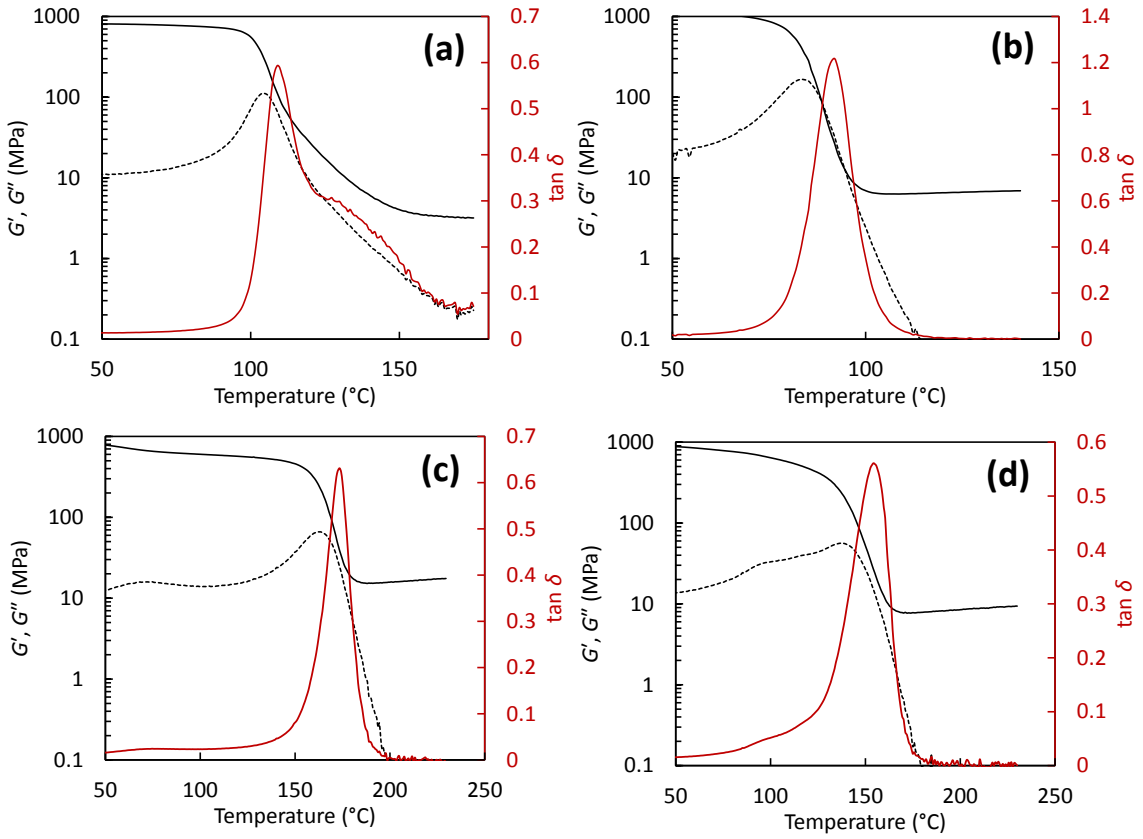

Figure 3-16. Temperature dependence of *G′* (solid), *G″* (dotted), and loss tangent (red) of (a) 828\FcDA, (b) 828\D-230, (c) 828\MDA, and (d) 828\IPD.

At the molecular level, stress relaxation in polymers deformed above their T_g arises from bond rotations that locally reorient the polymer's conformation in order to accommodate the applied stress.[91,92] Naturally, each unique chemical bond in a polymer possesses distinct energy barriers associated with such conformational isomerization. In the absence of chain connectivity, the energy barrier to Cp rotation in 828\FcDA would be given by 0.9-2.3 kcal/mol, *i.e.*, the measured activation energy for Cp rotation in ferrocene.[93-95] This is significantly less than the activation energy for C-C bond rotation, which has been measured at 3-3.5 kcal/mol.[96] However, the integration of Cp units, or any chemical bond, into a polymeric chain causes any individual rotation event to be restricted by the presence of neighboring bonds. The corresponding energy barriers increase dramatically and stress relaxation is only possible through cooperative and coordinated conformational isomerization among many interconnected bonds. In an entangled, linear polymer, such segmental motion is manifested as the well-known phenomenon of reptation. Crosslinks, though, represent fixed, topological constraints that prevent segmental motion; hence, stress relaxation is rapidly inhibited with increasing crosslink density. The prevailing notion is that stress relaxation in crosslinked rubbers only occurs through segmental motion of free chain ends and other network defects.[97-105]

Our observations concerning 828 cured with FcDA do not necessarily conflict with the accepted theories described above. Although we have attempted to use a stoichiometrically balanced system, we have already noted unmistakable evidence of a slight imbalance attributed to the purity of FcDA. This fact implies that a non-negligible concentration of defects exists in the current 828\FcDA network that can relax stress in fully cured samples. By the nature of the condensation polymerization employed (as opposed to, for example, crosslinking of a preformed, high molecular weight polymer), such defects should be short and unentangled, which is consistent with the observed time scale of relaxation (Figure 3-12). Besides, as cure progresses from gelation to vitrification or full cure, a monotonically decreasing fraction of chain ends must exist that can relax stresses arising from shrinkage. It is important to note, however, that the *difference* in stress relaxation between 828\FcDA and the traditional systems cannot simply be attributed to the presence of network defects and\or non-reactive impurities alone. Figure 3-17 illustrates the stress relaxation behavior of 828\D-230 with 5% residual epoxy from added DMSO impurity, in which it is readily apparent that there is no profound difference relative to pure, stoichiometrically-balanced 828\D-230, aside from small changes in T_g and G_r'. Instead, we propose that torsional flexing of the Cp rings[68-70] of the FcDA curing agent (Figure 1-3) dramatically enhances stress relaxation by facilitating chain end motion. In addition to its comparatively low activation energy, Cp rotation offers the possibility for reorientation of a chain segment within an effective 360° of 2-D space. The contribution of Cp rotation to stress relaxation is apparently augmented with increasing cure temperature, such that the stress due to cure with FcDA exhibits a fundamentally different, advantageous dependence on cure temperature (Figure 3-8). Furthermore, the effect of Cp rotation may be reflected in the broad, asymmetric peak exhibited in the loss tangent (Figure 3-16). Previous work in radical-cured thermosets has revealed that networks with heterogeneous distributions in chain mobility present broad loss tangent peaks.[106] In light of the narrow loss tangent peak observed in all variations of 828\D-230 (Figure 3-16 and Figure 3-17), the broad decay in the loss tangent of 828\FcDA above T_g suggests that the mobility of chain ends in the FcDA-based network is quite atypical relative to traditional epoxy-amine networks. Indeed, Cp rotation has been shown to occur in linear, ferrocene-based polymers only above T_g.[68-70]

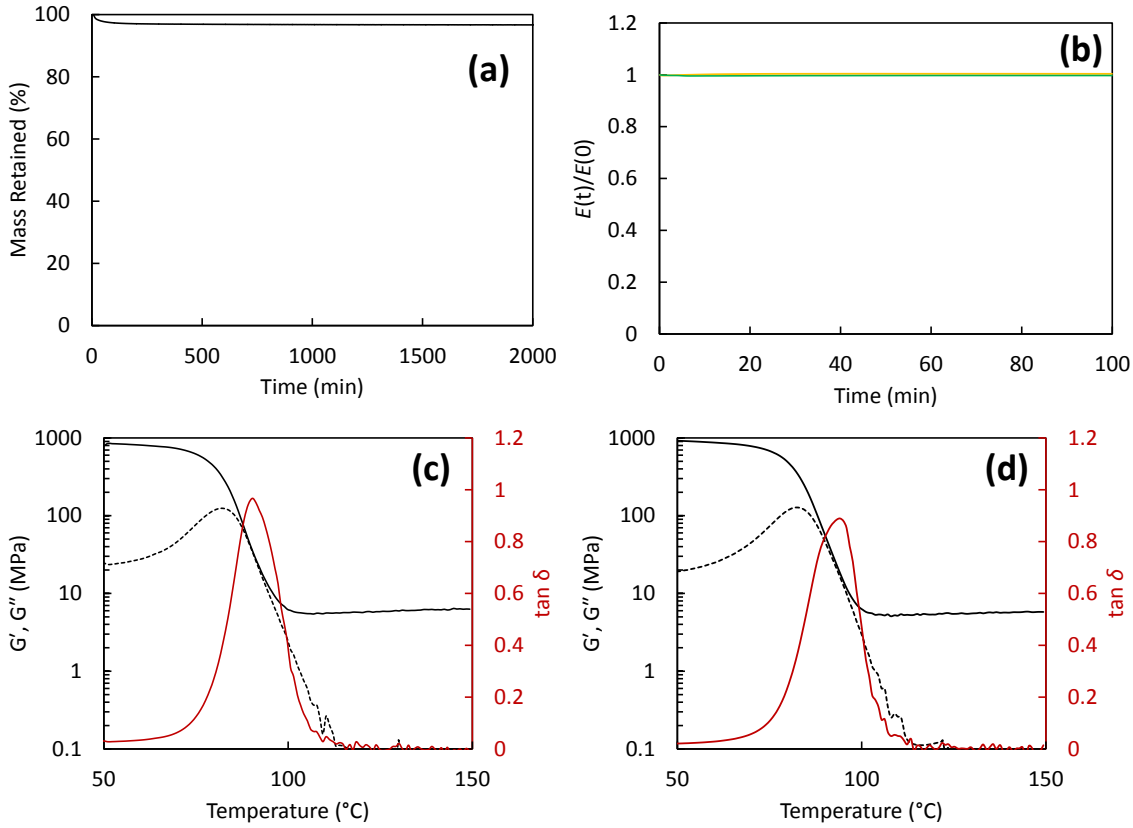

Figure 3-17. (a) TGA and (b)-(d) stress relaxation behavior of 828\D-230 containing 5% added DMSO. Panel (a), yellow line in (b), and panel (c): stoichiometrically-balanced w/ 5 wt, % added DMSO. Green line in (b) and panel (d): stoichiometrically-imbalanced mixture with 5% D-230 substituted by DMSO.

To further highlight these propositions, we intentionally introduced additional defects by adjusting stoichiometry. In Figure 3-18, we examine a series of stress build-up curves during isothermal cure of an excess of 828 with FcDA or D-230. The parameter r defines the initial concentration of amine hydrogens to epoxy groups. For D-230, as r is decreased to 0.8 and to 0.67, the final stress level is *ca*. 25% and 10%, respectively, of the final stress level with r = 1. Unsurprisingly, a similar decrease in G_r' of the fully cured material is observed (Figure 3-19). For FcDA, however, as r is decreased to 0.8, the final stress level is *ca*. 6% of the final stress level with r = 1. At r = 0.67, the mixture exhibits no detectable stress within the resolution of the instrument (~ 1 kPa), from which a final stress level < 0.6% relative to r = 1 is implied. Thus, the introduction of defects into a FcDA-cured network produces an incredibly more profound effect on cure stress than a D-230-cured network.

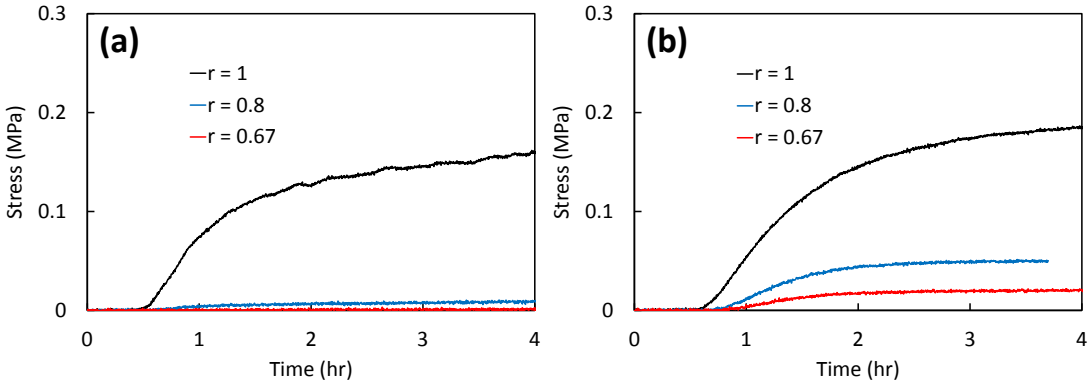

Figure 3-18. Stress build-up during isothermal cure at 90 °C of 828 with (a) FcDA and (b) D-230 using different compositions.

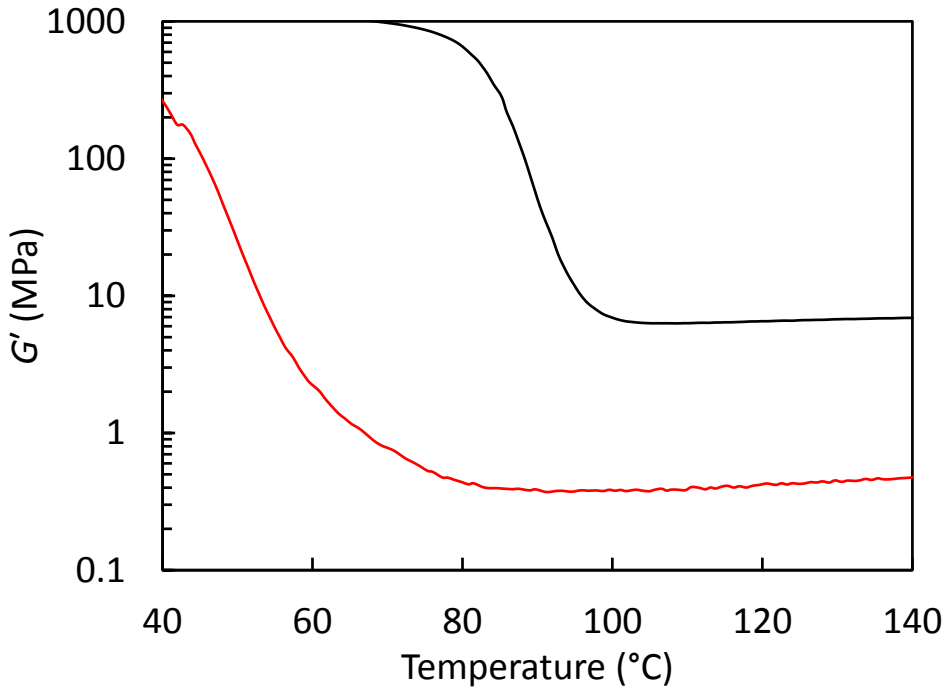

Figure 3-19. Temperature dependence of *G′* of 828\D-230 using a composition of (black) *r* = 1 and (red) *r* = 0.67.

Finally, we present the room-temperature mechanical properties of 828 fully cured with FcDA in comparison to the traditional curing agents. Figure 3-20 shows the stress-strain relationship of these materials in response to uniaxial tension. Interestingly, 828\FcDA appears to be substantially more brittle than 828\MDA, 828\IPD, and, in particular, 828\D-230, which was the only material to consistently yield in tension. This fact is further highlighted by Figure 3-21, where the average strain at break of 828\FcDA is observed to be considerably less than 828\D-230. Conversely, when brittle fracture is suppressed by applying uniaxial compression, the

yield strengths of 828\FcDA, 828\MDA, and 828\IPD are all comparable and considerably greater than the yield strength of 828\D-230.

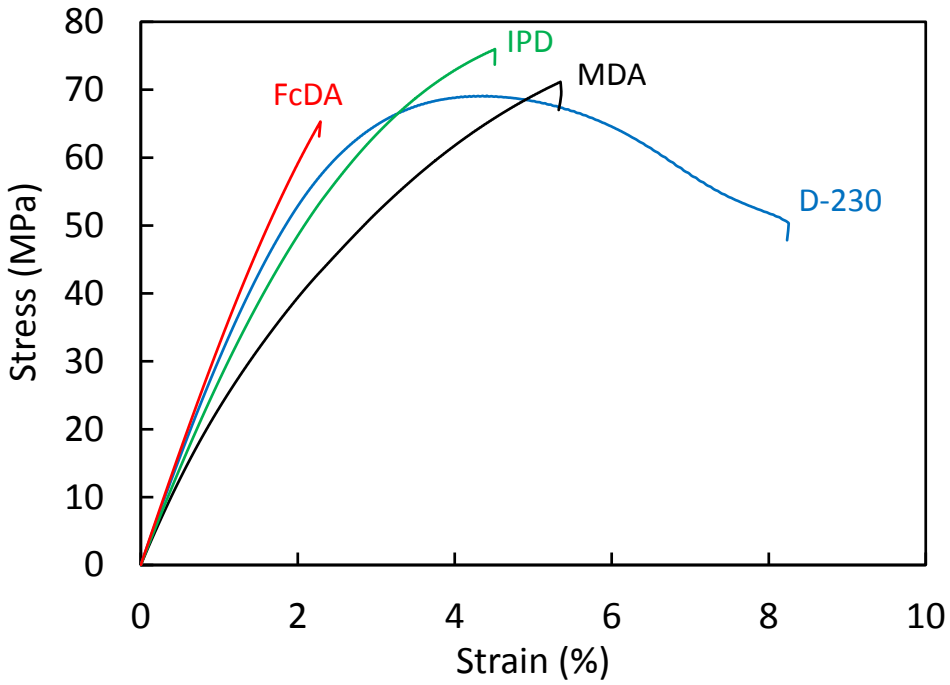

Figure 3-20. Representative stress-strain curves measured in uniaxial tension at room temperature.

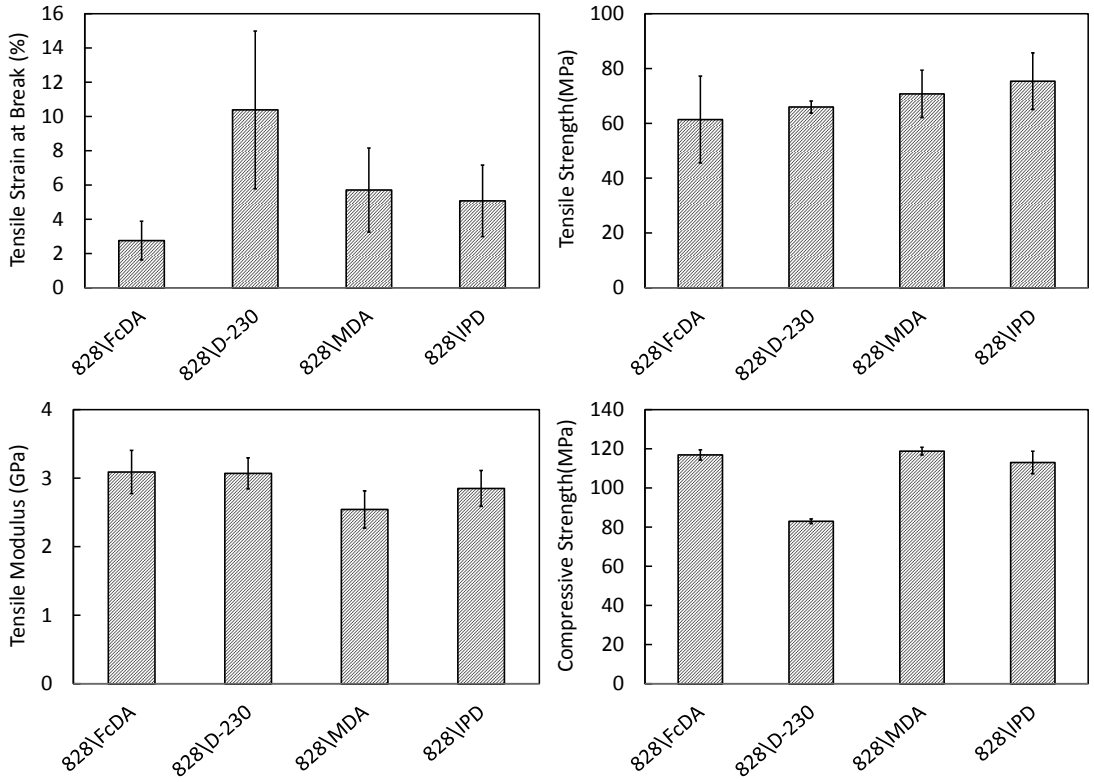

Figure 3-21. Mechanical properties measured at room temperature. Error bars represent one standard deviation.

Previous publications have examined the effect of curing agent structure on the mechanical properties of epoxy thermosets, from which several general trends are apparent.[107-112] For example, an aliphatic amine-crosslinked epoxy was observed to transition from brittle fracture to yield at *ca.* 60-70 °C below its T_g.[107] Since D-230 produces the lowest T_g value among the curing agents studied, this may explain, at least in part, why 828\D-230 is the only material to consistently yield in tension. On the other hand, however, curing agents with decreased chain flexibility have been shown to produce materials exhibiting increased brittle character. Therefore, the measured mechanical properties of 828\FcDA are suggestive of a rigid curing agent, seemingly in conflict with its stress relaxation behavior. More precisely, however, the macroscopic properties of epoxies in this regime are connected to a sub-T_g relaxation process (commonly referred to as the β-relaxation), which is suspected to be associated with specific motion of certain components of the network.[113] Thus, reconciliation of the room-temperature mechanical properties in the context of stress relaxation above T_g will require additional characterization of sub-T_g relaxation processes, a subject discussed in more detail in Chapter 4.

3.4. Conclusions

In summary, we have shown that FcDA can be used to substantially reduce the stress arising from cure of an epoxy resin. Traditional curing agents lead to increased cure stress with increasing isothermal cure temperature, whereas the ferrocene-based curing

agent exhibits reduced cure stress with increasing temperature. To reiterate, we postulate that this phenomenon is fundamentally due to fluxional motion of the ferrocene moieties – specifically, torsional flexing of interconnected Cp units – that are integrated into the backbone of the polymer network. In support of this concept, we have demonstrated that increasing the concentration of network defects, which are the entities responsible for stress relaxation in rubbers, causes cure stress in the ferrocene-based thermoset to rapidly vanish. Moreover, we have shown that the fully cured material is capable of relaxing a significant fraction of applied stress above T_g, in a manner that is clearly distinct from the traditional materials. Despite these benefits to stress relaxation at elevated temperature, the ferrocene-based thermoset possesses room-temperature stiffness and strength that are comparable to the traditional materials, although it is also prone to brittle fracture.

4. SOLID STATE ^{1}H NMR INVESTIGATION OF DYNAMICS IN EPOXY THERMOSETS

Although the results of Chapter 3 clearly show that thermosets derived from FcDA are distinguished from traditional thermosets in the context of stress relaxation and residual stress, it remains an open question as to whether such behavior truly arises from torsional flexing or other fluxional motion of incorporated ferrocene units (Figure 3-1). Therefore, we attempted to use solid state NMR spectroscopy to gain further insight into the molecular dynamics of these epoxy thermosets. Line shape analysis of static ^{1}H NMR spectra as a function of temperature was used to monitor the chain dynamics for the fully cured materials through T_g, allowing the measurement of the associated E_a values. Double quantum (DQ) ^{1}H NMR experiments were also employed to measure the residual ^{1}H-^{1}H residual dipolar coupling (RDC) well above T_g where there is an averaging of the segmental motions between crosslinks and entanglements. The RDC is a measure of the bond order parameter (S_b), and is directly proportional to the concentration of topological constraints, both crosslinks and entanglements, or the relative flexibility of the polymer chain between adjacent crosslinks. We also show that the thermosets produced with different curing agents have inhomogeneous distributions of RDC (*i.e.*, crosslink densities). These results are discussed below in terms of possible fluxional stress relief mechanisms.

4.1. Experimental Methods

The solid state ^{1}H NMR spectra were obtained on a Bruker Avance III instrument operating at an ^{1}H observe frequency of 400.14 MHz with a 7 mm high temperature DOTY MAS probe used under static (non-spinning) conditions. The reported sample temperature was calibrated using known melting points of secondary external standard materials. The 1D ^{1}H NMR spectra were obtained using a Hahn echo pulse sequence with an inter-pulse delay of 10 μs, 16 scan averages, and a 5 s recycle delay for temperatures ranging between −40 °C and +281 °C. The epoxy samples were allowed to equilibrate 5 min at each temperature prior to acquisition. The temperature results were scaled to the glass transition temperature T/T_g or various equivalent representations as shown in equation 4-1.

$$\frac{T-T_g}{T_g} = \frac{\Delta T}{T_g} = \frac{T}{T_g} - 1 \qquad (4\text{-}1)$$

The intensities for the DQ $\left(I_{DQ}\right)$ and reference longitudinal magnetization $\left(I_{ref}\right)$ were obtained using a standard 5-pulse sequence (Figure 4-1) during the DQ excitation and reconversion period, with π refocusing pulses incorporated to reduce frequency offset and chemical shift effects.[114-116] The DQ buildup curves were obtained by measuring the signal intensity as a function of the inter-pulse delay τ_{DQ}. The evolution time t_1 and the z-filter time τ_f were fixed to 2 μs and 100 μs, respectively.

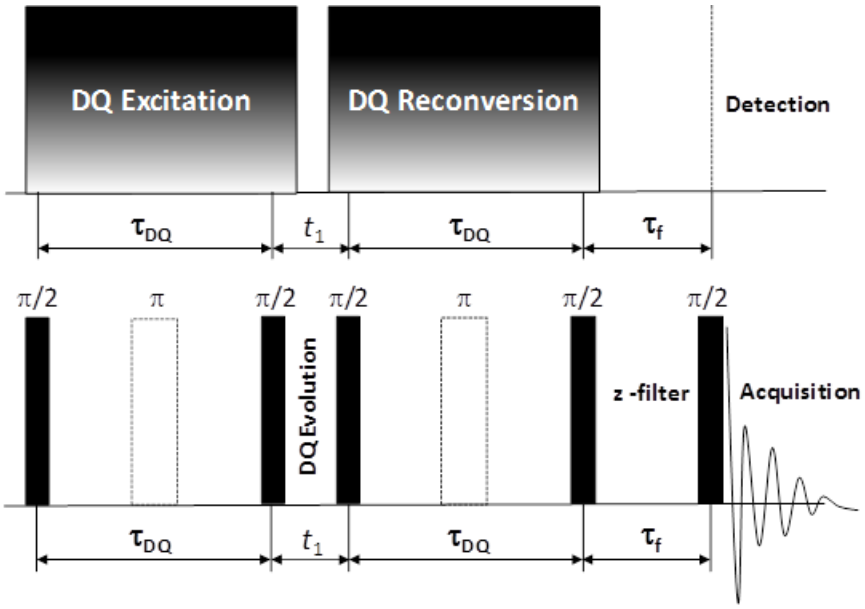

Figure 4-1. Schematic representation of the 5-pulse NMR sequence used for excitation and reconversion of the DQ NMR coherences. The DQ buildup curves were obtained by varying τ_{DQ} while keeping t_1 and τ_f fixed.

The DQ selection was obtained using a 4-step phase cycle of the carrier phase during the excitation period combined with receiver phase inversion on alternating scans to give I_{DQ}, while the reference intensity I_{ref} was measured using the same sequence without the 4-step phase cycling. The I_{DQ} includes signal from dipolar coupled protons and all 4n+2 multiple quantum coherences, while I_{ref} includes contributions from the dipolar-encoded longitudinal magnetization plus signal from uncoupled isotropically mobile fragments (*i.e.*, chain ends). A normalized DQ intensity (I_{nDQ}) was defined as detailed previously,[117,118]

$$I_{nDQ} = \frac{I_{DQ}}{I_{DQ}+I_{ref}-Be^{-2\tau_{DQ}/T_2}} \tag{4-2}$$

For temperatures significantly above (and below) T_g, the contributions from the isotropic signal (B) is small with the normalization procedure (Eqn. 4-1) being effective and compensating for thermally induced motions and relaxation effects. Near T_g, the contributions from these isotropic components become more apparent, impacting the normalization procedure. This observation suggests that, near T_g, there are slow motions on a time scale that interfere with the measurement of the RDC (D_{res}). The initial rise of the normalized DQ intensity as a function of τ_{DQ} were fit using a second moment approximation:

$$I_{nDQ}(D_{res}) = \frac{1}{2}\left(1 - e^{-\frac{2}{5}D_{res}\tau_{DQ}^2}\right) \tag{4-3}$$

where D_{res} is an apparent residual coupling corresponding to an average over multiple ^{1}H-^{1}H dipolar coupling within the thermoset material. With increasing temperature, marked deviations from this inverted Gaussian were observed, suggesting that a

distribution of D_{res} was present. Assuming a Gaussian distribution, the DQ buildup was analyzed using:

$$I_{\mathrm{nDQ}}(\overline{D}_{\mathrm{res}},\sigma_{\mathrm{D}}) = \frac{1}{2}\left(1-\exp\left\{-\frac{\frac{2}{5}\overline{D}_{\mathrm{res}}^{2}\tau_{\mathrm{DQ}}^{2}}{1+\frac{4}{5}\sigma_{\mathrm{D}}^{2}\tau_{\mathrm{DQ}}^{2}}\right\}\left[1+\frac{4}{5}\sigma_{\mathrm{D}}^{2}\tau_{\mathrm{DQ}}^{2}\right]^{-1/2}\right) \quad (4\text{-}4)$$

where $\overline{D}_{\mathrm{res}}$ is the average residual dipolar coupling constant with standard deviation σ_{D}. For the FcDA-cured thermosets at temperatures above T_g, the normalized DQ intensity buildups were very heterogeneous showing significant deviations from even a Gaussian distribution. In this case, it was assumed that the buildups were described by the bimodal model:

$$I_{\mathrm{nDQ}}\left(D_{\mathrm{res}}^{(1)},D_{\mathrm{res}}^{(2)},f\right) = fI_{\mathrm{nDQ}}\left(D_{\mathrm{res}}^{(1)}\right)+(1-f)I_{\mathrm{nDQ}}\left(D_{\mathrm{res}}^{(2)}\right) \quad (4\text{-}5)$$

where f and $1-f$ are the relative weights of the two domains with $D_{\mathrm{res}}^{(1)}$ and $D_{\mathrm{res}}^{(2)}$, respectively.

The heterogeneous nature of the crosslinking was evaluated from the distribution in D_{res} (related to the bond order parameter S_b) as a function of temperature using the program *ftikreg*, which is based on a fast Tikhonov regularization of the I_{nDQ} buildups. This regularization utilizes the Feldhome Integral equation:

$$g(\tau_{\mathrm{DQ}}) = \int_0^{\infty} K\left[D_{\mathrm{res}},\tau_{\mathrm{DQ}}\right]f(D_{\mathrm{res}})dD_{\mathrm{res}} \quad (4\text{-}6)$$

where $K\left[D_{\mathrm{res}},\tau_{\mathrm{DQ}}\right]$ is the Kernel utilized in this integral. We have employed the empirical "Abragam-like" (A-1) Kernel for our transforms defined as:[119]

$$I_{\mathrm{nDQ}}\left(\tau_{\mathrm{DQ}},D_{\mathrm{res}}\right) = \frac{1}{2}\left(1-\exp\left\{-\left(0.378D_{\mathrm{res}}\tau_{\mathrm{DQ}}\right)^{1.5}\right\}\right)\cos[0.583]\,D_{\mathrm{res}}\tau_{\mathrm{DQ}} \quad (4\text{-}7)$$

4.2. Solid State ^{1}H NMR Line Shape Variation

The static ^{1}H NMR spectra as a function of temperature for 828\FcDA, 828\D-230, and 828\MDA are shown in Figure 4-2. The high temperature limits correspond to equivalent reduced temperatures of $T/T_g \sim 1.2$. Here, as with the mechanical analysis and stress relaxation presented in Chapter 3, the 828\FcDA was annealed at 175 °C under nitrogen for 24 hr to remove unreacted impurities (Figure 3-13). The annealed material is indicated by the post cure label; however, the ^{1}H NMR spectra for the material prior to annealing is similar and is shown in Figure 4-3. All of the thermosets show a very broad NMR resonance with a full width at half maximum (FWHM) line width of ~ 37 to 50 kHz at low temperature resulting from the significant homonuclear ^{1}H-^{1}H dipolar coupling present in these rigid materials. With increasing temperature below T_g, the line widths gradually become narrower as different polymer motions (various β relaxation modes) begin to partially average the ^{1}H-^{1}H dipolar coupling.

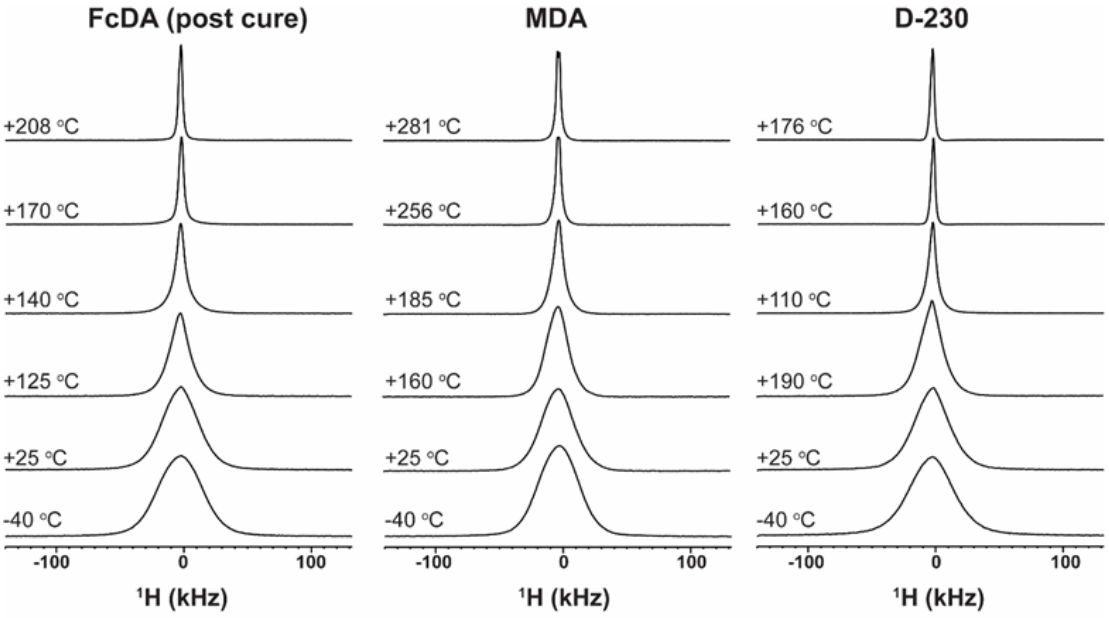

Figure 4-2. Static ^{1}H NMR spectra of fully cured thermosets as a function of temperature.

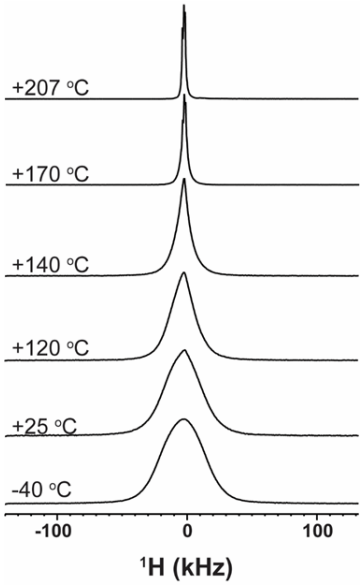

Figure 4-3. Static ^{1}H NMR spectra of fully cured 828\FcDA thermoset prior to annealing.

The most dramatic change in the line widths occurs at T_g due to a sudden increase in the chain dynamics (α relaxation) to produce a highly motionally averaged line shape at high temperatures. This line width change can be fit to obtain an estimate of T_g and the width of the glass transition. More specifically, the line width variation with temperature $W_i(T)$ was fit with a 4-parameter sigmoid function as follows:

$$W_{\mathrm{i}}(T) = W_i' + \frac{W_i''}{1+\exp\left[-\frac{T-T_{\mathrm{g}}}{b}\right]} \tag{4-8}$$

where T_{g} is defined as the mid-point of this transition, W_i' is the low temperature line width, W_i'' is the line width change during the transition, and $1/b$ is the rate of temperature-induced change occurring at T_{g}. We have chosen line width limits near T_{g} to separate this transition from the other β relaxation-induced line width changes occurring with temperature. The various fits for the different thermosets are shown in Figure 4-4, while the fitting results are given in Table 4-1. From Table 4-1, the T_{g} values determined by this method are found to be consistently greater than those determined by DMA (Section 3.2.6). Interestingly, the reduction in T_{g} observed by DMA after annealing of 828\FcDA is not mirrored in the NMR results. It is unclear whether this discrepancy is simply a product of inherent error associated with the determination of T_{g} by both methods, or whether it reflects physical changes in the material to which mechanical measurements are more sensitive.

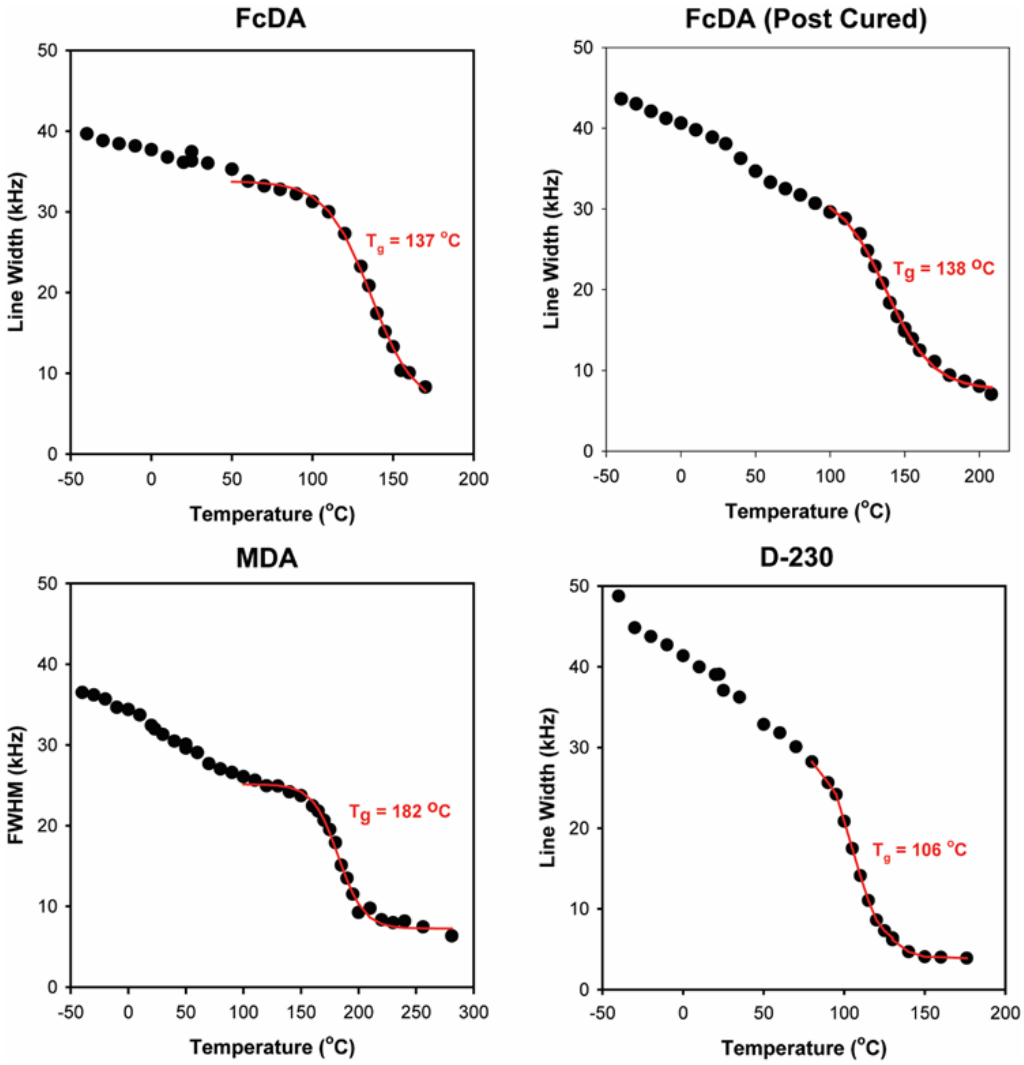

Figure 4-4. Static ^{1}H NMR line width vs. temperature for fully cured thermosets with 4-parameter Sigmoid fits used to estimate T_g.

Table 4-1. T_g and E_a values estimated from static ^{1}H NMR line width fitting.

Thermoset	T_g DMA (°C)	T_g NMR (°C)[a]	b[a]	E_a (kJ/mol)[b]	E_a' (kJ/mol)[c]
828\MDA	180	182	-11.1	33.5	2.8
828\D-230	90	106	-9.6	62.1	2.9
828\FcDA	125	137	-13.8	35.3	1.8
828\FcDA (postcure)	113	138	-15.6	27.4	2.0

[a]From fitting according to Eqn. 4-6. [b]Activation energy for the T_g (α) transition. [c]Activation energy for the low temperature (β relaxation) line width variation.

It is well established that polymer segmental relaxations should scale with reduced temperature T/T_g or the equivalent representations of Eqn. 4-1.[120-122] The variation in line width with temperature offset (T-T_g) and with reduced temperature ($\Delta T/T_g$) are shown in Figure 4-5. The line widths for the different materials show similar overall trends, but do reveal distinct differences in the impact of local segmental motions on averaging of the dipolar coupling both below and above T_g. 828\D-230 reveals the highest rigidity in local segmental motions at lower temperatures, as indicated by the largest line widths. In contrast, 828\MDA shows the presence of significant segmental motion at lower temperatures, even though the material has the highest T_g (Table 4-1). A somewhat tenuous parallel can be drawn between these data and the room temperature mechanical properties discussed in Figure 3-21. Boye, *et al.*, have previously examined MDA-cured DGEBA of varying stoichiometry and shown that increased modulus is accompanied by a suppression of the β relaxation, assessed in their case by thermally stimulated creep recovery.[113] This suppression is, in effect, a freezing out of segmental dynamics over the associated temperature range. In light of such information, it is reassuring then to note that both the moduli and low-temperature line widths of the present materials follows the trend D-230 > FcDA > MDA. Above T_g, the measured line widths become similar with 828\D-230 showing the highest degree of motional averaging at higher temperatures. This is consistent with the overall similarities in crosslink density among the materials, as noted in Table 3-1 and discussed at length in Chapter 3 with regards to measurements of epoxy conversion and G_r'. It is important to note that, despite the substantial differences in stress relaxation above T_g among these materials (Figure 3-11 and Figure 3-16), a similar distinction in motional averaging above T_g should not necessarily be expected from these experiments. The NMR line width is indicative of the motion of all protons in the entire sample; therefore, it is entirely reasonable that the signal from a small fraction of the sample responsible for stress relaxation (*e.g.*, chain ends) would be, in effect, diluted. Such considerations aside, a slight reduction in the temperature variation (increased transition width) of the ^{1}H NMR line width at T_g for the annealed 828\FcDA (post cure) can be seen in Figure 4-5, and is also evident in the T_g activation energies presented below. The ^{1}H NMR spectra of 828\FcDA after annealing also have broader line widths at low temperature (Figure 4-5), which likely reflects the loss of comparatively mobile, unreactive species.

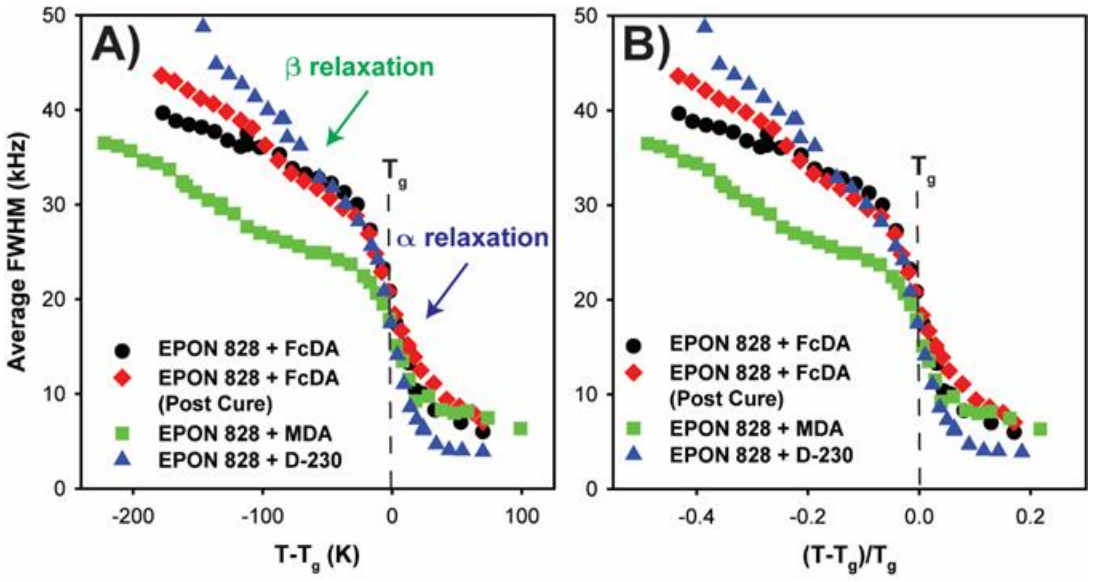

Figure 4-5. Static ^{1}H NMR line width (FWHM – full width at half maximum) vs. (a) temperature offset and (b) reduced temperature for fully cured thermosets.

The effective molecular correlation times at different temperature (τ_i, i = *T*) for these different polymer chain motions can be estimated using:

$$\tau_i = \frac{1}{W_i} \tan\left[\frac{\pi}{2}\frac{W_i^2 - \langle W\rangle^2}{W_0^2 - \langle W\rangle^2}\right] \quad (4\text{-}9)$$

where W_i is the line width at temperature i, while W_0 and W are the rigid limit and high temperature-averaged line widths, respectively. The temperature variation τ_i of these line widths is shown in Figure 4-6, and over small temperature ranges allows E_a for T_g and for the β relaxation region to be determined assuming an Arrhenius behavior (Table 4-1).

$$\tau_i = \tau_0 \exp\left[\frac{E_a}{RT}\right] \quad (4\text{-}10)$$

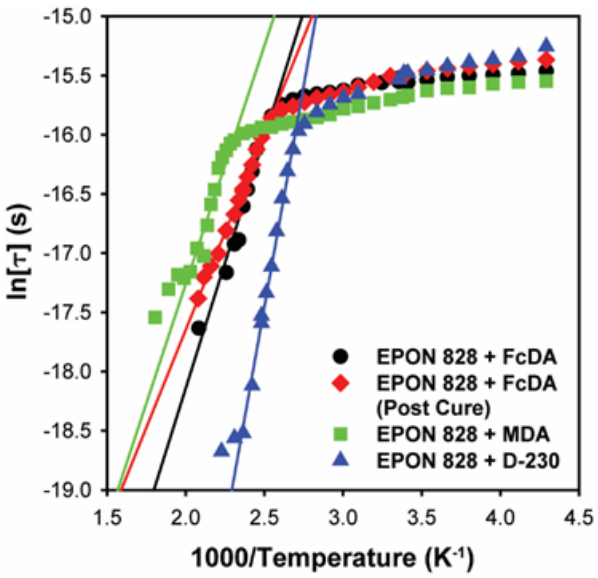

Figure 4-6. Arrhenius behavior of the average motional correlation time.

4.3. Double Quantum NMR

The normalized DQ intensity (I_{nDQ}) variations with increasing excitation period τ_{DQ} (see Figure 4-1 for pulse sequence definitions) observed for the different cured materials are shown in Figure 4-7 as a function of temperature through T_g (the equivalent scaled temperature T/T_g are included in Table 4-2 through Table 4-5). These DQ build-ups can be analyzed to obtain the RDC as a function of temperature. A few qualitative observations can be made concerning the different build-up behavior. As expected, at temperatures (−40 °C) well below T_g, the ^{1}H-^{1}H dipolar coupling is very strong with D_{res} ranging from 40 to 50 kHz, producing the rapid rise in I_{nDQ}. This behavior was observed for all the materials and is consistent with the glassy nature of these thermosets. With increasing temperatures the I_{nDQ} buildup becomes slower, reflecting a reduction in D_{res}. This is particularly apparent if one looks at the expansions in panels (b), (d), (f), and (h) of Figure 4-7. At and above T_g, this reduction in D_{res} increases (Table 4-2 through Table 4-5), until the build-ups begin to converge at very high temperature (T/T_g ~ 1.2). At high temperature, the relative D_{res} for D-230 (Table 4-3) is less than that for MDA (Table 4-2). The DQ build-ups for FcDA before and after annealing (Table 4-4 and Table 4-5, respectively) are significantly different, but as noted in the experimental discussion, significant correction was required for an isotropic component (~ 6% to 10%) in the DQ normalization, consistent with the presence of unreactive impurities that are mobile enough not to produce DQ intensity. For this reason, the remainder of the discussion will concentrate on the FcDA-based material only after annealing. The latter also reveals a reduction in D_{res} with increasing temperature, but is clearly heterogeneous in nature with a rapid increase in the I_{nDQ} at short τ_{DQ} (reflecting a strong D_{res}) in combination with a second, much slower recovery arising from chain segments with a small D_{res} produced by motional averaging of the dipolar coupling. For an isotropic motion, the dipolar coupling would be zero as the ^{1}H-^{1}H inter-nuclear tensor visits all

orientations due to thermal fluctuations during the experiments. For the thermosets, this isotropic motion does not occur due to topological constraints of the polymer chain (*i.e.*, crosslinks), such that there remains a non-zero D_{res} even at temperatures above T_g. These DQ build-up curves were analyzed using Eqn. 4-4 for each temperature investigated with the results summarized in Table 4-5. At higher temperatures, it was necessary to include a distribution of D_{res} (Eqn. 4-5) in order to reproduce the DQ intensity response. Figure 4-8 shows examples of fits using Eqn. 4-3 and Eqn. 4-4 for 828\MDA, along with the need to include the bimodal response (Eqn. 4-5) to describe the annealed 828\FcDA material.

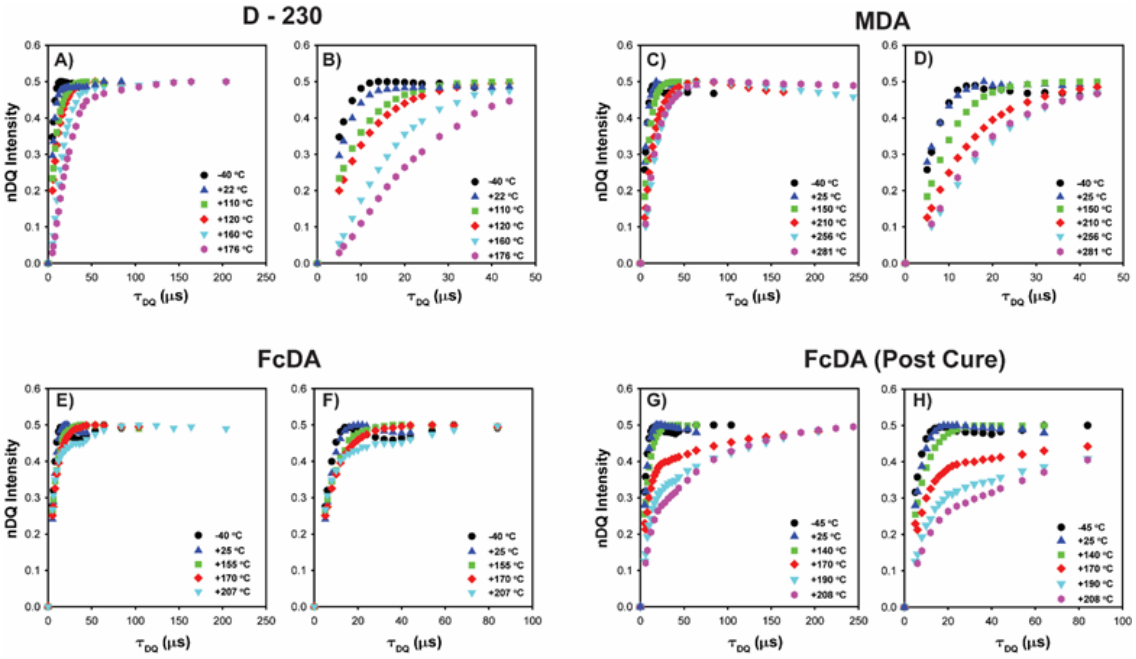

Figure 4-7. Normalized DQ intensity build-ups for the cured thermosets. The right panel for each curing agent shows expansions of the initial DQ intensity build-up.

Table 4-2. Residual dipolar coupling for 828\MDA (T_g = 455 K, 182 °C)

T (K) [°C]	T/T_g	ΔT (K)	$\Delta T/T_g$	$D_{res}/2\pi$ (kHz) [r^2]	$\bar{D}_{res}$, $\sigma_D/2\pi$ (kHz) [r^2]
233 [−40]	0.51	−222	−0.49	42.8 [0.9924]	43.1, 5.0 [0.9925]
298 [25]	0.65	−157	−0.35	42.8 [0.9897]	45.5, 14.6 [0.9973]
423 [150]	0.83	−32	−0.07	36.2 [0.9560]	38.9, 15.8 [0.9939]

448 [175]	0.98	−7	−0.02	29.1 [0.9763]	30.7, 12.3 [0.9962]
458 [185]	1.01	3	0.006	30.9 [0.9528]	30.9, 16.0 [0.9919]
473 [200]	1.04	18	0.04	21.9 [0.9534]	23.9, 12.7 [0.9917]
483 [210]	1.06	28	0.06	20.1 [0.9559]	21.6, 11.8 [0.9900]
529 [256]	1.16	74	0.16	15.4 [0.9668]	16.9,8.9 [0.9955]
554 [281]	1.22	99	0.22	15.4 [0.9697]	15.7, 7.4 [0.9947]

Table 4-3. Residual dipolar coupling for 828\D-230 (T_g = 379 K, 106 °C)

T (K) [°C]	T/T_g	ΔT (K)	$\Delta T/T_g$	$D_{res}/2\pi$ (kHz) [r^2]	$\bar{D}_{res}$, $\sigma_D/2\pi$ (kHz) [r^2]
233 [−40]	0.61	−146	−0.39	53.3 [0.9963]	56.2, 13.3 [0.9980]
295 [22]	0.78	−84	−0.22	45.6 [0.9889]	49.6, 18.7 [0.9984]
383 [110]	1.01	4	0.01	33.7 [0.9483]	36.5, 18.2 [0.9914]
393 [120]	1.04	14	0.04	29.0 [0.9368]	31.3, 17.2 [0.9894]
433 [160]	1.14	54	0.14	15.0 [0.9885]	15.8, 6.3 [0.9993]
449 [176]	1.18	70	0.18	11.04 [0.9869]	11.4, 5.1 [0.9990]

Table 4-4. Residual dipolar coupling for 828\FcDA before annealing (T_g = 410 K, 137 °C)

T (K) [°C]	T/T_g	ΔT (K)	$\Delta T/T_g$	$D_{res}/2\pi$ (kHz) [r^2]	$\bar{D}_{res}$, $\sigma_D/2\pi$ (kHz) [r^2]
233	0.57	−177	−0.43	44.5	51.4, 5.7

[−40]				[0.9657]	[0.9884]
298 [25]	0.73	−112	−0.27	38.9 [0.9657]	40.0, 8.5 [0.9950]
413 [140]	1.01	3	0.01	29.7 [0.9539]	31.7, 15.3 [0.9905]
443 [170]	1.08	33	0.08	60.1(54%), 20.3(46%)[a] [0.9993]	61.6, 24.8 (68%), 18.9, 2.0(32%)[b] [0.9990]
480 [207]	1.17	70	0.17	49.6(80%), 6.6(20%)[a] [0.9913]	50.3, 26.9 (91%): 4.7, 1.0(9%)[b] [0.9933]

[a]Multicomponent D_{res} distribution, fit with 2 build-ups. [b]Multicomponent Gaussian distribution with small D_{res} fixed.

Table 4-5. Residual dipolar coupling for 828\FcDA after annealing (T_g = 411 K, 138 °C)

T (K) [°C]	T/T_g	ΔT (K)	$\Delta T/T_g$	$D_{res}/2\pi$ (kHz) [r^2]	$\bar{D}_{res}$, $\sigma_D/2\pi$ (kHz) [r^2]
233 [−40]	0.57	−178	−0.43	49.0 [0.9935]	51.4 (12.2) [0.9959]
298 [25]	0.73	−113	−0.27	42.4 [0.9935]	44.8 (13.2) [0.9955]
413 [140]	1.005	2	0.005	37.1 [0.9578]	40.1 (18.7) [0.9934]
443 [170]	1.08	32	0.08	39.4 (75%), 3.7(25%)[a] [0.9194]	40.1, 25.0 (86%), 2.9, 2.2 (14%)[b] [0.9947]
463 [190]	1.13	52	0.13	29.6 (62%), 2.4 (27%)[a] [0.9873]	32.4, 16.2 (65%): 2.9, 2.5 (35%)[b] [0.9964]
481 [208]	1.17	70	0.17	27.5 (54%), 2.6 (46%)[a] [0.9757]	29.0, 15.9 (57%): 1.7, 1.3 (43%)[b] [0.9840]

[a]Multicomponent D_{res} distribution, fit with 2 build-ups. [b]Multicomponent Gaussian distribution with small D_{res} fixed.

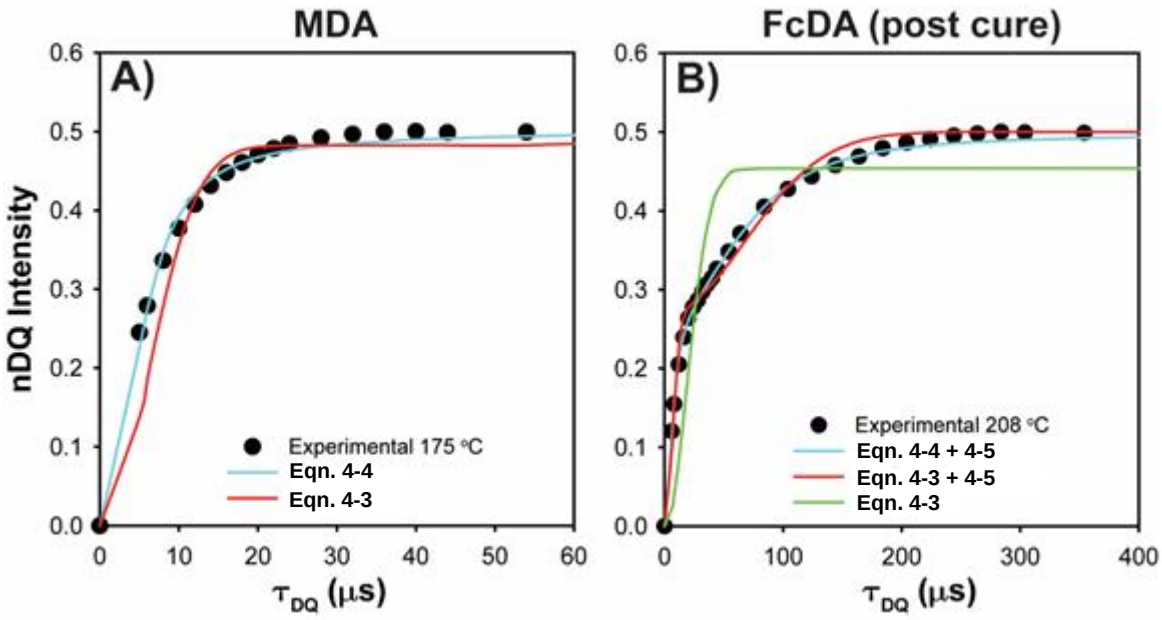

Figure 4-8. Examples of the different fits to I_{nDQ} intensity build-up for 828\MDA and 828\FcDA.

This mixture or distribution of local chain dynamics was directly evaluated by determining the distribution of dipolar couplings from DQ NMR build-up curves using the program *ftikreg* as shown in Figure 4-9 as a function of temperature. As predicted, in these fully cured epoxy thermoset materials there is a large distribution in D_{res} with the mean ~ 40 to 60 kHz. With increasing sample temperature, the dipolar coupling or, equivalently, the local bond order parameter S_b decrease, with a dramatic change at $T > T_g$ with $D_{res} < 12$ kHz. The behavior for the D-230- and MDA-cured epoxy thermosets is very similar for temperatures above T_g, revealing only a single broad distribution around $\langle D_{res} \rangle \sim 10$ kHz. In contrast, the FcDA-cured thermoset revealed a bimodal distribution in the dipolar coupling corresponding to a very mobile fraction $\langle D_{res} \rangle \sim 3$ kHz, and a more rigid fraction at $\langle D_{res} \rangle \sim 20$ kHz above the glass transition temperature (T/T_g = 1.2). The evolution of these residual dipolar coupling as a function of temperature is shown in Figure 4-10.

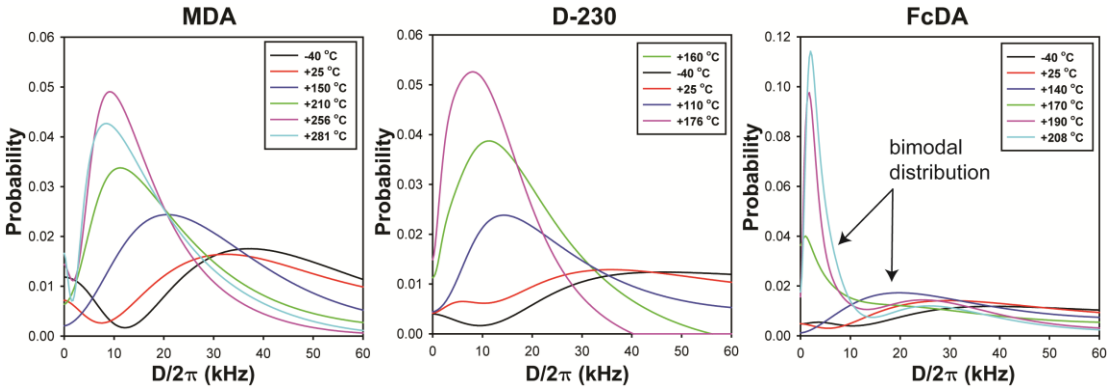

Figure 4-9. Distribution in dipolar coupling evaluated from DQ NMR build-up curves at several key temperatures.

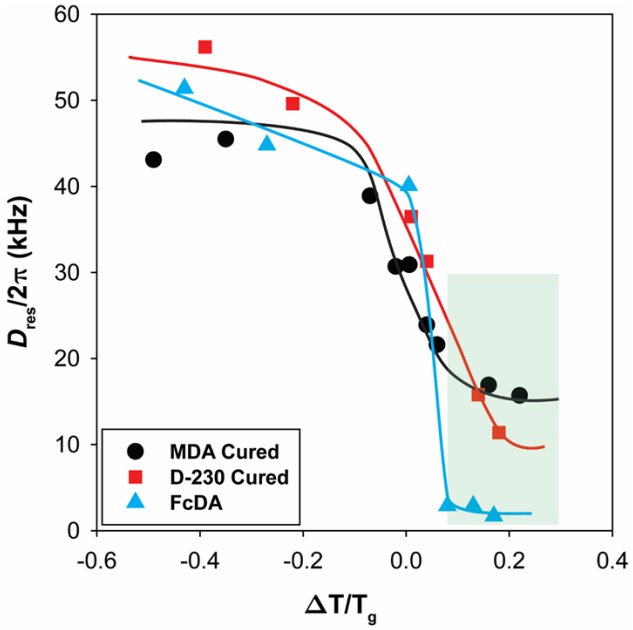

Figure 4-10. Residual dipolar coupling vs. scaled temperature for fully-cured thermosets.

At temperatures well above T_g, segmental dynamics should be fast enough for chain segments to rapidly explore all possible configurational states, with the observed D_{res} reflecting the density of crosslinks. DQ-derived D_{res} values have been utilized extensively for rubber systems and can also be used to evaluate the role of topological constraints in these thermosets. Under these high temperature conditions the order parameter S_b can evaluated from the ratio of D_{res} and the static dipolar coupling limit D_{stat} according to:

$$S_b = k\frac{D_{res}}{D_{stat}}\frac{1}{\langle P_2 \cos\alpha\rangle} = \frac{3}{5}\left(\frac{R}{L}\right)^2 \quad (4\text{-}11)$$

For the case of a Gaussian chain, the end-to-end distance $\boldsymbol{R}$ can be described by N statistical Kuhn segments of length a, with S_b proportional to $1/N$:

$$\boldsymbol{R}^2 = Na^2; L = Na; r = \frac{\boldsymbol{R}}{\boldsymbol{R}_0}$$
$$S_b = \frac{3}{5}\left(\frac{R}{L}\right)^2 = \frac{3}{5}\frac{r^2}{N} \tag{4-12}$$

The Kuhn segment can be related to the actual crosslink density using:

$$C_\infty = \lim_{N\to\infty} \boldsymbol{R}^2 \Big/ N_M l_M^2$$
$$\boldsymbol{R}^2 = C_\infty N_M l_M^2 \tag{4-13}$$

where the subscript M implies maximum extension, given by:

$$r_M = Na = fN_M l_M \tag{4-14}$$
$$N = \frac{f^2}{C_\infty} N_M$$
$$a = \frac{C_\infty}{f} l_M \tag{4-15}$$

where C_∞ is the characteristic ratio for the polymer chains, and f depends on the bond angle in the material. It is well known for rubbery materials, that DQ NMR experiments can provide the crosslink density using Eqn. 4-12. It is argued that for epoxy thermosets at temperatures $T > T_g$, the DQ NMR order parameters are also related to the crosslink or entanglement density. Unfortunately, an accurate estimate of C_∞ is not currently available for these epoxy thermosets, precluding using Eqn. 4-15 to relate the statistical segment to the actual chain segments. In addition, it is unclear what impact using the different curing agents would have on C_∞ for these materials.

Instead, we have taken a slightly different approach by looking at the ratio of the measured order parameters S_b to compare the epoxy thermosets obtained for the different curing agents. It is assumed that the static dipolar coupling and scaling factor are equivalent, such that by comparing the ratios of D_{res}, it is possible to obtain ratios of S_b and an effective measure of the chain flexibility

$$\frac{S_b^{(1)}}{S_b^{(2)}} \approx \frac{3}{5}\frac{r^2}{N^{(1)}} \Big/ \left\{\frac{3}{5}\frac{r^2}{N^{(2)}}\right\} = \frac{N^{(2)}}{N^{(1)}} = \frac{N_M^{(2)} C_\infty^{(1)}}{N_M^{(1)} C_\infty^{(2)}} \tag{4-16}$$

A smaller S_b ratio would imply greater mobility, corresponding to a larger number of statistical Kuhn segments describing the polymer chain. As we have discussed at length in Chapter 3, all experimental evidence suggests that 828\FcDA possesses similar crosslink density to the conventional materials. Therefore, the segment end-to-end distances between constraints are equivalent, meaning that the chain was more flexible with $C_\infty^{(2)} > C_\infty^{(1)}$. The ratio of order parameters at $\Delta T / T_g \sim 0.2$ is shown in Figure 4-11. These results show that the local order parameters S_b for the FcDA epoxy thermosets are only 10 to 15% of those observed in the MDA and D-230 epoxies. This

local measurement of chain dynamics is consistent with the increased fluxional properties of the FcDA curing agent.

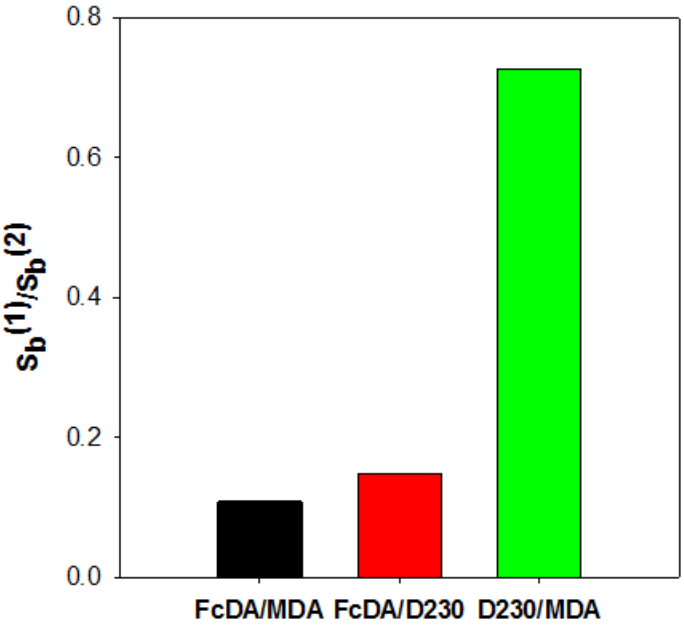

Figure 4-11. Order parameter ratios, indicating significantly enhanced average chain flexibility for FcDA-based networks.

4.4. Conclusions

In summary, the results of our solid state ^{1}H NMR investigation into chain dynamics in these epoxy thermosets mirror the stress relaxation phenomena described in Chapter 3. The static ^{1}H NMR spectra exhibited an abrupt change in line width ascribed to variation in motional averaging associated with the glass transition, as well as more subtle changes associated with lower temperature relaxation processes. More importantly, the DQ intensity build-up was comprehensively evaluated as a function of temperature, from which the residual dipolar coupling was estimated *via* non-linear fitting. The ferrocene-based thermoset exhibited a bimodal distribution in dipolar coupling at temperatures above T_g, indicative of chain segments exhibiting both rapid and slow dynamics. Finally, a comparison of residual dipolar coupling between different curing agents revealed that the order parameter of a FcDA-cured material is roughly an order of magnitude lower than either MDA-cured or D-230-cured materials. Although these observations are consistent with increased chain flexibility in ferrocene-based networks, they are not definitive proof of torsional flexing of Cp ligands in such materials. Future efforts should be directed at selective deuterium labeling of the Cp rings, so as to permit deconvolution of the Cp signal from the remainder of the polymer network *via* solid state ^{2}H NMR.

5. SUMMARY AND FUTURE WORK

The results presented in Chapter 3 and Chapter 4 give confidence that organometallic fluxionality can be exploited to profoundly alter chain dynamics in thermosets above T_g and thereby enable relaxation of stresses occurring in the rubbery state. In turn, this phenomenon leads to reduced overall residual stress due to cure in a like-for-like comparison between fluxional and conventional thermosets. Nevertheless, stress management in practical applications requires careful consideration of both cure stresses and thermal stresses. Unfortunately, condensation polymerizations, such as those based on epoxy-amine chemistry, typically yield stress profiles in which the overall residual stress is dominated by thermal effects, rather than cure shrinkage. This has been described previously by Lange, *et al.*, in a series of publications comparing residual stresses in epoxy and acrylate thermosets.[123,124]

As further illustration, Figure 5-1 compares the combined stress build-up due to cure and subsequent cooldown for 828 cured with FcDA and IPD. The initial portion of each curve, up to 10 or more hr, is the isothermal cure stress, *i.e.*, the same data previously depicted in Figure 3-8. The second, much larger increase in stress at later time is the stress due to cooling from the cure temperature to room temperature, *i.e.*, $\Delta T = -45$ °C, −65 °C, and −85 °C, for cure temperatures of 70 °C, 90 °C, and 110 °C, respectively. Two important facts are immediately apparent from these data. First, the thermal stress is over an order of magnitude larger than the cure stress, and this disparity increases with increasing cure temperature. Second, for a given cure temperature, there is negligible difference in the overall residual stress when curing with FcDA compared to IPD. The final stress level after cooldown in both cases is approximately 3 MPa, 4 MPa, and 5 MPa when curing at 70 °C, 90 °C, and 110 °C, respectively.

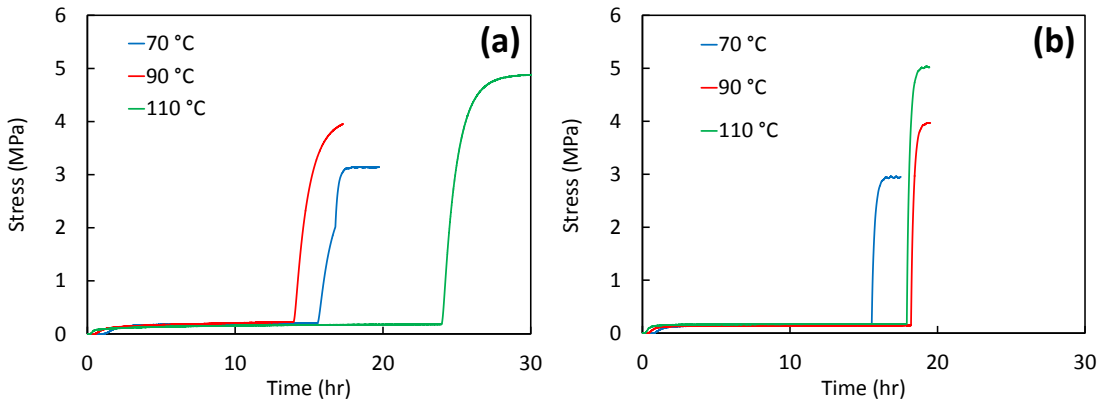

Figure 5-1. Stress build-up due to cure and subsequent cooldown to room temperature for 828 cured with (a) FcDA and (b) IPD.

Clearly, then, organometallic fluxionality does not substantially alter the *overall* residual stress in highly crosslinked thermosets based on condensation polymerizations, such as we have investigated in this work. These materials possess

comparatively high T_g values and residual stress is built up primarily in the glassy regime. To reiterate, the cure temperatures in Figure 5-1 are below $T_{g\infty}$, thus the materials are glassy through the entirety of cooldown. In conjunction, our solid state ^{1}H NMR data presented in Chapter 4 do not indicate any profound differences in segmental dynamics below T_g. This is reasonable to expect, as the glass transition defines the point below which segmental motion is arrested, particularly for the homogeneous networks typical of condensation polymerizations. Previous work has also shown that fluxionality is only apparent near or above T_g in polymers with backbone chain connectivity through ferrocene units.[68-70]

In light of this revelation, future work concerning stress management through fluxional materials should focus on polymer systems better suited to exploit rubbery chain dynamics. Among thermosets, radical-cured materials are an attractive choice for several reasons. These materials involve chain-growth polymerization mechanisms, in which gelation occurs at relatively low extents of functional group conversion. Consequently, the residual stress due to cure is significantly greater than condensation-cured materials, often approaching levels comparable to or greater than subsequent thermal stresses. In addition, chain-growth polymerizations yield highly heterogeneous networks, characterized by regions of high crosslink density interspersed among regions of low crosslink density populated with several types of network defects. In contrast, step-growth polymerizations (*e.g.*, epoxy-amine) yield homogeneous networks, where the concentration of network defects is effectively dependent only on the initial balance of reactive, functional groups. The heterogeneity inherent to radical-cured materials leads to considerable chain mobility below T_g (evident, for example, by broad loss tangent peaks), offering the possibility to exploit organometallic fluxionality to enhance stress relaxation in the glassy regime.

Organometallic fluxionality may also be of utility for stress management in linear polymers, particularly thermoplastics. Although many groups have incorporated ferrocene onto the backbone of linear polymers, the implications of fluxionality on stress relaxation apparently have not been considered. At a minimum, the low energy barrier associated with Cp rotation should lead to decreased relaxation times associated with terminal relaxation, *i.e.*, flow. This characteristic is expected to be useful for minimization of processing stresses as it will enable comparable final properties with reduced cycle time.

REFERENCES

1. Kamal, M. R. Thermoset Characterization for Moldability Analysis. *Polym. Eng. Sci.* **1974**, *14*, 231-239.
2. Adolf, D. B.; Martin, J. E.; Chambers, R. S.; Burchett, S. N.; Guess, T. R. Stresses during thermoset cure. *J. Mater. Res.* **1997**, *13*, 530-550.
3. Morgan, S. A.; Stavig, M. Model Validation Studies of 459 Epoxy. **2000**, SAND2000-2028C.
4. Russell, J. D.; Madhukar, M. S.; Genidy, M. S.; Lee, A. Y. A New Method to Reduce Cure-Induced Stresses in Thermoset Polymer Composites, Part III: Correlating Stress History to Viscosity, Degree of Cure, and Cure Shrinkage. *J. Compos. Mater.* **2000**, *34*, 1926-1947.
5. Lu, H.; Stansbury, J. W.; Bowman, C. N. Towards the elucidation of shrinkage stress development and relaxation in dental composites. *Dent. Mater.* **2004**, *20*, 979-986.
6. Stavig, M. Adolf, D. Kawaguchi, S. A TECHNIQUE TO CHARACTERIZE EPOXY CURE STRESSES FOR CURE PROFILE OPTIMIZATION. **2004**, SAND2004-2629C.
7. Ruiz, E.; Trochu, F. Comprehensive Thermal Optimization of Liquid Composite Molding to Reduce Cycle Time and Processing Stresses. *Polym. Compos.* **2005**, *26*, 209-230.
8. Yu, H.; Mhaisalkar, S. G.; Wong, E. H. Direct Measurement of Cure-Induced Stress in Thermosetting Materials by Means of a Dynamic Mechanical Analyzer. *Macromol. Rapid Comm.* **2006**, *27*, 1393-1397.
9. Merzlyakov, M.; McKenna, G. B.; Simon, S. L. Cure-induced and thermal stresses in a constrained epoxy resin. *Compos. A Appl. Sci. Manufact.* **2006**, *37*, 585-591.
10. Schubel, P. J.; Johnson, M. S.; Warrior, N. A.; Rudd, C. D. Characterisation of thermoset laminates for cosmetic automotive applications: Part III – Shrinkage control via nanoscale reinforcement. *Compos. A Appl. Sci. Manufact.* **2006**, *37*, 1757-1772.
11. Omrani, A.; Simon, L. C.; Rostami, A. A.; Ghaemy, M. Cure kinetics, dynamic mechanical and morphological properties of epoxy resin–Im_6NiBr_2 system. *Euro. Polym. J.* **2008**, *44*, 769-779.
12. Heinrich, C.; Aldridge, M.; Wineman, A. S.; Kieffer, J.; Waas, A. M.; Shahwan, K. W. Generation of heat and stress during the cure of polymers used in fiber composites. *Int. J. Eng. Sci.* **2012**, *53*, 85-111.
13. Soohyun, N.; Dongyoung, L.; Ilbeom, C.; Gil, L. D. Smart cure cycle for reducing the thermal residual stress of a co-cured E-glass/carbon/epoxy composite structure for a vanadium redox flow battery. *Compos. Struct.* **2015**, *120*, 107-116.
14. Rohr, G. D.; Rasberry, R. D.; Kaczmarowski, A. K.; Stavig, M. E.; Gibson, C. S.; Udd, E.; Roach, A. R.; Nation, B. Residual internal stress optimization for EPON 828/DEA thermoset resin using fiber Bragg grating sensors. **2015**, SAND2015-2114C.
15. Thurn, J.; Hermel-Davidock, T. Thermal stress hysteresis and stress relaxation in an epoxy film. *J. Mater. Sci.* **2007**, *42*, 5686-5691.

16. Barua, B.; Saha, M. C. Tensile Stress Relaxation Behavior of Thermosetting Polyurethane Solid and Foams: Experiment and Model Prediction. *J. Eng. Mater. Tech.* **2011**, *133*, 041007.

17. Odegard, G. M.; Bandyopadhyay, A. Physical Aging of Epoxy Polymers and Their Composites. *J. Polym. Sci. B Polym. Phys.* **2011**, *49*, 1695-1716.

18. Kropka, J. M.; Spangler, S. W.; Stavig, M. E.; Chambers, R. S. Residual Stress Developed During the Cure of Thermosetting Polymers. **2015**, SAND2015-2149C.

19. Jutzi, P. Fluxional η^1-Cyclopentadienyl Compounds of Main-Group Elements. *Chem Rev.* **1986**, *86*, 983-996.

20. Jutzi, P.; Reumann, G. Cp* Chemistry of main-group elements. *J. Chem. Soc. Dalton Trans.* **2000**, 2237-2244.

21. Powell, P. *Principles of Organometallic Chemistry*, 2nd Ed.; Springer: 1988.

22. Dewey, F. M. FERROCENE-CONTAINING PROPELLANT INGREDIENTS. **1968**, AFRPL-TR-68-170.

23. Yu, H.; Wang, L.; Huo, J.; Ding, J.; Tan, Q. Synthesis and Curing Behavior of a Novel Ferrocene-Based Epoxy Compound. *J. Appl. Polym. Sci.* **2008**, *110*, 1594-1599.

24. Yu, H.; Wang, L.; Huo, J.; Li, C.; Tan, Q. Synthesis of Glycidyl Ether of Poly(bisphenol-A 1,1'-ferrocene dicarboxylate) and Its Electrochemical Behavior. *Des. Monomers Polym.* **2009**, *12*, 305-313.

25. Wang, J.; Ding, H.; Ni, P.; Dai, L.; Gao, Q. Ferrocene-Based Epoxy Derivatives. *Prog. Chem.* **2015**, *27*, 853-860.

26. Woltersdorf, M.; Kranich, R.; Schmalz, H.-G. Enantioselective Synthesis of New C_2-Symmetric Ferrocenylalkylamines via Sonochemical Amination of 1-Ferrocenylalkyl Acetates. *Tetrahedron* **1997**, *53*, 7219-7230.

27. Schwink, L.; Knochel, P. Enantioselective Preparation of C_2-Symmetrical Ferrocenyl Ligands for Asymmetric Catalysis. *Chem. Eur. J.* **1998**, *4*, 950-968.

28. Zorić, Z.; Rapić, V.; Lisac, S.; Jukić, M. Ferrocene Compounds. XXV.* Synthesis and Characterization of Ferrocene-Containing Oligoamides, Their Precursors, and Analogues. *J. Polym. Sci. A Polym. Chem.* **1999**, *37*, 25-36.

29. Kim, T.-J.; Lee, H.-Y.; Ryu, E.-S.; Park, D.-K.; Cho, C. S.; Shim, S. C.; Jeong, J. H. Asymmetric addition of diethylzinc to aromatic aldehydes by chiral ferrocene-based catalysts. *J. Organomet. Chem.* **2002**, *649*, 258-267.

30. Ballistreri, F. P.; Patti, A.; Pedotti, S.; Tomaselli, G. A.; Toscano, R. M. Synthesis of novel chiral 'salen-type' ferrocenyl ligands. *Tetrahedron: Asymmetry* **2007**, *18*, 2377-2380.

31. Kim, H.-K.; Park, J.-A.; Kim, K. M.; Md., N. S.; Kang, D.-S.; Lee, J.; Chang, Y.; Kim, T.-J. Gd-complexes of macrocyclic DTPA conjugates of 1,1'-bis(amino)ferrocenes as high relaxivity MRI blood-pool contrast agents (BPCAs). *Chem. Commun.* **2010**, *46*, 8442-8444.

32. Kanbayashi, N.; Akutsu, H.; Yamada, J.; Nakatsuji, S.; Turner, S. S. A new ferrocene-containing charge-transfer salt, $(TTF)_2[Fe(C_5H_4\text{-}CH(CH_3)NHCOCH_2SO_3)_2]$. *Inorg. Chem. Commun.* **2012**, *21*, 122-124.

33. Qian, H.; Yan, S.; Cui, X.; Pi, C.; Liu, C.; Wu, Y. A Highly Efficient Synthesis of Optically Active Ferrocenylethylamines via Hydride Reduction of Chiral Ferrocenylketimines. *Chin. J. Chem.* **2013**, *31*, 992-996.

34. Ochi, M.; Yamazaki, K.; Shimbo, M. Internal stress of epoxide resin modified with spiro ortho-ester type resin. *J. Mater. Sci.* **1989**, *24*, 3189-3195.

35. Bailey, W. J. Matrices that expand on curing for high strength composites and adhesives. *Mater. Sci. Eng.* **1990**, *A126*, 271-279.

36. He, P.; Zhou, Z. Epoxy resin copolymer with zero shrinkage. *J. Mater. Sci.* **1991**, *26*, 3792-3796.

37. Alcoutlabi, M.; McKenna, G. B.; Simon, S. L. Analysis of the development of isotropic residual stresses in a bismaleimide/spiro orthocarbonate thermosetting resin for composite materials. *J. Appl. Polym. Sci.* **2003**, *88*, 227-244.

38. Morikawa, H.; Sudo, A.; Nishida, H.; Endo, T. Volume-expandable monomer 5,5-dimethyl-1,3-dioxolan-2-one: Its copolymerization behavior with epoxide and its applications to shrinkage-controlled epoxy-curing systems. *J. Appl. Polym. Sci.* **2005**, *96*, 372-378.

39. Chen, X.; Dam. M. A.; Ono, K.; Mal, A.; Shen, H.; Nutt, S. R.; Sheran, K.; Wudl, F. A Thermally Re-mendable Cross-Linked Polymeric Material. *Science* **2002**, *295*, 1698-1702.

40. Scott, T. F.; Schneider, A. D.; Cook, W. D.; Bowman, C. N. Photoinduced Plasticity in Cross-Linked Polymers. *Science* **2005**, *308*, 1615-1617.

41. Kloxin, C. J.; Scott, T. F.; Bowman, C. N. Stress Relaxation via Addition-Fragmentation Chain Transfer in a Thiol-ene Photopolymerization. *Macromolecules* **2009**, *42*, 2551-2556.

42. Ghosh, B.; Urban, M. W. Self-Repairing Oxetane-Substituted Chitosan Polyurethane Networks. *Science* **2009**, *323*, 1458-1460.

43. Park, H. Y.; Kloxin, C. J.; Scott, T. F.; Bowman, C. N. Stress Relaxation by Addition-Fragmentation Chain Transfer in Highly Cross-Linked Thiol-Yne Networks. *Macromolecules* **2010**, *43*, 10188-10190.

44. Nicolaÿ, R.; Kamada, J.; Van Wassen, A.; Matyjaszewski, K. Responsive Gels Based on a Dynamic Covalent Trithiocarbonate Cross-Linker. *Macromolecules* **2010**, *43*, 4355-4361.

45. Montamal, D.; Capelot, M.; Tournilhac, F.; Leibler, L. Silica-Like Malleable Materials from Permanent Organic Networks. *Science* **2011**, *334*, 965-968.

46. Amamoto, Y.; Kamada, J.; Otsuka, H.; Takahara, A.; Matyjaszewski, K. Repeatable Photoinduced Self-Healing of Covalently Cross-Linked Polymers through Reshuffling of Trithiocarbonate Units. *Angew. Chem. Int. Ed.* **2011**, *50*, 1660-1663.

47. Capelot, M.; Unterlass, M.; Tournilhac, F.; Leibler, L. Catalytic Control of the Vitrimer Glass Transition. *ACS Macro Lett.* **2012**, *1*, 789-792.

48. Bowman, C. N.; Kloxin, C. J. Covalent Adaptable Networks: Reversible Bond Structures Incorporated in Polymer Networks. *Angew. Chem. Int. Ed.* **2012**, *51*, 4272-4274.

49. Lu, Y.-X.; Tournilhac, F.; Leibler, L.; Guan, Z. Making Insoluble Polymer Networks Malleable via Olefin Metathesis. *J. Am. Chem. Soc.* **2012**, *134*, 8424-8427.

50. Capelot, M.; Montarnal, D.; Tournilhac, F.; Leibler, L. Metal-Catalyzed Transesterification for Healing and Assembling of Thermosets. *J. Am. Chem. Soc.* **2012**, *134*, 7664-7667.

51. Park, H. Y.; Kloxin, C. J.; Abuelyaman, A. S.; Oxman, J. D.; Bowman, C. N. Stress Relaxation via Addition-Fragmentation Chain Transfer in High T_g, High Conversion Methacrylate-Based Systems. *Macromolecules* **2012**, *45*, 5640-5646.

52. Kloxin, C. J.; Bowman, C. N. Covalent adaptable networks: smart, reconfigurable and responsive network systems. *Chem. Soc. Rev.* **2013**, *42*, 7161-7173.

53. Pepels, M.; Filot, I.; Klumperman, B.; Goossens, H. Self-healing systems based on disulfide-thiol exchange reactions. *Polym. Chem.* **2013**, *4*, 4955-4965.

54. Yu, K.; Taynton, P.; Zhang, W.; Dunn, M. L.; Qi, H. J. Influence of stoichiometry on the glass transition and bond exchange reactions in epoxy thermoset polymers. *RSC Adv.* **2014**, *4*, 48682-48690.

55. Brutman, J. P.; Delgado, P. A.; Hillmyer, M. A. Polylactide Vitrimers. *ACS Macro Lett.* **2014**, *3*, 607-610.

56. Martin, R.; Rekondo, A.; de Luzuriaga, A. R.; Cabañero, G.; Grande, H. J.; Odriozola, I. The processability of a poly(urea-urethane) elastomer reversibly crosslinked with aromatic disulfide bridges. *J. Mater. Chem. A* **2014**, *2*, 5710-5715.

57. Fortman, D. J.; Brutman, J. P.; Cramer, C. J.; Hillmyer, M. A. Dichtel, W. R. Mechanically Activated, Catalyst-Free Polyhydroxyurethane Vitrimers. *J. Am. Chem. Soc.* **2015**, *137*, 14019-14022.

58. Obadia, M. M.; Mudraboyina, B. P.; Serghei, A.; Montarnal, D.; Drockenmuller, E. Reprocessing and Recycling of Highly Cross-Linked Ion-Conducting Networks through Transalkylation Exchanges of C-N Bonds. *J. Am. Chem. Soc.* **2015**, *137*, 6078-6083.

59. Romano, F.; Sciortino, F. Switching Bonds in a DNA Gel: An All-DNA Vitrimer. *Phys. Rev. Lett.* **2015**, *114*, 078104.

60. Denissen, W.; Rivero, G.; Nicolaÿ, R.; Leibler, L.; Winne, J. M.; Du Prez, F. E. Vinylogous Urethane Vitrimers. *Adv. Funct. Mater.* **2015**, *25*, 2451-2457.

61. Imbernon, L.; Norvez, S.; Leibler, L. Stress Relaxation and Self-Adhesion of Rubbers with Exchangeable Links. *Macromolecules* **2016**, *49*, 2172-2178.

62. Denissen, W.; Winne, J. M.; Du Prez, F. E. Vitrimers: permanent organic networks with glass-like fluidity. *Chem. Sci.* **2016**, *7*, 30-38.

63. Snijkers, F.; Pasquino, R.; Maffezzoli, A. Curing and viscoelasticity of vitrimers. *Soft Matter* **2017**, *13*, 258-268.

64. Kuang, X.; Liu, G.; Dong, X.; Wang, D. Correlation between stress relaxation dynamics and thermochemistry for covalent adaptive networks polymers. *Mater. Chem. Front.* **2017**, *1*, 111-118.

65. Manners, I. Polymer science with transition metals and main group elements: Towards functional, supramolecular inorganic polymeric materials. *J. Polym. Sci. A Polym. Chem.* **2002**, *40*, 179-191.

66. Williams, K. A.; Boydston, A. J.; Bielawski, C. W. Main-chain organometallic polymers: synthetic strategies, applications, and perspectives. *Chem. Soc. Rev.* **2007**, *36*, 729-744.

67. Abd-El-Aziz, A. S.; Agatemor, C.; Etkin, N. Sandwich Complex-Containing Macromolecules: Property Tunability Through Versatile Synthesis. *Macromol. Rapid Comm.* **2014**, *35*, 513-559.

68. Kulbaba, K.; Macdonald, P. M.; Manners, I. Molecular Motions in Poly(ferrocenes): Solid-State Deuterium NMR Studies of Poly(ferrocenylsilanes) near Their Glass Transition Temperature. *Macromolecules* **1999**, *32*, 1321-1324.

69. Kulbaba, K.; Macdonald, P. M.; Manners, I. Molecular Motions in Poly(ferrocenes): Solid State Deuterium NMR Study of Poly(ferrocenylsilanes) near the Glass Transition Temperature. *Polym. Mater. Sci. Eng.* **2000**, *82*, 179-180.

70. Kulbaba, K.; Manners, I.; Macdonald, P. M. Molecular Motions in Metal-Containing Polymers: Solid-State Deuterium NMR Studies of Polyferrocenylsilanes near Their Glass Transition Temperature. *Macromolecules* **2002**, *35*, 10014-10025.

71. Mijović, J.; Andjelić, S. A Study of Reaction Kinetics by Near-Infrared Spectroscopy. 1. Comprehensive Analysis of a Model Epoxy/Amine System. *Macromolecules* **1995**, *28*, 2787-2796.

72. Horie, K.; Hiura, H.; Sawada, M.; Mita, I.; Kambe, H. Calorimetric investigation of polymerization reactions. III. Curing reaction of epoxides with amines. *J. Polym. Sci. A-1* **1970**, *8*, 1357-1372.

73. Charlesworth, J. M. Effect of crosslink density on molecular relaxations in diepoxide-diamine network polymers. Part 2. The rubbery plateau region. *Polym. Eng. Sci.* **1988**, *28*, 230-236.

74. Hiemenz, P. C.; Lodge, T. P. *Polymer Chemistry*, 2nd ed.; CRC Press: Boca Raton, FL, 2007.

75. Haider, M.; Hubert, P.; Lessard, L. Cure shrinkage characterization and modeling of a polyester resin containing low profile additives. *Compos. A* **2007**, *38*, 994-1009.

76. Khoun, L.; Hubert, P. Cure Shrinkage Characterization of an Epoxy Resin System by Two in Situ Measurement Methods. *Polym. Compos.* **2010**, *31*, 1603-1610.

77. Shah, D. U.; Schubel, P. J. Evaluation of cure shrinkage measurement techniques for thermosetting resins. *Polym. Test.* **2010**, *29*, 629-639.

78. Lee, S. H.; Chang, J.; Ferracane, J.; Lee, I. B. Influence of instrument compliance and specimen thickness on the polymerization shrinkage stress measurement of light-cured composites. *Dent. Mater.* **2007**, *23*, 1093-1100.

79. Min, S.-H.; Ferracane, J.; Lee, I.-B. Effect of shrinkage strain, modulus, and instrument compliance on polymerization shrinkage stress of light-cured composites during the initial curing stage. *Dent. Mater.* **2010**, *26*, 1024-1033.

80. Chiang, M. Y. M.; Giuseppetti, A. A. M.; Qian, J.; Dunkers, J. P.; Antonucci, J. M.; Schumacher, G. E.; Gibson, S.-L. Analyses of a cantilever-beam based instrument for evaluating the development of polymerization stresses. *Dent. Mater.* **2011**, *27*, 899-905.

81. Gonçalves, F.; Boaro, L. C.; Ferracane, J. L.; Braga, R. R. A comparative evaluation of polymerization stress data obtained with four different mechanical testing systems. *Dent. Mater.* **2012**, *28*, 680-686.

82. Braga, R. R.; Yamamoto, T.; Tyler, K.; Boaro, L. C.; Ferracane, J. L.; Swain, M. V. A comparative study between crack analysis and a mechanical test for assessing the polymerization stress of restorative composites. *Dent. Mater.* **2012**, *28*, 632-641.

83. Wang, Z.; Landis, F. A.; Giuseppetti, A. A. M.; Lin-Gibson, S.; Chiang, M. Y. M. Simultaneous measurement of polymerization stress and curing kinetics for photo-polymerized composites with high filler contents. *Dent. Mater.* **2014**, *30*, 1316-1324.

84. Harsch, M.; Herzog, F.; Karger-Kocsis, J. Cure-induced Normal Force Development in Unfilled and Filled Epoxy Resins. *J. Compos. Mater.* **2008**, *42*, 2299-2309.

85. Offenbach, J. A.; Tobolsky, A. V. Chemical Relaxation of Stress in Polyurethane Elastomers. *J. Colloid Sci.* **1956**, *11*, 39-47.

86. Colodny, P. C.; Tobolsky, A. V. Chemorheological Study of Polyurethan Elastomers. *J. Am. Chem. Soc.* **1957**, *79*, 4320-4323.

87. Chasset, R.; Thirion, P. Viscoelastic relaxation of rubber vulcanizates between the glass transition and equilibrium. *Proceedings of the Conference on Physics of Non-Crystalline Solids*; North Holland Publishing: Amsterdam, 1965, pp. 345-359.

88. de Nograro, F. F.; Llano-Ponte, R.; Mondragon, I. Dynamic and mechanical properties of epoxy networks obtained with PPO based amines/mPDA mixed curing agents. *Polymer* **1996**, *37*, 1589-1600.

89. Galy, J.; Sabra, A.; Pascault, J.-P. Characterization of epoxy thermosetting systems by differential scanning calorimetry. *Polym. Eng. Sci.* **1986**, *26*, 1514-1523.

90. Mezzenga, R.; Luciani, A.; Manson, J.-A. E. Phase separation and gelation of epoxy resin/hyperbranched polymer blends. *Polym. Eng. Sci.* **2002**, *42*, 249-257.

91. Matsuoka, S. Thermodynamic Theory of Viscoelasticity. *J. Therm. Anal.* **1996**, *46*, 985-1010.

92. Matsuoka, S.; Hale, A. Cooperative relaxation processes in polymers. *J. Appl. Polym. Sci.* **1997**, *64*, 77-93.

93. Mulay, L. N.; Attalla, A. Activation Energies for Reorientation Processes in Ferrocene and Some of its Derivatives: A Study of Proton Magnetic Resonance Spectra. *J. Am. Chem. Soc.* **1963**, *85*, 702-706.

94. Bohn, R. K.; Haaland, A. On the molecular structure of ferrocene, $Fe(C_5H_5)_2$. *J. Organomet. Chem.* **1966**, *5*, 470-476.

95. Haaland, A.; Nilsson, J.-E. The Determination of the Barrier to Internal Rotation in Ferrocene and Ruthenocene by Means of Electron Diffraction. *Chem. Commun.* **1968**, 88-89.

96. Abe, A.; Jernigan, R. L.; Flory, P. J. Conformational Energies of n-Alkanes and the Random Configuration of Higher Homologs Including Polymethylene. *J. Am. Chem. Soc.* **1966**, *88*, 631-639.

97. Ferry, J. D. *Viscoelastic Properties of Polymers*, 3rd ed.; John Wiley and Sons: New York, 1980.

98. de Gennes, P. G. Reptation of a Polymer Chain in the Presence of Fixed Obstacles. *J. Chem. Phys.* **1971**, *55*, 572-579.

99. de Gennes, P. G. Reptation of stars. *J. Phys. France* **1975**, *36*, 1199-1203.

100. Curro, J.; Pincus, P. A Theoretical Basis for Viscoelastic Relaxation of Elastomers in the Long-Time Limit. *Macromolecules* **1983**, *16*, 559-562.

101. Curro, J.; Pearson, D. S.; Helfand, E. Viscoelasticity of Randomly Cross-Linked Polymer Networks. Relaxation of Dangling Chains. *Macromolecules* **1985**, *18*, 1157-1162.

102. Thirion, P.; Monnerie, L. Double-Step Retraction of a Polyisoprene Vulcanizate: Comparison with Molecular Models. *J. Polym. Sci. B Polym. Phys.* **1986**, *24*, 2307-2318.

103. Gaylord, R. J.; Weiss, G. H.; Dimarzio, E. A. Nonequilibrium Mechanical Response of a Cross-Linked Network. *Macromolecules* **1986**, *19*, 927-929.

104. Thirion, P.; Monnerie, L. Response of Polyisoprene and Polybutadiene Vulcanisates to Double-Step Retractions: Analysis by a Disengagement Process of Pendant Chains. *J. Polym. Sci. B Polym. Phys.* **1987**, *25*, 1033-1041.

105. McKenna, G. B.; Gaylord, R. J. Relaxation of crosslinked networks: theoretical models and apparent power law behaviour. *Polymer* **1988**, *29*, 2027-2032.

106. Lu, H.; Lovell, L. G.; Bowman, C. N. Exploiting the Heterogeneity of Cross-Linked Photopolymers To Create High-T_g Polymers from Polymerizations Performed at Ambient Conditions. *Macromolecules* **2001**, *34*, 8021-8025.

107. Schroeder, J. A.; Madsen, P. A.; Foister, R. T. Structure/property relationships for a series of crosslinked aromatic/aliphatic epoxy mixtures. *Polymer* **1987**, *28*, 929-940.

108. Kody, R. S.; Lesser, A. J. Deformation and yield of epoxy networks in constrained states of stress. *J. Mater. Sci.* **1997**, *32*, 5637-5643.

109. Crawford, E. D.; Lesser, A. J. Brittle to Ductile: Fracture Toughness Mapping on Controlled Epoxy Networks. *Polym. Eng. Sci.* **1999**, *39*, 385-392.

110. Garcia, F. G.; Soares, B. G.; Pita, V. J. R. R.; Sánchez, R.; Rieumont, J. Mechanical properties of epoxy networks based on DGEBA and aliphatic amines. *J. Appl. Polym. Sci.* **2007**, *106*, 2047-2055.

111. Blanco, M.; Ramos, J. A.; Goyanes, S.; Rubiolo, G.; Salguiero, W.; Somoza, A.; Mondragon, I. Intermolecular Interactions on Amine-Cured Epoxy Matrices with Different Crosslink Densities. Influence on the Hole and Specific Volumes and the Mechanical Behavior. *J. Polym. Sci. B Polym. Phys.* **2009**, *47*, 1240-1252.

112. Amaral, C. R.; Rodriguez, R. J. S.; Garcia, F. G.; Junior, L. P. B.; Carvalho, E. A. Impact of aliphatic amine comonomers on DGEBA epoxy network properties. *Polym. Eng. Sci.* **2014**, *54*, 2132-2138.

113. Boye, J.; Demont, P.; Lacabanne, C. Secondary retardation modes in diglycidyl ether of bisphenol A-diamino diphenyl methane networks. *J. Polym. Sci. B Polym. Phys.* **1994**, *32*, 1359-1369.

114. Munowitz, M.; Pines, A. Principles and Applications of Multiple-Quantum NMR. In *Advances in Chemical Physics*, John Wiley & Sons, Inc.: 2007; pp 1-152.

115. Schneider, M.; Gasper, L.; Demco, D. E.; Blümich, B. Residual dipolar couplings by ^{1}H dipolar-encoded longitudinal magnetization, double- and triple-quantum nuclear magnetic resonance in cross-linked elastomers. *J. Chem. Phys.* **1999,** *111*, 402-415.

116. Voda, M. A.; Demco, D. E.; Perlo, J.; Orza, R. A.; Blümich, B. Multispin moments edited by multiple-quantum NMR: application to elastomers. *J. Magn. Reson.* **2005,** *172*, 98-109.

117. Saalwächter, K.; Herrero, B.; López-Manchado, M. A. Chain Order and Cross-Link Density of Elastomers As Investigated by Proton Multiple-Quantum NMR. *Macromolecules* **2005,** *38*, 9650-9660.

118. Saalwächter, K.; Klüppel, M.; Luo, H.; Schneider, H. Chain Order in Filled SBR Elastomers: a Proton Multiple-Quantum NMR Study. *Appl. Magn. Reson.* **2004,** *27*, 401.

119. Chassé, W.; Valentín, J. L.; Genesky, G. D.; Cohen, C.; Saalwächter, K. Precise Dipolar Coupling Constant Distribution Analysis in Proton Multiple-Quantum NMR of Elastomers. *J. Chem. Phys.* **2011,** *134*, 044907.

120. Plazek, D. J.; Ngai, K. L. Correlation of polymer segmental chain dynamics with temperature-dependent time-scale shifts. *Macromolecules* **1991,** *24*, 1222-1224.

121. Roland, C. M.; Ngai, K. L. Segmental relaxation and molecular structure in polybutadienes and polyisoprene. *Macromolecules* **1991,** *24*, 5315-5319.

122. Roland, C. M.; Ngai, K. L. Normalization of the temperature dependence of segmental relaxation times. *Macromolecules* **1992,** *25*, 5765-5768.

123. Lange, J.; Toll, S.; Månson, J.-A. E.; Hult, A. Residual stress build-up in thermoset films cured above their ultimate glass transition temperature. *Polymer* **1995**, *36*, 3135-3141.

124. Lange, J.; Toll, S.; Månson, J.-A. E.; Hult, A. Residual stress build-up in thermoset films cured below their ultimate glass transition temperature. *Polymer* **1997**, *37*, 809-815.

DISTRIBUTION

1	MS0346	Kurtis Ford	1556 (electronic copy)
1	MS0734	Timothy Lambert	8824 (electronic copy)
1	MS0840	Kevin Long	1554 (electronic copy)
1	MS0878	Carlton Brooks	2585 (electronic copy)
1	MS0878	Ryan Davis	2585 (electronic copy)
1	MS0886	Todd Alam	1853 (electronic copy)
1	MS0888	James McElhanon	1853 (electronic copy)
1	MS0889	Wahid Hermina	1850 (electronic copy)
1	MS0958	Jamie Kropka	1853 (electronic copy)
1	MS0958	Mark Stavig	1853 (electronic copy)
1	MS0971	Amy Kaczmarowski	6782 (electronic copy)
1	MS1217	David Wheeler	5864 (electronic copy)
1	MS1411	Mathias Celina	1853 (electronic copy)
1	MS0899	Technical Library	9536 (electronic copy)
1	MS0359	D. Chavez, LDRD Office	1911
1	MS0161	Legal Technology Transfer Center	11500


Sandia National Laboratories